AD-A203 015

DTIC
ELECTED
JAN 2 3 1989
S H

A STUDY OF FAILURE CHARACTERISTICS IN

A THERMOPLASTIC COMPOSITE MATERIAL AT

HIGH TEMPERATURE

THESIS

James M. Fisher
Capt, USAF

AFIT/GAE/AA/88D-15

DEPARTMENT OF THE AIR FORCE

AIR UNIVERSITY

AIR FORCE INSTITUTE OF TECHNOLOGY

Wright-Patterson Air Force Base, Ohio

A STUDY OF FAILURE CHARACTERISTICS IN

A THERMOPLASTIC COMPOSITE MATERIAL AT

HIGH TEMPERATURE

THESIS

James M.Fisher
Capt, USAF

AFIT/GAE/AA/88D-15

DTIC
ELECTE
JAN 2 3 198
H

Approved for public release; distribution unlimited

(

A STUDY OF FAILURE CHARACTERISTICS IN

A THERMOPLASTIC COMPOSITE MATERIAL AT

HIGH TEMPERATURE

THESIS

Presented to the Faculty of the School of Engineering

of the Air Force Institute of Technology

Air University

In Partial Fulfillment of the

Requirements for the Degree of

Master of Science in Aeronautical Engineering

James M.Fisher
Capt, USAF
AFIT/GAE/ENG/88D-15

December 1988

Preface

The purpose of this thesis was to study the nonlinear
behavior and failure characteristics of Gr/PEEK at 250 F
using both experimental and analytic methods. For the
experimental work, a total of 71 specimens were fabricated,
instrumented, and tested. For the analytic work, a number
of techniques were employed to analyze the behavior of the
model numerically. Almost all of this work was accomplished
over a five month period while I was attending classes part
time. Obviously, I had help!

I had the privilege of having two advisors on this work:
Dr. Palazotto (from AFIT) was my thesis advisor and Dr.
Sandhu (from FDL) was my technical advisor. Dr. Palazotto
was instrumental in directing me toward a thesis topic and
then keeping tabs on what I was doing to make sure I wasn't
getting too far off in left field (not to mention providing
invaluable roundball tips). Dr. Sandhu walked me through
each new stage of both the experimental and analytic work so
that I could proceed on my own. Both of these gentlemen were
always there to answer my naive questions, to help me through
the times where I wasn't sure what I was doing, and to
provide the creative spark that got me over the problems.

The experimental work required a great deal of effort
involving the AFIT Model Shop, Instrumentation, the Fracture
Lab, and a variety of other shops. Much of the coordination
required between these shops was done by Patty Lachey at

ii

FDL/FIBC. She seemed to always be there making sure things got done on time, slipping work into people between higher priority jobs, and taking care of the details that I never seemed to get to. The experimental work for this thesis could not have been completed on time had it not been for her diligence and care.

A lot of people helped me at the technician level. These were the guys who actually cut the material and instrumented the specimens and operated the equipment. I can't mention all the names so I'll risk slighting someone by mentioning the most important. Of all the people I had the privilege of working with on this thesis, the two I worked most closely with were Larry Bates and Don Cook in the Fracture Lab. I relied heavily on these guys to solve a lot of the equipment related problems and they always came through. I'd also like to thank Marlin North, Jim Weiher, and Cliff Hitchcock for their efforts in getting my specimens gaged and Bob Graf for whatever he did to the data collection software (and for fixing it afterward).

Lastly, and most importantly, I'd like to thank my lovely wife Jan for her understanding and patience. It seemed like she always knew when I was under the gun and responded by being extra supportive. I'd like to thank her mostly for all the times that she reminded me that there are more important things to grow grey hairs over than AFIT.

Table of Contents

List of Figures

List of Tables

AFIT/GAE/AA/88D-15

Abstract

The purpose of this thesis was to study the failure
characteristics of the thermoplastic composite Graphite/
Polyetheretherketone (Gr/PEEK) at 250 F. Specimens of Gr/PEEK
containing a hole (1/3 diameter to width ratio) were tested at
250 F to determine stress-strain response, the progression of
failure, and ultimate tensile strength. The ply lay-ups of
these specimens were: $[0]_{16}$, $[90]_{16}$, $[\pm45]_{4s}$, and
$[0,\pm45,90]_{2s}$. Using ASTM standards, specimens of Gr/PEEK
were also tested at 250 F to determine the nonlinear material
properties of Gr/PEEK. These material properties were used
in a nonlinear finite element program designed to predict the
stress-strain behavior and ultimate failure of structures
made from materials with nonlinear material properties.

Testing of the specimens containing $\pm45^{\circ}$ fibers was
complicated when the high temperature coupled with the high
strains caused the strain gages to come unglued a third of the
way through testing. Optical techniques of measuring high
strains were used on both the basic property $[\pm45]_{4s}$ specimens
and the $[\pm45]_{4s}$ specimens containing a hole primarily to
determine the feasibility of these techniques and to provide a
basis for comparison for the analysis. These techniques
showed promise for measuring high strains in extreme
environmental conditions.

The experimental results compared well with the predicted behavior determined by using the nonlinear finite element program. The model used was designed to predict failure transverse to the load at the hole, fairly reasonable for isotropic materials. This geometry was quite effective for the $[90]_{46}$, $[\pm45]_{4s}$, and $[0,\pm45,90]_{2s}$ ply lay-ups. The stress-strain behavior, progression of failure, and ultimate failure predicted for these ply layups compared well with the available experimental data. The stress-strain correlation was limited to lower load levels for the $[\pm45]_{4s}$ and $[0,\pm45,90]_{2s}$ specimens because of the failure of the gage adhesive. Results from the $[0]_{46}$ analysis indicate that since failure in this lay-up occurred parallel to the load, the geometry of the model was not appropriate. Results from a model with elements oriented in the direction of the fibers but with less refinement at the hole were significantly better.

One of the assumptions made in this study was that the effect of time dependent (viscoelastic) material properties would be minimal. Based on experimental data discovered accidentally, this may not be an appropriate assumption. Ply lay-ups containing $\pm45^\circ$ fibers are shown to unload themselves under static deformation at load levels as low as 65% of ultimate failure.

A high speed video camera was used to record failure of the specimens with holes. Data on approximately how rapidly the different ply lay-ups fail is valuable in modeling the

progression of failure analytically. Although the video camera used was capable of frame rates high enough to capture the failure process, the high frame rates are at the expense of photographic resolution. Although the images do provide some insight into how fast the specimens fail, the images recorded are of relatively poor quality.

A STUDY OF THE FAILURE CHARACTERISTICS OF A THERMOPLASTIC COMPOSITE MATERIAL AT HIGH TEMPERATURE

I. Introduction

The study of materials and their failure characteristics probably began with the advent of the wheel. As buildings, transportation systems, and manufactured goods have evolved, so have the materials used to make these products. Insight into how structures fail when subjected to different loads and environmental conditions is instrumental to effectively use these new materials and in the development of even more advanced materials. In the past twenty years this insight has been used to develop advanced composites. These materials are a combination of two or more constituents and can be optimized for given loading conditions during the fabrication of the material. The ability to accurately predict the failure characteristics of these composites analytically is essential for expanded use of these materials in industry.

As the aerospace industry searches for ways to fly farther, faster, and more economically, use of high strength materials will undoubtedly be employed. Composites offer a wide variety of advantages including high fracture toughness, high strength-to-weight ratio, and low thermal expansion. The polyether-based thermoplastic composite material graphite

polyetherether-ketone (Gr/PEEK) promises many advantages over Gr/Ep: lower manufacturing costs, lower part weight, higher operating temperatures, improved maintainability, lower susceptibility to delamination, and higher fracture toughness than that of graphite epoxy (Gr/Ep) [7]. These characteristics make Gr/PEEK a very promising material for use in aerospace applications.

The ability to accurately predict the stress-strain response and failure characteristics of Gr/PEEK is essential before this material can be used in aerospace applications. Previous research has revealed significant nonlinearities in the relationship between stress and strain for Gr/PEEK [9,12]. This complicates the study of its failure characteristics significantly because assuming a linear relationship between stress and strain in no longer accurate. This thesis contributes to the current research on Gr/PEEK by using analytic results from a fully nonlinear finite element program (developed by Dr. Sandhu of the Flight Dynamics Lab at Wright-Patterson AFB) in conjunction with experimental data to investigate the initiation and progression of failure at 250 F.

A. Purpose.

As previously stated, the purpose of this thesis is to investigate the initiation and progression of failure in Gr/PEEK at 250 F. The geometry will consist of a circular discontinuity (hole) with a diameter to width (d/w) ratio of 1/3 subjected to tensile loading. The objectives of this

study are the following:

(1) To determine the basic material properties for
Gr/PEEK at 250 F for use in the nonlinear finite element
program.

(2) To determine the experimental stress-strain
response of $[0_{16}]$ and $[90_{16}]$ unidirectional laminates,
$[+45]_{4s}$ angle-ply laminates, and $[0,\pm45,90]_{2s}$ quasi isotropic
laminates of Gr/PEEK specimens containing a .4-inch (in) diameter
circular discontinuity (hole) and loaded to ultimate strength
at 250 F.

(3) To experimentally investigate the initiation and
progression of failure in similar specimens loaded to a
reduced percentage of average failure stress,

(4) To analytically model the failure process of the
unidirectional, angle ply, and quasi-isotropic laminates
using a fully nonlinear finite element program, and

(5) To compare and contrast these experimental and
analytic results.

This thesis contains all theories and procedures used
to accomplish these objectives along with the results and
conclusions.

B. Background and Overview.

A composite material can be considered as any material
made from two or more materials combined on a macroscopic
scale. This definition would normally include a wide range
of materials, some dating back to the dawn of civilization.
Although the origins of composite materials are unknown, all

1-3

recorded history contains some references to composite materials. For example, straw was used by the Israelites to strengthen mud bricks. Plywood was used by the Egyptians when they realized that wood could be rearranged to achieve superior strength and thermal characteristics. Medieval swords and armor were constructed using layers of different material. More recently, both reinforced concrete and fiberglass have provided engineers with materials that could be optimized to suit a particular application.

The common thread between these seemingly diverse materials is the ability to optimize a material for a specific application. This gives the engineer or designer a great deal of flexibility. A prime example of how a composite material can be used to optimize a design is the X-29 aircraft. The X-29 incorporates a forward-swept-wing, a design that induces a large adverse moment on the wing. Engineers used a Graphite/Epoxy (Gr/Ep) composite in a ply lay-up aeroelastically tailored to counter this moment. Since conventional materials cannot be tailored this way, this aircraft could not have been developed without the use of composite materials.

Materials such as Gr/Ep are known as advanced composites. These composites typically consist of continuous fibers embedded in a matrix. These fibers are usually graphite and can be either unidirectional or woven (see Figure 1-1). The fibers are supported in a matrix which can either be a plastic or a metal. This fiber/matrix

1-4

combination is called a lamina or ply and is usually about
.00525 inches thick. These plies are combined by stacking
and bonding one ply upon another until the desired thickness
is reached. The strength of any single ply in the direction
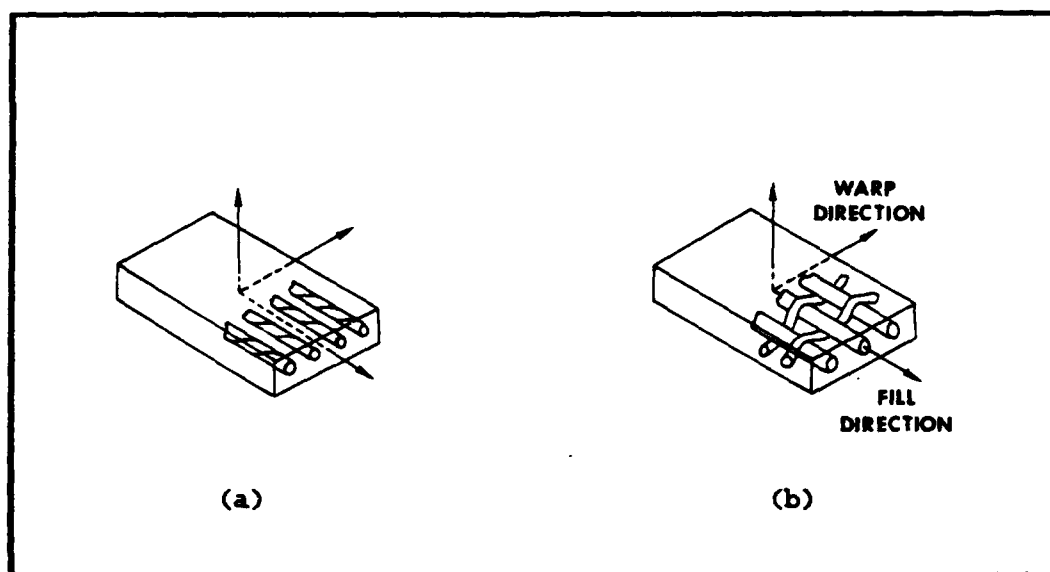
Figure 1-1. Fiber Format, (a) unidirectional, (b) woven

of the fibers is usually an order of magnitude higher than
transverse to the fibers. This characteristic is used to
optimize the material for an application by orienting the
fibers in the direction of the highest loads.

Gr/PEEK is very similar to Gr/Ep; the primary
difference is that the matrix is PEEK. The PEEK matrix in
Gr/PEEK provides the improvements in material
characteristics over Gr/Ep mentioned earlier.
Unfortunately, the matrix is also the constituent that

causes the nonlinear stress-strain response. Another
complexity that can be introduced as a result of the PEEK
matrix is viscoelasticity. Viscoelastic affects can become
important for any material that demonstrates a time
dependency to the stress strain relations [25]. The
techniques used to account for these phenomena in this
thesis are discussed in Chapter II.

In the design of structural components, one geometric
feature that almost always has to be accounted for is a
hole. Holes exist in structural components for a variety of
reasons: to accommodate bolts or rivets in a joint, as
through holes for wires or hydraulic lines, or even as a
result of being punctured by projectiles such as bullets.
Relatively simple techniques exist to accurately predict the
stress concentration at a hole for conventional isotropic
materials [11]. Unfortunately, these techniques are not
accurate for orthotropic materials. The stresses for these
materials cannot be evenly distributed around the hole and
discontinuous fibers cause effects which lead to design
difficulties [8].

A number of parameters must be considered to accurately
predict the strength of a composite containing a hole.
These parameters include:

(1) The infinite number of possible ply lay-ups, or
stacking sequences.

(2) The variety of fibers, matrices, and fiber/matrix
combinations available.

1-6

(3)   The infinite number of geometries (thicknesses, hole size, width-to-hole size).

(4)   The effect of environmental conditions on composites.

There are a number of techniques available for predicting strength reduction or ultimate strength in a composite. In general, the techniques include fracture mechanics approaches [1,8,23,24,26] and finite element methods [16,17,20,21].

Reference [1] includes a review of several fracture models for predicting the strength of a composite laminate containing a hole. These models require the use of semi-empirical techniques which are relatively simple to employ. The problem with these models is pointed out in Reference [18]:

> With the development of accurate non-destructive evaluation methods, it became apparent that the damage zone corrections (of fracture models) were arbitrary and subject to question [18].

Consequently, until better models are developed and assessed, the use of these models in general applications is of dubious value.

Even given a model that can accurately predict the behavior of a laminate containing a hole, the problem of determining failure still exists. At least 30 failure theories exist in the composite industry (as of late 1986). Another 12 theories exist to predict post-failure behavior

of composites [16]. Some of these theories can only be applied to special cases, some are only special cases of the maximum stress theory, and some are based on assumptions that are not always true for composites. Obviously, a great deal of consideration must be taken when selecting a failure theory for a specific application.

For theories such as Sandhu's strain energy failure criterion [16,17], theory-experiment correlation coefficients are included which make calculated and test results agree closely. Although these coefficients must be determined for each material (and environmental state), the coefficients can be applied to any geometry of interest. This is a vast improvement over those techniques that are inherently application sensitive.

There are several advantages to using a finite element program to predict the response of a composite: the nonlinear stress-strain response can be accounted for, the actual damage accumulation process can be modeled [8], and realistic ply failure schemes can be employed. Additionally, finite element techniques offer the advantage of being generally applicable to a wide range of geometries. The composite strength analysis proposed by Sandhu differs from the more conventional formulations in the following respects [14]:

(1) The nonlinear lamina stress-strain responses to failure are represented analytically by using a cubic-spline interpolation function on tabularized basic property data. The tangent moduli of these functions are employed to evaluate

lamina and laminate stiffness and compliance during load
increments.

   (2) Ply degradation is based on an energy to failure
criterion. This criterion is applied incrementally to
predict the failure of an element.

   (3) Equivalent strain increments are defined. (See
Section II C).

Previous works have described this technique in detail
[16,17] while others have used this technique for predicting
behavior in Gr/Ep [4,16,20,21,22] and Gr/PEEK [9]. Where the
work in Reference [9] was accomplished at room temperature,
this thesis is directed toward evaluating specimens at 250 F.
The results from the room temperature study indicate
that Sandhu's technique accurately predicts the failure of
both uniaxial specimens ([0_{16}] and [90_{16}]) and shear
specimens ([$\pm45]_{42}$) containing holes.

   Sandhu's technique uses a functional form of
stress-strain curves derived from experimental data. Basic
property tests are conducted (in this case at 250 F) to
obtain stress-strain curves. Tabular data derived from the
experimental curves are then provided to the program. The
program then fits a cubic spline interpolation function to
the tabular data. These cubic spline functions yield smooth
composite stress-strain curves from which the computer
program can determine accurate moduli of elasticity over the
entire range of the curves [17].

   The modulii determined by the program are used in

conjunction with an incremental constitutive relationship to

describe the stress-strain response of Gr/PEEK. The model is

subjected to incremental loading using a plywise application

of Sandhu's failure criterion using strain energy under

longitudinal, transverse, and shear loading as independent

parameters to determine the ultimate load carrying capacity

of the laminate [16,17]. The theory used to develop this

incremental approach is described in detail in Chapter II and

the actual procedures used to employ the approach are in

Chapter III.

The three types of testing conducted were basic property

tests, ultimate load tests, and percentage of ultimate load

tests. Basic property tests were conducted on specimens

without holes to determine the stress-strain relationships of

Gr/PEEK at 250 F. Ultimate load tests were conducted to

determine the ultimate strength of specimens containing a

hole. Finally, the percentage of ultimate load tests yielded

partially failed specimens containing a hole for further

examination. The test fixtures and procedures used to

conduct these tests are described in Chapter IV.

The specimens studied in this thesis were of fixed

geometry with a variety of ply lay-ups. All specimens were

1.2" wide with a .4" diameter hole at their centers

representing a finite-width plate containing a stress

concentrator. The ply lay-ups studied through both analysis

and experimentation were $[0_{16}]$ and $[90_{16}]$ unidirectional,

$[\pm 45]_{4s}$ angle-ply, and $[0/\pm 45/90]_{2s}$ quasi-isotropic. All

specimens were tested in tension at 250 F.

Several methods were employed to examine the failure of the specimens. The partially failed specimens were examined using stereo x-rays. Also, all of the specimen failures were videotaped with either a regular speed or a high speed video camera. The high speed video camera was used for ply lay-ups where the actual failure was too fast for a regular video to capture. These videos along with still shots from the videos provided insight into the progression of failure in these laminates.

II. Theory

The purpose of this chapter is to discuss the applicable theory used to accomplish this thesis: mechanics of composite materials, linear finite element theory, nonlinear finite element theory, failure criterion, and viscoelasticity. The mechanics of composite materials is normally divided into micromechanical and macromechanical considerations. Because this thesis is directed toward the macromechanical or gross properties of the laminate, micromechanical behavior is only discussed as it applies to the macromechanical properties. A short overview of linear finite element theory is included primarily as a basis for discussing the nonlinear finite element theory incorporated into a computer program. A failure criterion developed by Sandhu [16] for use with nonlinear materials is discussed in conjunction with the progressive-ply-failure technique used in the nonlinear finite element program to predict ply failure. Finally, a short discussion on viscoelasticity and how it applies to this thesis is included along with a summary.

A. **Mechanics of Composite Materials**.

This section provides a discussion of the mechanics of composite materials as they apply to this thesis. The topics included are the macromechanical behavior of a lamina, the macromechanical behavior of a laminate, and the strength of the laminate.

(1) **Macromechanical Behavior of a Lamina**. In describing the behavior of a single lamina, the

macromechanical approach is restricted to linear elastic
behavior. This approach is appropriate in this thesis
because the nonlinear behavior is modeled as increments of
linear behavior. This incremental approach is discussed in
detail in the nonlinear finite element section.

The equation that relates stresses to strains in linear
elastic theory (Hooke's Law written in contracted notation)
is:

$$\sigma_i = C_{ij}\, \varepsilon_j \qquad i,j = 1,2,\ldots,6 \qquad (1)$$

or

$$\varepsilon_i = S_{ij}\, \sigma_j \qquad i,j = 1,2,\ldots,6 \qquad (2)$$

where σ_i are the stress components, C_{ij} is the stiffness
matrix, ε_j are the strain components, and S_{ij} is the
compliance matrix, which is the inverse of C_{ij} [3]. Both C_{ij}
and S_{ij} are referred to as the elastic constants (keeping in
mind the incremental approach used to account for the
nonlinear behavior). Any individual ply (not containing woven
fibers) can be considered as an orthotropic material (that
is, there are three mutually orthogonal planes of material
property symmetry). For the lamina in which the fibers are
aligned with the coordinate axis, Eq (2) reduces to the
following

$$\begin{Bmatrix} \varepsilon_1 \\ \varepsilon_2 \\ \varepsilon_3 \\ \gamma_{23} \\ \gamma_{13} \\ \gamma_{12} \end{Bmatrix} = \begin{bmatrix} S_{11} & S_{12} & S_{13} & 0 & 0 & 0 \\ S_{12} & S_{22} & S_{23} & 0 & 0 & 0 \\ S_{13} & S_{23} & S_{33} & 0 & 0 & 0 \\ 0 & 0 & 0 & S_{44} & 0 & 0 \\ 0 & 0 & 0 & 0 & S_{55} & 0 \\ 0 & 0 & 0 & 0 & 0 & S_{66} \end{bmatrix} \begin{Bmatrix} \sigma_1 \\ \sigma_2 \\ \sigma_3 \\ \tau_{23} \\ \tau_{13} \\ \tau_{12} \end{Bmatrix} \qquad (3)$$

6x1   6x6   6x1

where $\gamma_{ij} = 2\,\varepsilon_{ij}$. The terms γ_{ij} are the engineering shear strain, whereas ε_{ij} are the tensorial shear strain.

The specimens in this study are thin plates so a state of plane stress is assumed. For a lamina in the 1-2 plane (as depicted in Figure 2-1), a state of plane stress is defined by setting

$$\sigma_3 = 0, \ \tau_{23} = 0, \ \tau_{13} = 0 \qquad (4)$$

from Eq (3). Applying the plane stress assumption, Eq (3) reduces to:

$$\begin{Bmatrix} \varepsilon_1 \\ \varepsilon_2 \\ \gamma_{12} \end{Bmatrix} = \begin{bmatrix} S_{11} & S_{12} & 0 \\ S_{12} & S_{22} & 0 \\ 0 & 0 & S_{66} \end{bmatrix} \begin{Bmatrix} \sigma_1 \\ \sigma_2 \\ \tau_{12} \end{Bmatrix} \qquad (5)$$

3x1   3x3   3x1

where the elastic constants are:

(

$$S_{11} = \frac{1}{E_{11}} \qquad\qquad S_{22} = \frac{1}{E_{22}}$$

$$S_{12} = S_{21} = -\frac{\nu_{12}}{E_{11}} = -\frac{\nu_{21}}{E_{11}}$$

$$S_{66} = \frac{1}{G_{12}} \tag{6}$$

The stress-strain relations in Eq (5) are inverted to obtain the following:

$$
\left\{ \begin{array}{c} \sigma_1 \\ \sigma_2 \\ \tau_{12} \end{array} \right\} = \left[\begin{array}{ccc} Q_{11} & Q_{12} & 0 \\ Q_{12} & Q_{22} & 0 \\ 0 & 0 & Q_{66} \end{array} \right] \left\{ \begin{array}{c} \varepsilon_1 \\ \varepsilon_2 \\ \gamma_{12} \end{array} \right\} \tag{7}
$$

3x1   3x3   3x1

(Note: m x n is the order of the matrix)

where the Q_{ij}, called the reduced stiffness terms, are defined as:

$$Q_{11} = \frac{E_1}{1 - \nu_{12}\nu_{21}} \qquad\qquad Q_{22} = \frac{E_2}{1 - \nu_{12}\nu_{21}}$$

$$Q_{12} = Q_{21} = \frac{\nu_{21}E_1}{1 - \nu_{12}\nu_{21}} \qquad\qquad Q_{66} = G_{12}$$

$$Q_{16} = Q_{26} = Q_{61} = Q_{62} = 0 \qquad (8)$$

For the lamina in which the fibers are not aligned with the coordinate axis, Eq (7) must be transformed from the principal material axis to the coordinate axis. The principal material axis is coincident with the fiber direction, as depicted in Figure 2-1.
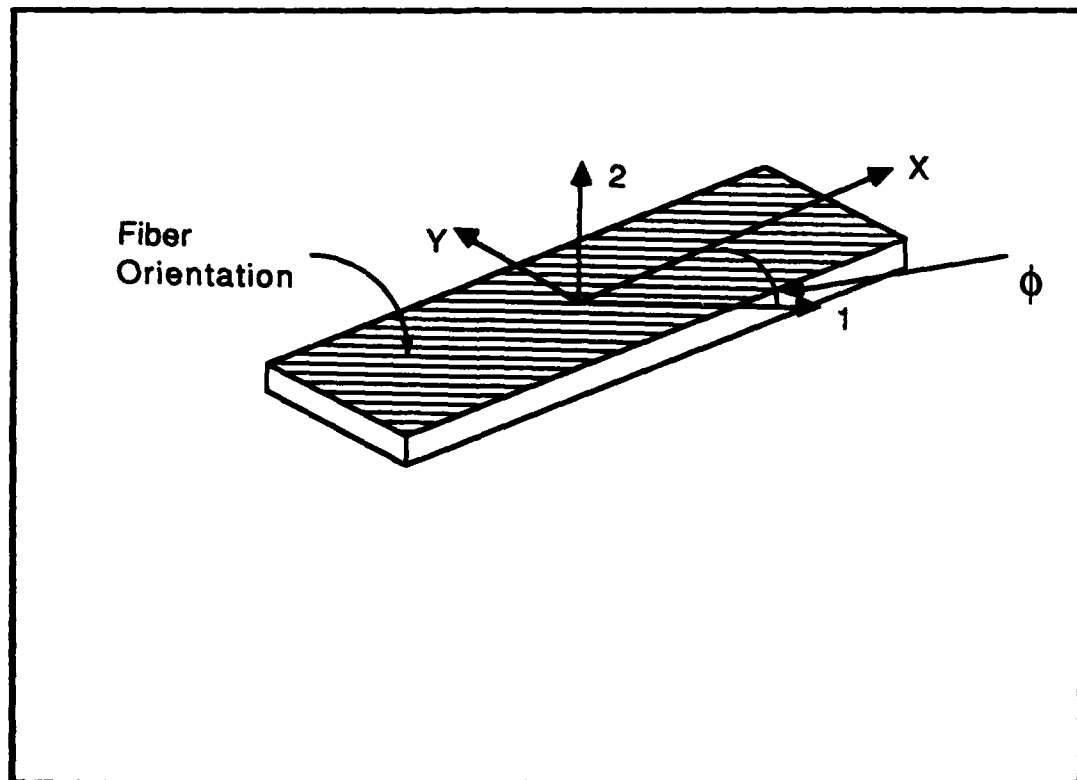
Figure 2-1. Principal Material Axis

Incorporating the transformations, Eq (7) is written as:

$$\left\{ \begin{array}{c} \sigma_x \\ \sigma_y \\ \tau_{xy} \end{array} \right\} = \left[\begin{array}{ccc} \bar{Q}_{11} & \bar{Q}_{12} & \bar{Q}_{16} \\ \bar{Q}_{12} & \bar{Q}_{22} & \bar{Q}_{26} \\ \bar{Q}_{16} & \bar{Q}_{26} & \bar{Q}_{66} \end{array} \right] \left\{ \begin{array}{c} \varepsilon_x \\ \varepsilon_y \\ \gamma_{xy} \end{array} \right\} \qquad (9)$$

3×1   3×3   3×1

where the $\bar{Q}_{ij}$ are the transformed reduced stiffness terms. The values of $\bar{Q}_{ij}$ are given as [3]:

$$\bar{Q}_{11} = Q_{11}m^4 + 2 (Q_{12} + 2Q_{66}) n^2m^2 + Q_{22}n^4$$

$$\bar{Q}_{12} = (Q_{11} + Q_{22} - 4Q_{66}) n^2m^2 + Q_{12}(n^4 + m^4) \qquad (10)$$

$$\bar{Q}_{22} = Q_{11}n^4 + 2(Q_{12} + 2Q_{66}) n^2m^2 + Q_{22}m^4$$

$$\bar{Q}_{16} = (Q_{11} - Q_{12} - 2Q_{66}) nm^3 + (Q_{12} - Q_{22} + 2Q_{66}) n^3m$$

$$\bar{Q}_{26} = (Q_{11} - Q_{12} - 2Q_{66}) n^3m + (Q_{12} - Q_{22} + 2Q_{66}) nm^3$$

$$\bar{Q}_{66} = (Q_{11} + Q_{22} - 2Q_{12} - 2Q_{66}) n^2m^2 + Q_{66}(n^4 + m^4)$$

where m is the cosine and n is the sine of the angle between the material and coordinate axis.

(2) <u>Macromechanical Behavior of Laminates</u>. The macromechanical behavior of a composite laminate is based on the summation of the individual lamina. The stress-strain relationship in Eq (9) is generalized for each ply as follows:

$$\left\{ \begin{array}{c} \sigma_x \\ \sigma_y \\ \tau_{xy} \end{array} \right\}_k = \left[\begin{array}{ccc} \bar{Q}_{11} & \bar{Q}_{12} & \bar{Q}_{16} \\ \bar{Q}_{12} & \bar{Q}_{22} & \bar{Q}_{26} \\ \bar{Q}_{16} & \bar{Q}_{26} & \bar{Q}_{66} \end{array} \right] \left\{ \begin{array}{c} \varepsilon_x \\ \varepsilon_y \\ \gamma_{xy} \end{array} \right\}_k \qquad (11)$$

3×1   3×3   3×1

where k is the kth ply. This procedure is conceptually easy but since the plies can not deform independently, Eq (11) has to be satisfied simultaneously for each ply. Also, since plies of different orientation deform with respect to its particular material axis, out of plane (interlaminar) stresses develop between layers. These stresses can substantially reduce the predicted strength of a laminate and must be considered when comparing analytic and experimental results.

The requirement to satisfy Eq (11) simultaneously for each ply is accomplished by forming an equivalent stiffness matrix using simple lamination theory. For this thesis, the equivalent stiffness matrix is formed in the finite element program. Finite element theory and the technique used to form the equivalent stiffness matrix is discussed in Section II B.

Interlaminar stresses for a typical plate are depicted in Figure 2-2 for τ_{xy} and τ_{xz}. Determining these interlaminar stresses and their effect on overall strength is not an easy task. The most predominant effect of interlaminar stresses is delamination along the edges. Sandhu [15,18] describes the tendency for a composite to delaminate through the use of a "delamination moment coefficient" (DMC), which is based on stacking sequence. The DMC for Gr/Ep specimens with geometry identical to those in this thesis approach the critical value for a $[0/\pm45/90]_{2s}$ laminate in tension. The conclusions reached in

Reference [9] indicate that Gr/PEEK is a much tougher
material than Gr/Ep and less likely to delaminate.
These conclusions were based on the close correlation between
experimental and analytic results without considering
delamination. Even though at higher temperatures a composite
could be more susceptible to delamination, we are assuming the
effects of delamination are minimal for this thesis.
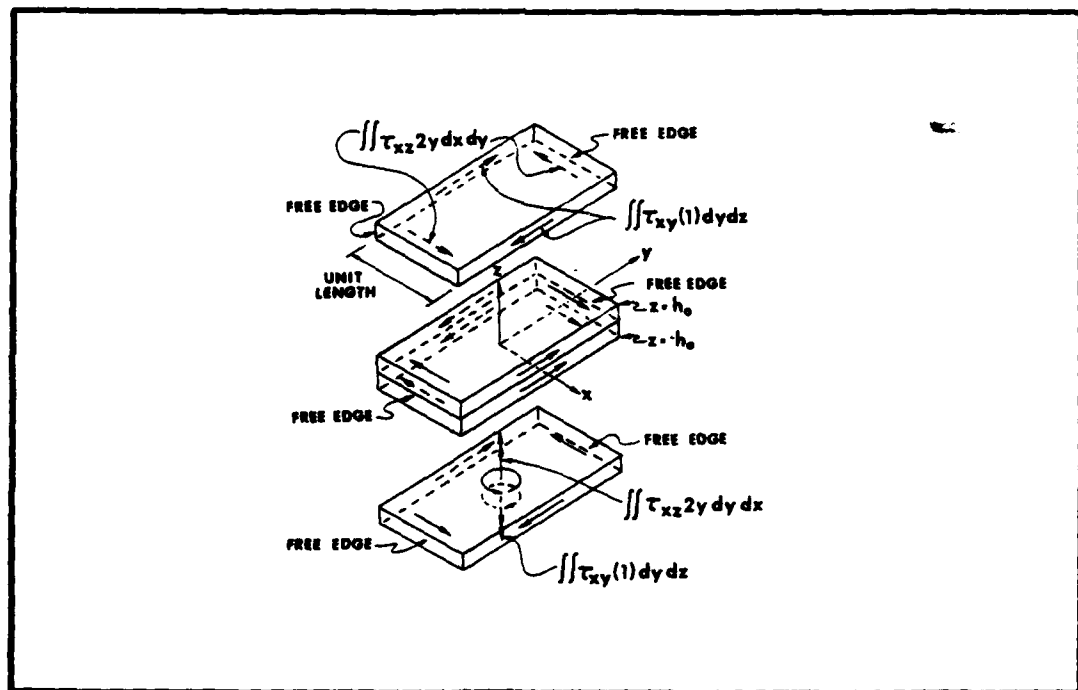
Figure 2-2. Interlaminar Stresses

(3) <u>Strength of Composite Laminates</u>. The strength of a
composite laminate is dependent on the strength of the
individual lamina. A variety of techniques exist for
predicting laminate strength, most of which are based on a

microscopic analysis of each lamina as it relates to the laminate. These techniques are discussed in detail in Reference [8]. These techniques are conceptually straight forward but are extremely tedious unless accomplished using a computer program. The method used for this thesis (developed by Sandhu [16,17]) is similar in both theory and application to these other techniques, but also accounts for nonlinearities. Because Sandhu's method directly relates to the nonlinear material behavior, the discussion on the application of his strength theory follows the discussion of his nonlinear finite element technique.

B. Linear Finite Element Theory.

The finite element method is a numerical method for solving problems in continuum mechanics. This discussion will be limited to solid mechanic applications. Two finite element programs were used for this thesis: a linear program used for model selection and a nonlinear program for the analysis. Both of these programs can be used to predict the strength of a composite laminate. The theory used to develop the linear program is discussed in this section. Included is a description of how the individual plies are accounted for in the stiffness matrix. The theory used to develop the nonlinear program is discussed in the subsequent section.

This finite element program uses constant strain triangle elements based on the assumed displacement field [2] (in cartesian coordinates)

2-9

$$u(x,y) = \alpha_1 + \alpha_2 x + \alpha_3 y$$

$$v(x,y) = \beta_1 + \beta_2 x + \beta_3 y \qquad (12)$$

Written in matrix form, Eq (12) becomes

$$\left\{ \begin{array}{c} u(x,y) \\ v(x,y) \end{array} \right\} = [H]_{2\times6} \left\{ \begin{array}{c} u_1 \\ u_2 \\ u_3 \\ v_1 \\ v_2 \\ v_3 \end{array} \right\}_{6\times1} \qquad (13)$$

where H is given by:

$$[H] = \begin{bmatrix} 1 & x & y & 0 & 0 & 0 \\ 0 & 0 & 0 & 1 & x & y \end{bmatrix}_{2\times6} [A]^{-1}_{6\times6} \qquad (14)$$

$[A]^{-1}$ is given by:

$$[A]^{-1} = \begin{bmatrix} A_1^{-1} & 0 \\ 0 & A_1^{-1} \end{bmatrix}_{6\times6} \qquad (15)$$

and:

$$[A_1] = \begin{bmatrix} 1 & x_1 & y_1 \\ 1 & x_2 & y_2 \\ 1 & x_3 & y_3 \end{bmatrix}_{3\times3} \qquad (16)$$

2-10

To evaluate the strains for this element, we differentiate
the displacements to obtain the following linear strain
relationships for small strain:

$$\varepsilon_{xx} = \frac{\partial u}{\partial x} \qquad \varepsilon_{yy} = \frac{\partial v}{\partial y} \qquad \gamma_{xy} = \frac{\partial u}{\partial y} + \frac{\partial v}{\partial x} \qquad (17)$$

Using the assumed displacement field, these strains
can be written in matrix form as follows:

$$\left\{ \begin{array}{c} \varepsilon_x \\ \varepsilon_y \\ \gamma_{xy} \end{array} \right\}_{3 \times 1} = [B]_{3 \times 6} \left\{ \begin{array}{c} u_1 \\ u_2 \\ u_3 \\ v_1 \\ v_2 \\ v_3 \end{array} \right\}_{6 \times 1} \qquad (18)$$

where

$$[B] = \begin{bmatrix} 0 & 1 & 0 & 0 & 0 & 0 \\ 0 & 0 & 0 & 0 & 0 & 1 \\ 0 & 0 & 1 & 0 & 1 & 0 \end{bmatrix}_{3 \times 6} [A]^{-1}_{6 \times 6} \qquad (19)$$

The stiffness equation can now be formed using [B] and [E] (a
matrix of material stiffnesses) with the equation:

$$[K] = \int [B]^T [E] [B] \, dx \, dy = [B]^T [E] [B] \, tA \qquad (20)$$

where t is the element thickness, A is the area, and [E] is given for an isotropic material (assuming plane stress conditions) by [5]:

$$[E] = \frac{E}{1 - \nu^2} \begin{bmatrix} 1 & \nu & 0 \\ \nu & 1 & 0 \\ 0 & 0 & \frac{1-\nu}{2} \end{bmatrix}_{3 \times 3}$$

where E and ν are the elastic coefficients for Young's modulus and Poisson's ratio, respectively.

These constant strain triangles are used to create quadrilateral elements as depicted in Figure 2-3. The resulting stiffness matrix from this combination of elements is a 10 X 10, however, two of the rows and columns are based on the internal node 0 at the centroid and which result in reductions of the stiffness matrix. These quadrilateral elements can be manipulated into triangular and bar elements by co-locating nodes, as shown in Figure 2-4.

2-12
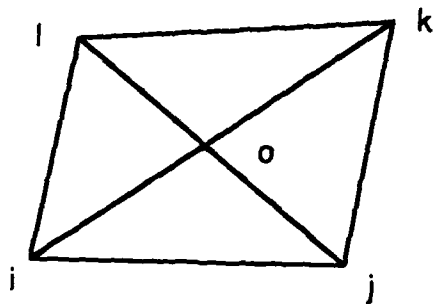
Note: o is the centroid of the element

Figure 2-3. Rectangular Element Made From Constant

Strain Triangles
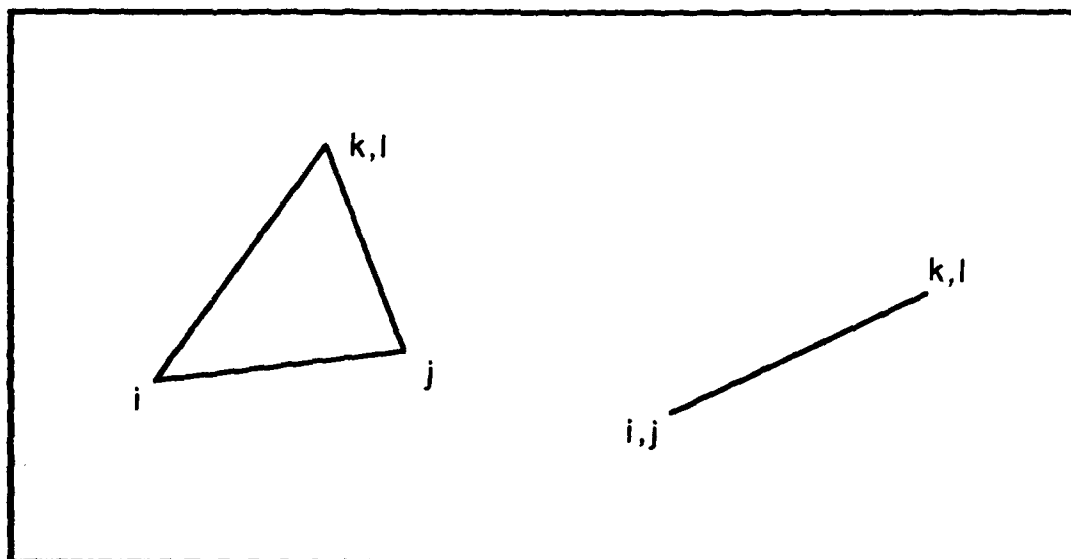
Figure 2-4. Triangular and Bar Elements

For an orthotropic material such as an individual lamina, the orientation must be considered when forming the stiffness matrix. Eq (9) is repeated here for convenience:

$$\begin{Bmatrix} \sigma_x \\ \sigma_y \\ \tau_{xy} \end{Bmatrix}_{3\times1} = \begin{bmatrix} \bar{Q}_{11} & \bar{Q}_{12} & \bar{Q}_1 \\ \bar{Q}_{12} & \bar{Q}_{22} & \bar{Q}_2 \\ \bar{Q}_{16} & \bar{Q}_{26} & \bar{Q}_6 \end{bmatrix}_{3\times3} \begin{Bmatrix} \epsilon_x \\ \epsilon_y \\ \gamma_{xy} \end{Bmatrix}_{3\times1} \tag{9}$$

The $\bar{Q}_{ij}$ in this equation is analogous to E in the elasticity stress-strain relationship and, consequently, to E in Eq (20). Substituting $[\bar{Q}]$ for $[E]$ in Eq (20) we obtain:

$$[K] = \int [B]^T [\bar{Q}] [B] dx\ dy = [B]^T [\bar{Q}] [B] t A \tag{21}$$

In order to account for a material consisting of more than one ply orientation, an equivalent stiffness matrix is formed. The assumption is made simple lamination theory applies (that is, that displacements through the thickness are the same). Additionally, the ply lay up is assumed symmetric at the mid plane of the model. The equivalent stiffness matrix is simply a summation of the ply stiffness matrices

$$[K_{eq}] = A \sum_{i=1}^{n} [B]^T [\bar{Q}]_i [B] t_i \tag{22}$$

2-14

where i is the ith lamina, n is the total number of plies, $[Q]_i$ is the stiffness of the ith ply, and t_i is the thickness of the ith ply.

Note that even though multiple layers have been allowed through the thickness of the element, the layers have common nodes. Due to the assumptions made in simple lamination theory, strain or displacement gradients through the thickness or stacked elements are constant. Therefore, the behavior of an element is dependent on the particular material properties of the ply and the state of stress of the element.

Finally, the displacements are related to the loads in a relationship similar to a spring-mass system. The force-displacement relationship written in matrix form is:

$$[K_{eq}]\{u\} = \{f\} \tag{23}$$

where u are the displacements and f are the loads. This equation relates the forces to displacements on an element basis.

C. Nonlinear Finite Element Theory

As mentioned previously, Gr/PEEK has material properties which are too nonlinear to neglect. The numerical analysis of these specimens was accomplished using a fully

nonlinear finite element program developed by Sandhu [16] to
account for material nonlinearities. These material
nonlinearities are the nonlinear elastic properties and do
not include the effects of plasticity. The nonlinear finite
element program (called PLSTREN) was developed by Sandhu to
predict the following:

(1) the damage initiation and accumulation process in
composite laminates and

(2) the static strength of composite laminates
containing. The program contains several modular sections
providing for the use of a variety of finite elements, ply
failure criteria, and post-ply-failure unloading schemes. A
complete development of Sandhu's technique is in References
16 and 17. This section describes the theory used to develop
the part of the program that models material nonlinearities
and is divided into three subsections:

(1) a discussion as to exactly how the material
nonlinearities are accounted for,

(2) a short discussion as to how imposed biaxial stress
states are related to the experimental data obtained by
testing specimens under simple load conditions, and

(3) an outline on how these two techniques are used in
the overall program.

Material Nonlinearities. To account for the material
nonlinearities, the response of the laminate under general
states of stress is modeled using an incremental form of the
constitutive law of Eq (1). The three assumptions used to

formulate this incremental constitutive relationship are as follows:

(1) The increment of strain depends on the strain state and the increment of stress,

(2) The increment of strain is proportional to the increment of stress, and

(3) The principles of linear elasticity in each increment are applicable. Using these assumptions, the incremental law for orthotropic lamina under plane stress can be written as:

$$d\varepsilon_i = S_{ij}(\varepsilon_i)\, d\sigma_j \qquad\qquad i,j = 1,2,6 \qquad\qquad (24)$$

where:

$d\varepsilon_i$ = strain increment

S_{ij} = incremental compliance matrix (a function of the current strain state)

$d\sigma_j$ = stress increment

Assuming that the lamina remains orthotropic at all load levels, Eq (24) can be reduced to:

$$\begin{Bmatrix} d\varepsilon_1 \\ d\varepsilon_2 \\ d\varepsilon_{12} \end{Bmatrix} = \begin{bmatrix} S_{11} & S_{12} & 0 \\ S_{12} & S_{22} & 0 \\ 0 & 0 & S_{66} \end{bmatrix} \begin{Bmatrix} d\sigma_1 \\ d\sigma_2 \\ d\sigma_{12} \end{Bmatrix} \qquad (25)$$

$$\underset{3\times1}{} \qquad\qquad \underset{3\times3}{} \qquad\qquad \underset{3\times1}{}$$

for an orthotropic lamina. For clarity, in Eq (25)

2-17

$d\sigma_1$, $d\varepsilon_1$ = normal stress and strain increments in the fiber direction,

$d\sigma_2$, $d\varepsilon_2$ = normal stress and strain increments in the transverse direction,

$d\sigma_{12}$ = shear stress increment,

$d\varepsilon_{12}$ = shear strain increments,

Equation (24) can be inverted for the incremental version of Eq (25):

$$d\sigma_i = C_{ij}(\varepsilon_j) \, d\varepsilon_j \qquad\qquad i,j = 1,2,6 \qquad (26)$$

where C_{ij} is the inverse of S_{ij}.

For laminates that are made up of two or more lamina, Eq (26) is written as:

$$(d\sigma_i)_k = [C_{ij}(\varepsilon_j)]_k \, (d\varepsilon_j)_k \qquad\qquad (27)$$

where the subscript k denotes the kth ply for each term in the equation. Rewriting Eq (27) for the general case of multidirectional laminates as discussed in an earlier section, the incremental constitutive law becomes:

$$(d\sigma_i)_k = [\bar{Q}_{ij}]_k \, (d\varepsilon_j)_k \qquad\qquad (28)$$

where $[\bar{Q}]$ is given in Eq (10).

The incremental strains for each ply in a uniaxial laminate

can be solved for by applying the definitions for S_{ij} from Section II. Substituting for S_{ij} the incremental strains are:

$$d\varepsilon_1 = \frac{d\sigma_1 \ (1 - \nu_{12}\beta)}{E_{11}}$$

$$d\varepsilon_2 = \frac{d\sigma_2 \ (1 - \frac{\nu_{21}}{\beta})}{E_{22}}$$

$$d\varepsilon_6 = \frac{d\sigma_6}{G_{12}} \tag{29}$$

where

$$\beta = \frac{|d\sigma_2|}{|d\sigma_1|} \quad \text{(provided that } |d\sigma_1| \text{ and } |d\sigma_2| \text{ are} > 0)$$

The finite element equation, Eq (23), developed in the linear finite element theory section can also be written on an incremental basis:

$$d\{f\} = [k(\varepsilon)_{eq}] \ d\{u\} \tag{30}$$

where $d\{f\}$ and $d\{d\}$ are the increments of load and displacement and the stiffness matrix $[k(\varepsilon)_{eq}]$ is a function

of the current strain state. This strain dependence exists
because the stiffness matrix is a function of the matrix
[$\bar{Q}$] as shown in Eq (22) and repeated here for convenience:

$$[k_{eq}] = A \sum_{i=1}^{n} [B]^T [\bar{Q}]_i [B] \, t_i \qquad (22)$$

Since Gr/PEEK exhibits nonlinear behavior, the basic
engineering properties E^t, E^t, E^c, E^c, G_{12}, ν_{12}^t, ν_{12}^c will
vary with strain. Obviously [$\bar{Q}$] and therefore [k]$_{eq}$ will
also vary with strain.

For this thesis the incremental elastic constants in
[$\bar{Q}$] (or [S]) are determined using stress-strain curves
obtained experimentally with unidirectional laminates. The
laminates tested and the corresponding curves and material
properties are shown in Table 2-1. These tests are described
in detail in Chapter IV of this thesis.

In order to make the experimental curves usable by the
computer program, the data is entered in tabular form and is
represented analytically by using a piecewise cubic spline
interpolation functions [20]. The use of the spline function
renders stress-strain curves smooth, which are desirable for
determination of elastic moduli under incremental and
iterative computations [20]. These functions are then used to
calculate the tangent moduli of E_1, E_2, and G_{12} (as functions
of strain) by differentiating the appropriate cubic spline
function with respect to strain.

Table 2-1. Basic Property Tests, Curves, and
Corresponding Basic Properties

Test	Curve	Basic Property
0° Tension	σ_1^t vs ϵ_1	E_1^t
0° Compression	σ_1^c vs ϵ_1	E_1^c
90° Tension	σ_2^t vs ϵ_2	E_2^t
90° Compression	σ_2^c vs ϵ_2	E_2^c
$\pm\,45^\circ$ Tension	γ_{12} vs τ_{12}	G_{12}
0° Tension	$\dfrac{-\epsilon_2}{\epsilon_1}$ vs ϵ_1	ν_{12}^t
0° Compression	$\dfrac{-\epsilon_2}{\epsilon_1}$ vs ϵ_1	ν_{12}^c

As implied by Eq (30), the loads must also be applied
incrementally using this technique. Because $[k_{eq}]$ may vary
within a load increment, a "predictor-corrector and iterative
technique" is used in this program. At the first load
increment, $[k_{eq}]$ is calculated using material properties
which are equal to the initial slope of the basic property
curves. For subsequent increments, $[k_{eq}]$ is calculated using
material properties that correspond to the state of strain at
the end of the previous load increment. When each new load
increment is applied, an increment of displacement is

calculated using Eq (30). Since the displacement is calculated based on the previous strain state, Eq (30) will take on the form:

$$d\{f\}_{n+1} = [k(\varepsilon)_{eq}]_n \ d\{u\}_{n+1} \qquad (31)$$

where n denotes the nth load increment [4]. The new displacements are then used to calculate an increment of strain using:

$$d\{\varepsilon\} = [B] \ d\{u\} \qquad (32)$$

and an increment of stress using:

$$d\{\sigma\}_i = [\overline{Q}]_i \ d\{\varepsilon\} \qquad (33)$$

Given the current levels of stress and strain, new increments of stress and strain are calculated and added to the end of the current level to obtain a new level. A mean level of strain is then calculated by averaging the new level of strain with the previous level at the end of the increment. These mean strains are then used to determine a new set of material properties since they are readily available as functions of strain through the cubic spline functions [4].

Given the new elastic properties, $[\overline{Q}]$ and $[k_{eq}]$ are recalculated and the same load increment (not an additional

2-22

one) is again applied. The incremental displacements, strains, and stresses are recalculated using Eq (31) through Eq (33) never using their values previously computed. This procedure is repeated for a given load increment until the change of the strain increment converges to:

$$\frac{d\varepsilon_{n+1} - d\varepsilon_n}{d\varepsilon_n} < 0.001 \tag{34}$$

where n denotes the nth reapplication of a given load increment. Finally, when Eq (32) is satisfied, a new load increment is applied and the entire process is repeated.

Graphically, this procedure is shown in Figure 2-5. A one-dimensional case of shear loading is shown for clarity, but the program actually recalculates the elastic properties for all seven curves during a load increment. Stepping through the example, in (a) an initial strain exists due to a previous load increment. A new increment of load is applied and the resulting strain is calculated based on G_{12} at point 0. In (b), a new modulus is calculated corresponding to the average of γ_0 and γ_1 at point 1. In (c) the new modulus is applied to the initial strain, γ_0, and a new strain, γ_2, is calculated. This new strain is used to calculate a new modulus in (d) which is then applied to the initial strain in (e). This procedure is repeated until Eq (34) is satisfied. Frame (f) is an overview of the steps accomplished in (a) through (e).
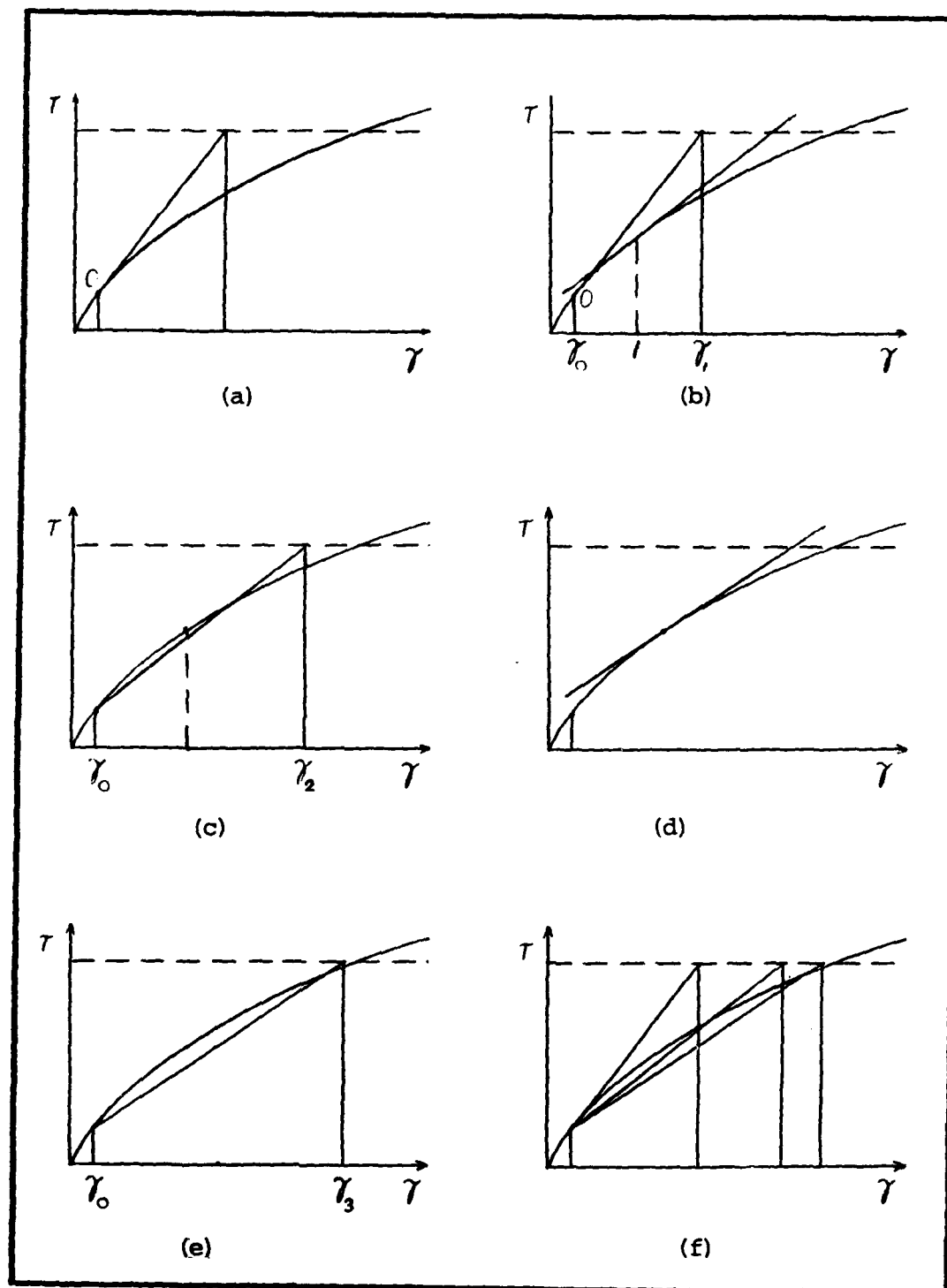
Figure 2-5.   Incremental Fitting of G_{12} Curve

<u>Biaxial Stress State</u>. The use of strain
components σ_1 and σ_2 to determine tangent moduli from basic
property curves generated experimentally under simple load
conditions is erroneous because typically plies are subject
to biaxial stresses. For example, ε_2 in Figure 2-6
under a biaxial stress state (σ_1, σ_2) corresponds to the
curve ON on the plane OEDC. The simple stress-strain curve
OM lies on the plane OEDC. Experimental data to correlate
these two stress states is currently not available so it is
assumed that, for each ply, simple equivalent strain
increments can be computed from the following expressions
[16].

$$d\varepsilon_1 \Big|_{eq} = \frac{d\sigma_1}{E_1} = \frac{d\varepsilon_1}{1 - \nu_{12} \dfrac{d\sigma_2}{d\sigma_1}}$$

$$d\varepsilon_2 \Big|_{eq} = \frac{d\sigma_2}{E_2} = \frac{d\varepsilon_2}{1 - \nu_{21} \dfrac{d\sigma_1}{d\sigma_2}} \qquad (35)$$

provided that $|d\sigma_1|$ and $|d\sigma_2| > 0$. Note that these equations
(for the equivalent incremental strain) differ from Eq 26 (for
the uncorrected incremental strain) by a factor of $\nu_{12}\beta$ for
$d\varepsilon_1$ and ν_{21}/β for $d\varepsilon_2$.

2-25
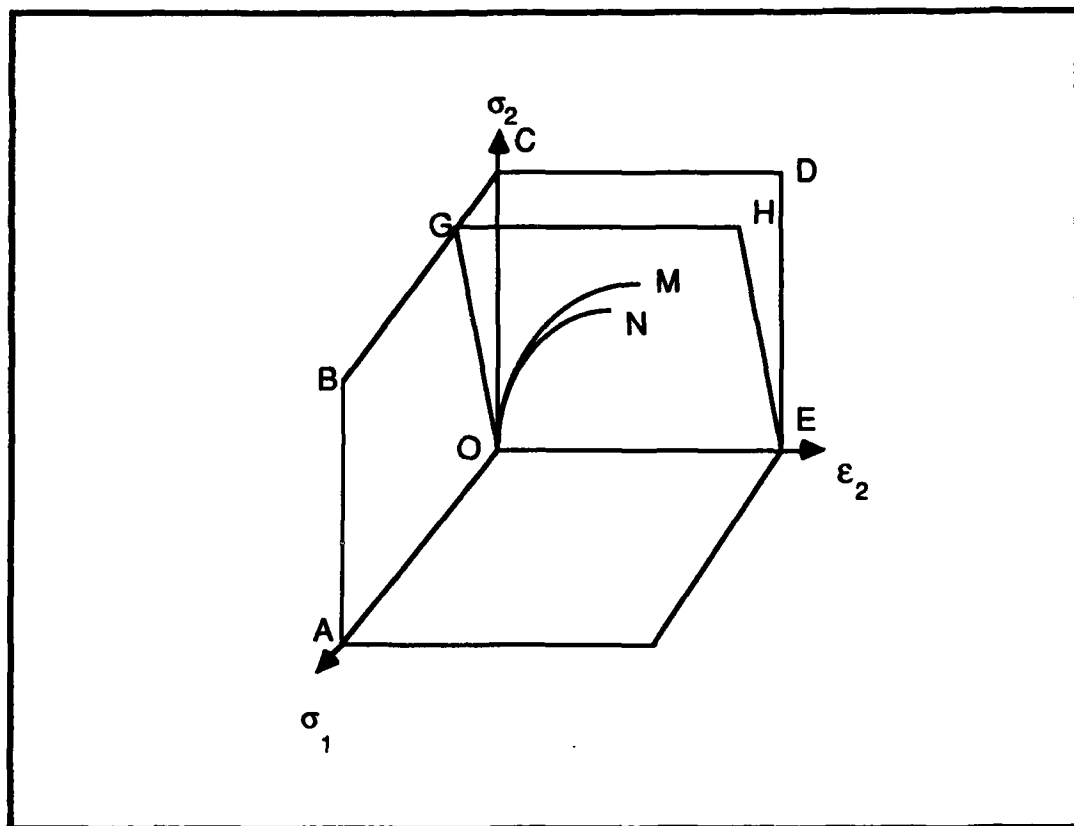
Figure 2-6. Biaxial Stress State

Outline of Nonlinear Finite Element Program. The
nonlinear finite element program uses the preceding
techniques to accomplish the following:

(1) Assuming that the stresses are uniformly
distributed through the thickness of each ply, stress
resultant increments, [dN], in the x, y coordinate system
are given by

$$[dN] = \sum_{k=1}^{p} [d\bar{\sigma}]_k \; t_k \tag{36}$$

where

$d\bar{\sigma}$ = the (transformed) stress increments in the x, y
coordinate system

t_k = thickness of the kth ply

p = number of plies in a laminate

Substituting the incremental constitutive law, Eq (33), into Eq (36), the stress resultants become:

$$[dN] = \sum_{k=1}^{P} [\bar{Q}]_k \ [du]_k \ t_k \qquad (37)$$

where [dN] are (transformed) stress resultant/force increments and du are incremental displacements in the x, y coordinate system.

(2) Since the stress resultant/force increments [dN] are the same for all plies in the laminate, Eq 37 can be rewritten:

$$[dN] = [K_{eq}] \ [du] \qquad (38)$$

where

(

2-27

$$[K_{eq}] = \sum_{k=1}^{p} [Q]_k \, t_k \tag{39}$$

Inversion of Eq (39) yields:

$$[du] = [K_{eq}]^{-1} [dN] \tag{40}$$

where $[K_{eq}]^{-1}$ represents the average compliance properties of the laminate during the (n+1)th load increment. The two techniques discussed previously are then employed to calculate the equivalent stress and strain increments. These increments are applied for the complete stress-strain response of the plies of the laminates [20]. Loads are applied as either forces or displacements at specific nodes. Forces and displacements are applied through the [dN] matrix. For example, if loads dN_1, dN_2, and dN_3 are specified the system of equations might look like

$$\begin{bmatrix} a_{11} & a_{12} & a_{13} \\ a_{12} & a_{22} & a_{23} \\ a_{13} & a_{23} & a_{33} \end{bmatrix} \begin{Bmatrix} du_1 \\ du_2 \\ du_3 \end{Bmatrix} = \begin{Bmatrix} dN_1 \\ dN_2 \\ dN_3 \end{Bmatrix}$$

where [a] is the stiffness matrix ($[K_{eq}]$ in Eq 40). If, however, du_2 is specified with dN_1 and dN_3 the system of equations become

$$\begin{bmatrix} a_{11} & 0 & a_{13} \\ 0 & a_{22} & 0 \\ a_{13} & 0 & a_{33} \end{bmatrix} \begin{Bmatrix} du_1 \\ du_2 \\ du_3 \end{Bmatrix} = \begin{Bmatrix} dN_1 - a_{12}d\varepsilon_2 \\ d\varepsilon_2 \\ dN_3 - a_{23}d\varepsilon_2 \end{Bmatrix}$$

An example of the output from this program is included at Appendix A in which a single element containing four plies is loaded to failure. A complete development of Sandhu's technique is in References 16 and 17.

D. Failure Criterion.

Numerically, the incremental loading procedure described in the preceding section cannot continue indefinitely. A failure criterion must be employed that would predict the failure of the individual plies and ultimately the entire laminate. The technique used to apply this failure criterion should account for the redistribution of stresses when any particular element fails. A variety of failure criterion have been proposed for the failure of anisotropic materials [18]. This section describes the criterion developed by Sandhu [16,17] which accounts for nonlinear material behavior.

The failure of an element is defined as the level of loads above which no additional loads can be sustained. Following the development in References [16] and [17], a scalar function, f, defining the failure condition of nonlinear materials can be written as:

$$f(\sigma, \varepsilon, K) = 1 \tag{41}$$

where σ and ε are the stress and strain states and K describes the material characteristics. One scalar function that depends on both the stress and strain states is the strain energy. For orthotropic materials, strain energies due to uniaxial tension and compression along and transverse to the material axes and shear are independent parameters. To measure the level of effect of both stress and strain states on the orthotropic materials under a combined stress state, a scalar function, which is a linear combination of functions of different strain energies, is used. It's form can be written as:

$$\sum_{i=1}^{3} \sum_{j=1}^{3} K_{ij} \left[\int_{\varepsilon} \sigma_{ij} \, d\varepsilon_{ij} \right]^{m_{ij}} = 1 \qquad (42)$$

where ε_{ij} are the current strain components and m_{ij} are the parameters defining the shape of the failure surface in the strain-energy space. The K_{ij} are the material characteristics. The failure criterion is based on the total strain energy, including the effect of hydrostatic loading. This inclusion is necessary to allow for the heterogeneous deviatoric stress field caused in fiber-reinforced composites by the hydrostatic loading [5].

Using contracted notation and assuming a plane stress condition, Eq 44 becomes:

$$K \left[\int_{\hat{\varepsilon}_i} \sigma_i \, d\varepsilon_i \right]^{m_i} = 1 \qquad i = 1,2,6 \qquad (43)$$

Using the results of tests under simple load conditions,

$$K \left[\int_{\varepsilon_{iu}} \sigma_i \, d\varepsilon_i \right]^{-m_i} = 1 \qquad i = 1,2,6 \qquad (44)$$

where ε_{iu} are the ultimate normal (tensile or compressive) and shear strains [17].

The shape of the failure surface (Eq 42) in the strain-energy space is determined by the shape factor m_i. For $m_1 = m_2 = m_6 = m = 2$, it is spherical and for m1=m2=m6=m=1, it is a pyramidal surface. This criterion in the stress space for three values of m_i (1/2,1,2) is compared with other failure theories in Figure 2-7 for a boron-epoxy material system. The comparison is confined to the first quadrant of the stress space. Since there is no reliable experimental data for boron-epoxy unidirectional laminas under biaxial stress states which could be used to determine suitable values of m, it is assumed to be unity. In this form, the three terms of Eq 43 are the ratios of current energy levels (due to longitudinal, transverse, and shear loading) to the maximum available energy levels. Therefore, when the sum of the three ratios equals unity, the lamina degrades completely.

2-31
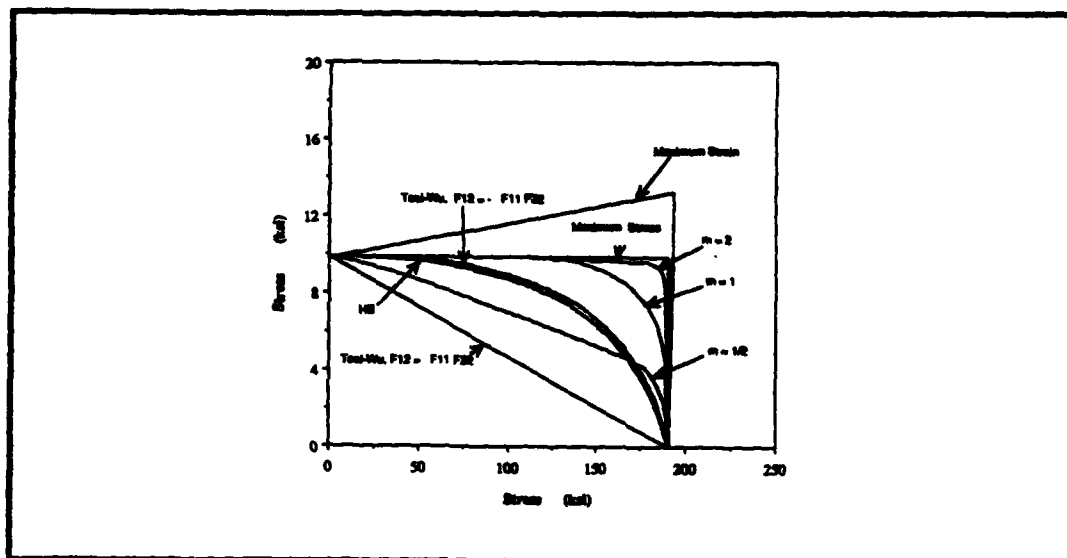
Figure 2-7. Comparison of Failure Theories

The three ratios at that time are contributions to degradation
made by longitudinal, transverse, and shear stress acting on
the lamina [17].

When considering a composite, two failure phenomena are
possible: matrix failure and fiber failure. Matrix failure
can occur in either tension, compression, or shear whereas;
fiber failure can only occur due to tension or compression.
Matrix failure can occur without necessarily precipitating
fiber failure. In this situation, the lamina is unloaded in
transverse tension and shear while continuing to carry loads
in the fiber direction. If the fiber failure mode occurs,
the lamina is assumed to be completely failed and is
completely unloaded. In both cases the applicable loads are
transferred to adjacent lamina. Unloading schemes used for

this program are described in subsequent paragraphs. The
occurrence of either matrix or fiber failure is determined by
using the strain energy failure criterion [20]. Fiber failure
is assumed to occur if both

$$\frac{K_1 \left[\int_{\varepsilon_1} \sigma_1 \, d\varepsilon_1 \right]}{\sum K_i \left[\int_{\varepsilon_i} \sigma_i \, d\varepsilon_i \right]} \geq 0.1 \tag{45}$$

and the criterion of Eq (43) is satisfied. Matrix failure
is assumed to occur when Eq (43) is satisfied and the
inequality, Eq (45), is not.

Finally, when failure occurs in one or more elements
the load must be redistributed to the surrounding elements.
The program PLSTREN uses two unloading schemes: a gradual
unloading scheme to model multidirectional laminates and a
rapid unloading scheme to model unidirectional laminates.

Gradual unloading of multidirectional laminates is
assumed because as elements of laminas fail, adjacent elements
are able to pick up the load previously sustained by the
failing element. Although this phenomenon is realistic it is
not easy to model numerically because the proportion of the
load retained by the failed lamina and the unloading rate are
both impossible to measure and difficult to even postulate.
This phenomena is complicated by the fact that at least some
of the load would reasonably be assumed by other plies through

2-33

interlaminar effects. For PLSTREN, the unloading is
accomplished by assigning negative values to the affected
moduli as determined by the failure mode. This unloading
scheme is depicted in Figure 2-8 for transverse tension. The
slope of the negative tangent modulus (the rate of unloading)
is the negative of the initial slope of the respective basic
property curve at the increment the element failed.
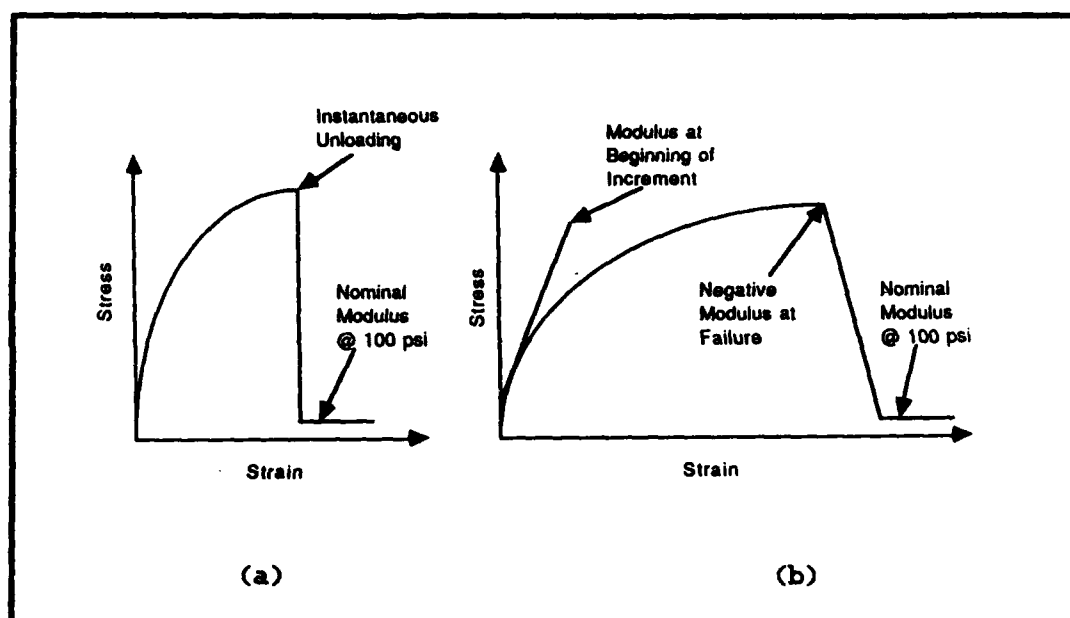
Figure 2-8. Unloading Schemes, (a) Unidirectional,
(b) Multidirectional

Rapid unloading for unidirectional laminates is
reasonable because failure occurs through the thickness and
is usually quite sudden. The affected moduli of a failed
element are set to nominally small values (100 psi) and the
same load increment is applied again. This reapplication of

2-34

the load increment can cause failure of additional elements. These failures are secondary in that they are caused by load redistribution without an increase in load. If secondary failures occur, the load increment is repeated until no further secondary failures occur before the next load increment is applied. Generally, this unloading scheme results in lower strength predictions than the gradual unloading scheme [20].

E. Viscoelasticity.

Materials that exhibit viscoelastic behavior complicate stress analysis because the stress-strain relation is time dependent. The normal elastic analysis of a conventional material is based on the stress-strain relationship

$$\{\sigma\} = [E]\{\epsilon\} \qquad (46)$$

where E is either a constant or dependent on the strain state as in this analysis. Nonlinear materials such as Gr/PEEK have to be evaluated incrementally because E is a function of strain. These relationships are based on the basic spring-mass equation for force-displacement which is independent of time. Consequently, to effectively model a viscoelastic material we have to go to the differential equation of motion and include the time dependent terms.

In general, Gr/PEEK can be shown to exhibit viscoelastic properties at elevated temperatures. Gr/PEEK

is also nonlinear and, in the ply layups investigated, orthotropic. Analytic prediction of the stress- strain relation of a viscoelastic, nonlinear, orthotropic material is well beyond the scope of this thesis. The nonlinear and orthotropic characteristics of this material cannot be suppressed. The variation in response from one specimen to another due to the viscoelastic characteristic can be reduced by using consistent strain rates when testing the specimens. Viscoelastic characteristics may still exist because this does not guarantee that the material will deform at consistent rates from one specimen to another. This effect, and consequently the viscoelastic effects, are assumed to be minimal.

F. Summary. As a summary of the development presented for the program PLSTREN, a diagram of Sandhu's program is shown in Figure 9. PLSTREN is configured for either linear or nonlinear analysis but only the nonlinear analysis is depicted in Figure 2-9 for clarity. Appendix A contains a sample PLSTREN data file for one of the models in this thesis. Additionally, Appendix A contains a copy of the output printout from PLSTREN for a single element containing four cross-ply laminas. The displacements, stresses, and strains are all suppressed in this output leaving only the energy levels of the elements for each iteration. The element is loaded incrementally through failure of the 90 degree plies, redistribution of the load to the 0 degree plies, to ultimate failure of the entire element. Hopefully, this will provide a

2-36

valuable visualization as to how PLSTREN works.

The material presented in this chapter consists
of the theory behind both the analytic and experimental
investigations of this thesis. The procedures used in both
the analytic and experimental phases along with the results
and discussion are presented in subsequent chapters.
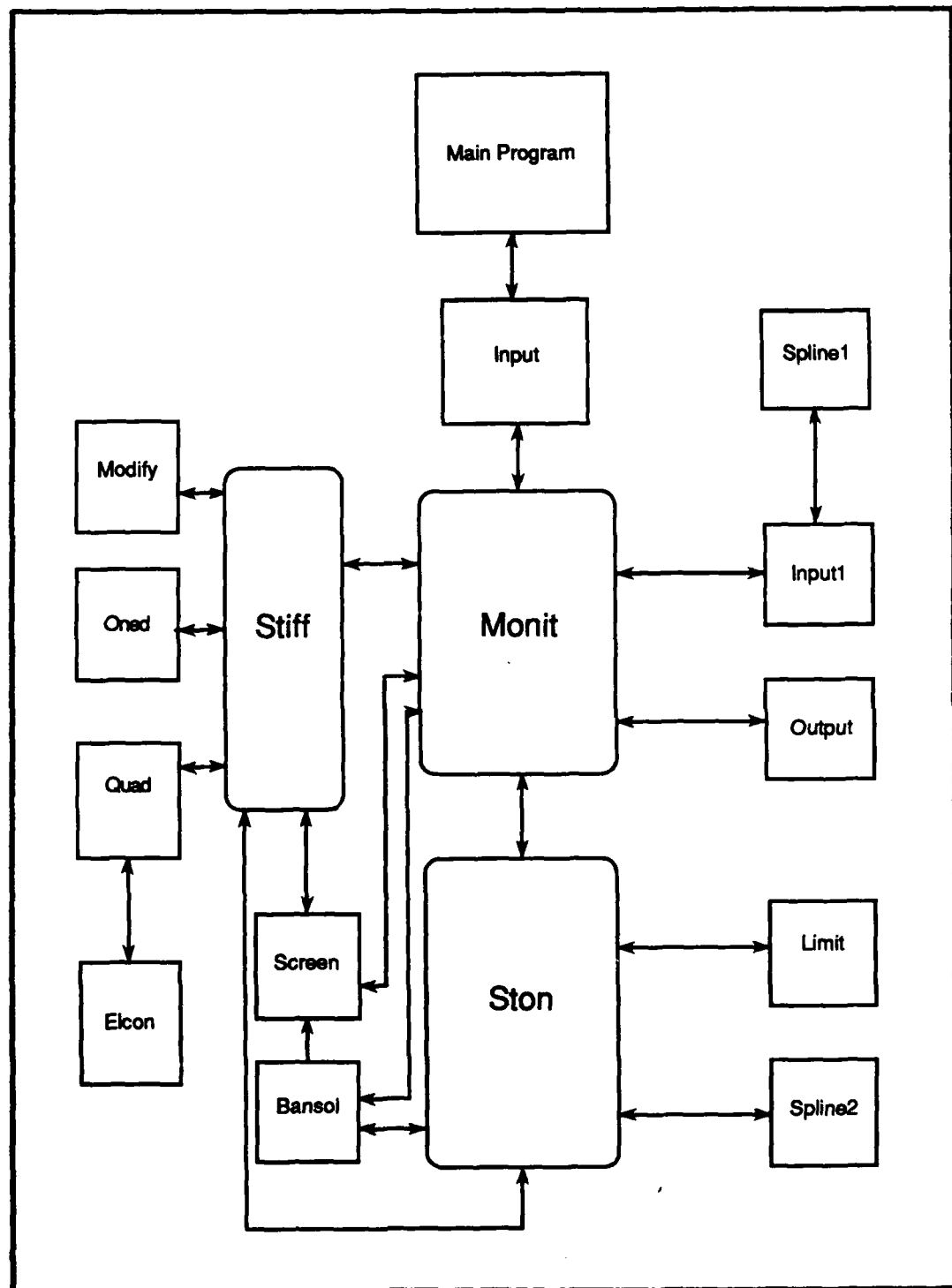
Figure 2-9.   PLSTREN Flow Chart

III. Analysis

As discussed in Chapter I, the ability to accurately analyze the failure characteristics of composite materials is critical to the implementation of composites in aerospace applications. One critical geometry is a hole in a finite width plate. The nonlinear finite element technique described in Chapter II was used to analyze three stacking sequences of Gr/PEEK laminates, each containing a .4" hole. This chapter includes a description of the specimen geometry, the modeling technique employed in developing the finite element models, the method used to differentiate between finite element models, and the procedures used for the nonlinear program.

A. Specimen Geometry

The specimen geometry depicted in Figure 3-1 was chosen to analyze the failure characteristics of Gr/PEEK. These specimens were machined from 16 ply sheets of commercially procured Gr/PEEK. Note that the diameter to width ratio (w/d) is one third. The stacking sequences modeled and analyzed are listed in Table 3-1.

B. Finite Element Modeling

An acceptable finite element model of a structure should accurately predict the displacements and stress fields of the actual structure. In creating these models the size, shape, loads, and boundary conditions of the structure must be accounted for. The model should also provide refinement in areas of interest so that stress

3-1

Note: All dimensions in inches
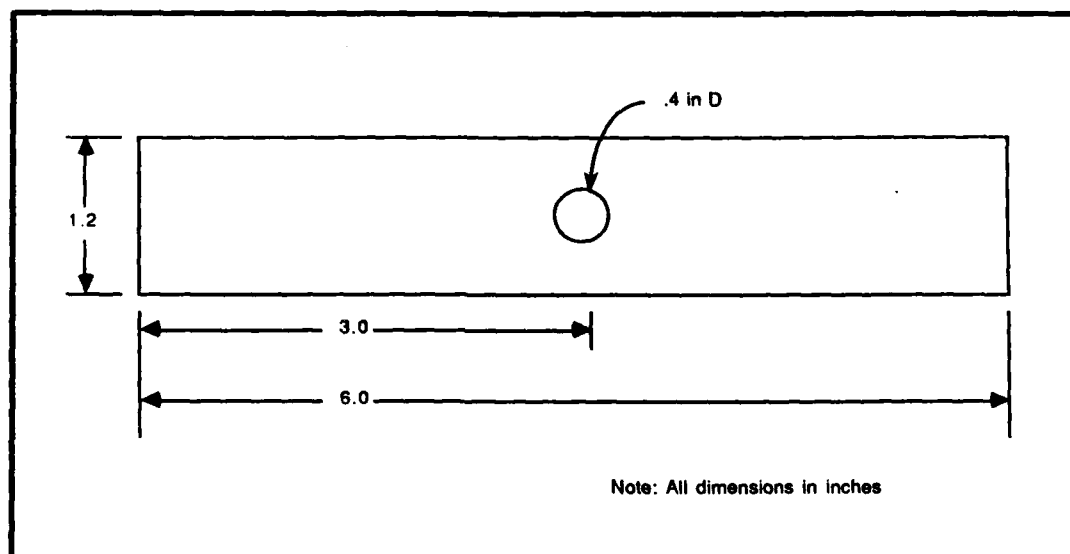
Figure 3-1. Specimen Model

Table 3-1. Modeled Stacking Sequences

Ply Lay-up	Symbol	Type
[0]	OT	Unidirectional
[90]	90T	Unidirectional
[+45]	SH	Angle-Ply
[0/±45/90]	Q	Quasi-isotropic

gradients or displacements can be accurately predicted. Each
of these issues will be discussed in describing the
methodology used to create the finite element model.

The size and shape of the model are inherently linked and will be discussed concurrently. Because of the symmetry of the specimen, a variety of geometric reductions were possible. These reductions are advantageous in terms of analysis time and computer costs as long as the impact on accuracy is minimal. Modeling a quarter of the specimen (as shown in Figure 3-2) was considered first. Since the program
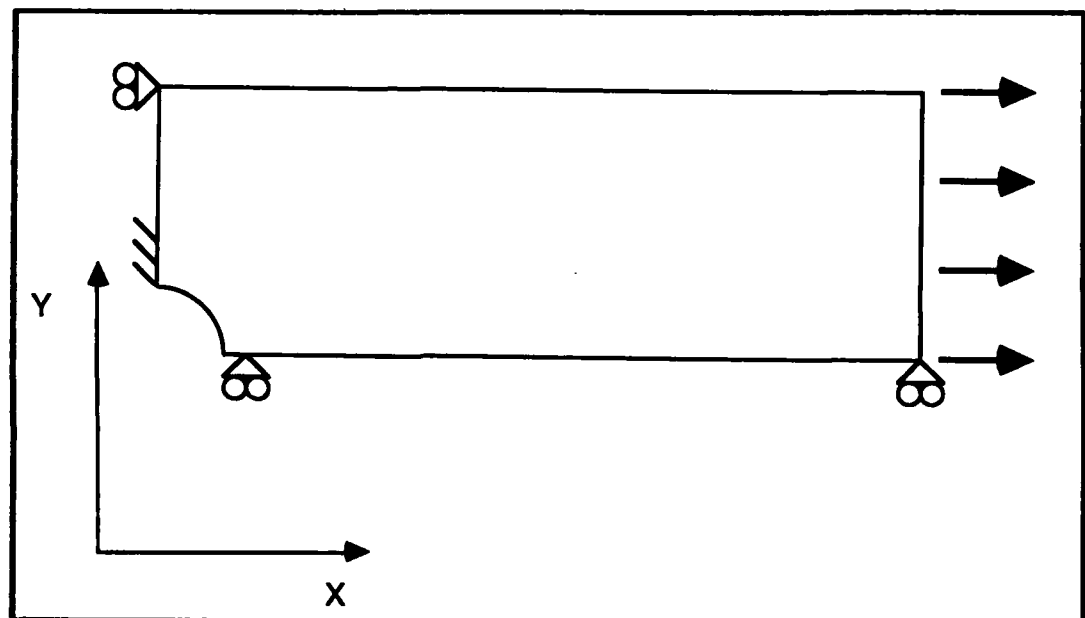
Figure 3-2. Quarter Specimen Model

calculates stresses at the center of each element, this would require the stresses of interest along the the center line of the specimen to be extrapolated. Extrapolation is inherently inaccurate, therefore this type of model was rejected. Modeling a half of the specimen (as shown in Figure 3-3) was then considered. Since the half
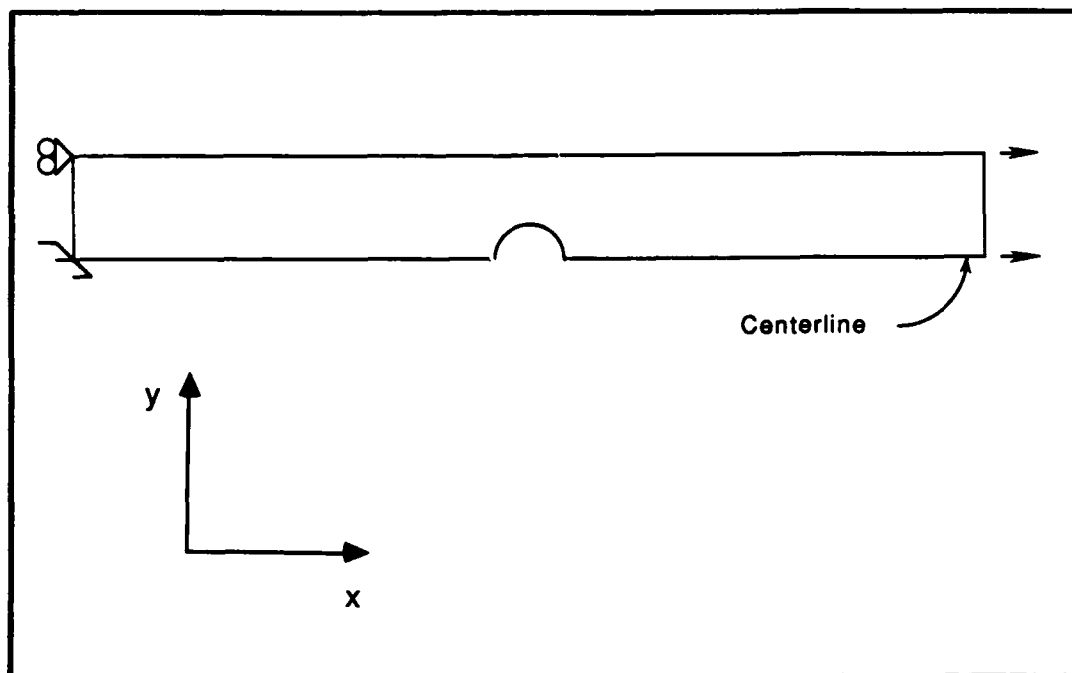
Figure 3-3. Half Specimen Model

model did not require stresses to be extrapolated at the
center line it was selected as the model geometry. The only
issue of concern for this geometry was whether it could
accurately predict stresses in the shear specimen. This
issue was resolved by creating a complete model of the
specimen using the crudest mesh (as shown in Figure 3-4) and
comparing the results. The stresses predicted in the
complete model vary from the half model by less than .5% at
any location and are typically less than .1%.

Choosing the half specimen geometry required additional
considerations in determining the boundary conditions. The
nodes at the fixed end were set with the innermost node fixed
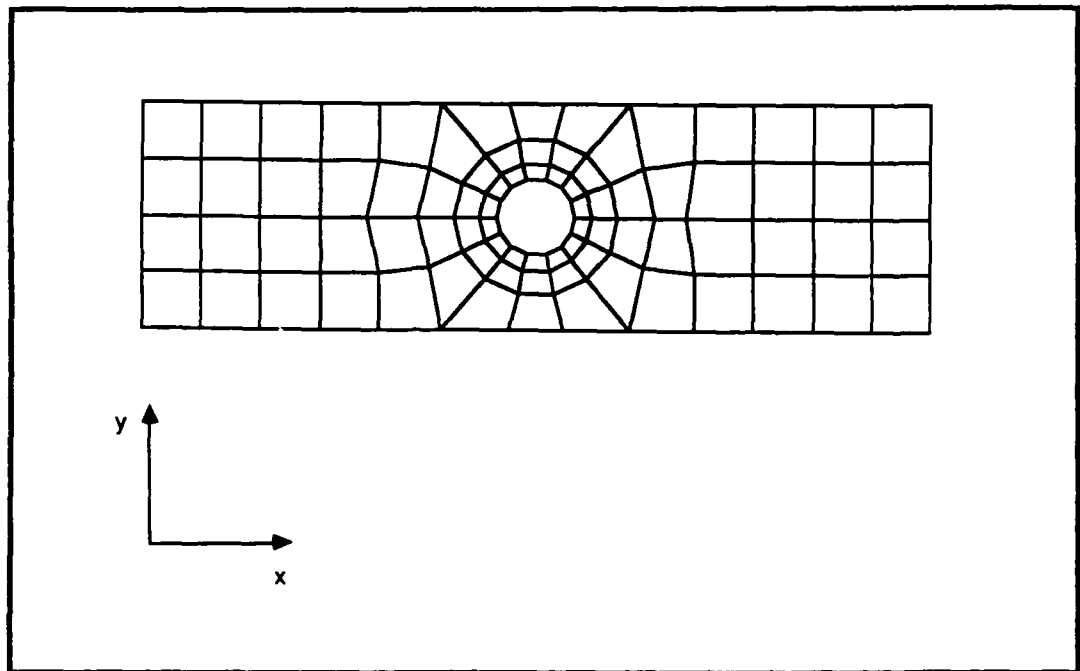
Figure 3-4. Whole Specimen Model

and the other nodes fixed in the x direction and free in the
y direction to accommodate the Poisson effect. The nodes
along the inside length of the specimen were fixed in the y
direction and free in the x direction. These boundary
conditions are depicted in Figure 3-5. The remainder of the
nodes were free.

Finally, the models required refinement around the
hole to accurately predict stresses at the center line. The
elements around the hole were built upon radial lines
extending from the center of the hole with two goals in
mind: to keep the elements as square as possible (for
accuracy) and to get stresses along the center line without
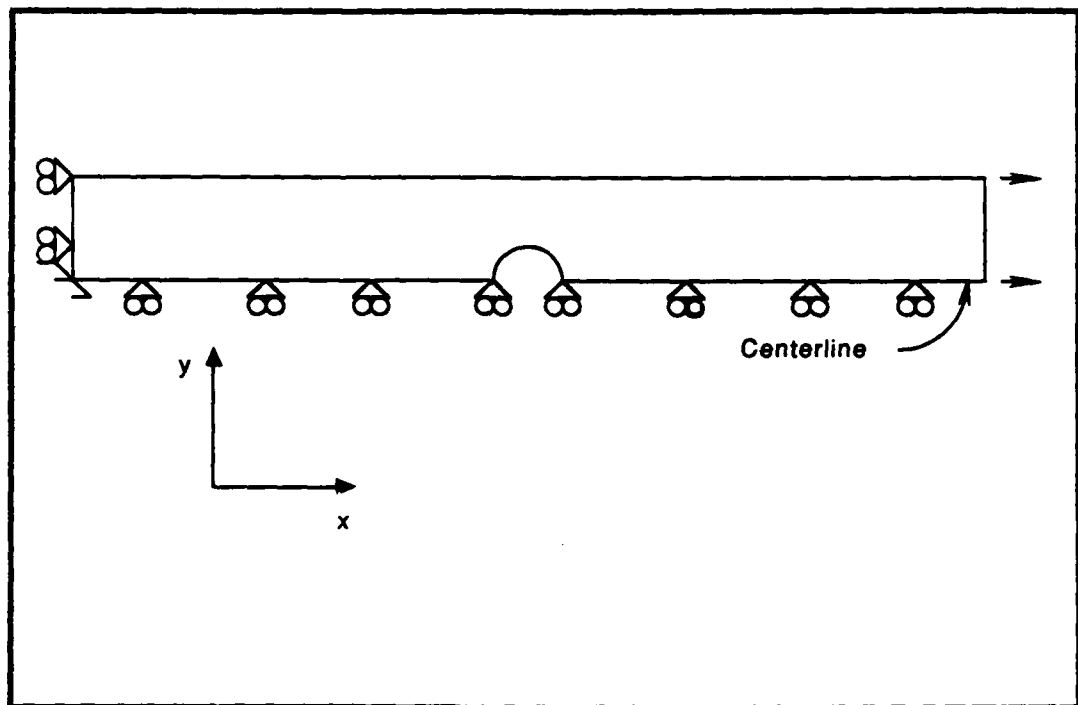
Figure 3-5.   Half Model Boundary Conditions

having to interpolate. To keep the elements as square as
possible, the elements were enlarged from the center with
three of the four sides equal in length. To eliminate the
need to interpolate the stresses the elements were built
upon evenly spaced radial lines at even angle increments
(producing an odd number of sectors).

Based on the preceding discussions, four finite
element models were developed. These models are as shown in
Figure 3-6. The final model selected for use in the
nonlinear program was selected based on results from the
linear version of this program. The selection process is
discussed in the following section.

Coarse Model

Medium Model

Fine Model

y

x

Extra Fine Model
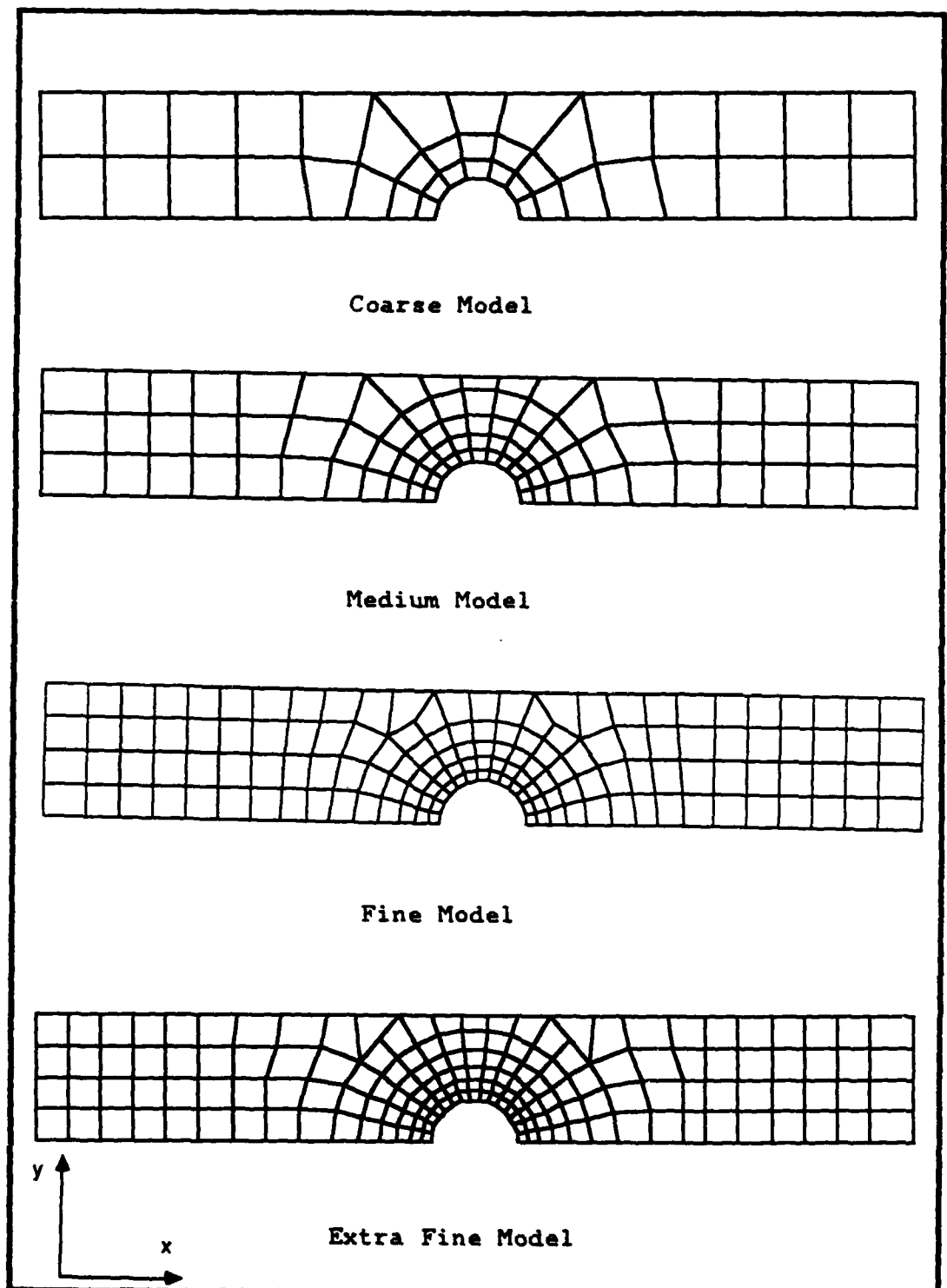
Figure 3-6.   Finite Element Models

C. Finite Element Model Selection

Three methods were used to differentiate between the four finite element models in an effort to get accurate results in a minimum of computer time. For simplicity, these methods are referred to as the Stress Concentration Method, the Ray Method, and the Stress Contour Method. Appendix B contains samples of all the graphs created to help differentiate between models using the Ray Method and the Stress Contour Method.

(1) Stress Concentration Method. In the Stress Concentration Method, each of the models was used to predict a stress concentration factor (SCF) at the hole, assuming the material was isotropic. The predicted SCF from each model was then compared to theoretical results as a measure of accuracy. To model an isotropic material, the plies were all given a 0-degree orientation and the material properties were set as elastic engineering constants such that:

$$E_1 = E_2 = 19.2 \times 10^6 \qquad G_{12} = 7.27 \times 10^6$$
$$\nu = .32$$

With these values set, the models were used to determine the corresponding stresses due to an end load of 500 pounds (tension) using the linear version of the finite element program.

To predict the SCF, the stresses corresponding to the center line of the coupon and perpendicular to the load

3-8

direction were used to predict the stress at the hole.
These stresses were extrapolated using an algorithm based on
Lagrange's interpolating polynomial [3]. Finally, the SCF
was calculated by simply dividing the stress at the hole by
the applied stress.

The results of the Stress Concentration Method are
listed in Table 3-2 and shown graphically in Figure 3-7. The

Table 3-2.   Results of Stress Concentration Method

Model	Stress at hole(kpsi)	Stress Concentration	Accuracy (%)	Time of Execution (sec)
Coarse	26.9	2.71	78.3	15.839
Medium	31.9	3.22	93.1	17.461
Fine	32.5	3.28	94.8	29.762
Extra Fine	33.4	3.37	97.4	63.902

theoretical SCF was determined using Figure 3-8 [11]. A d/w
ratio of 1/3 yielded an SCF of 3.46. Note that the only
model that failed to predict the SCF within 10% was the
coarse model. Based on these results, the coarse model was
discarded from consideration as the model to be used in the
nonlinear analysis. Note also that each level of refinement
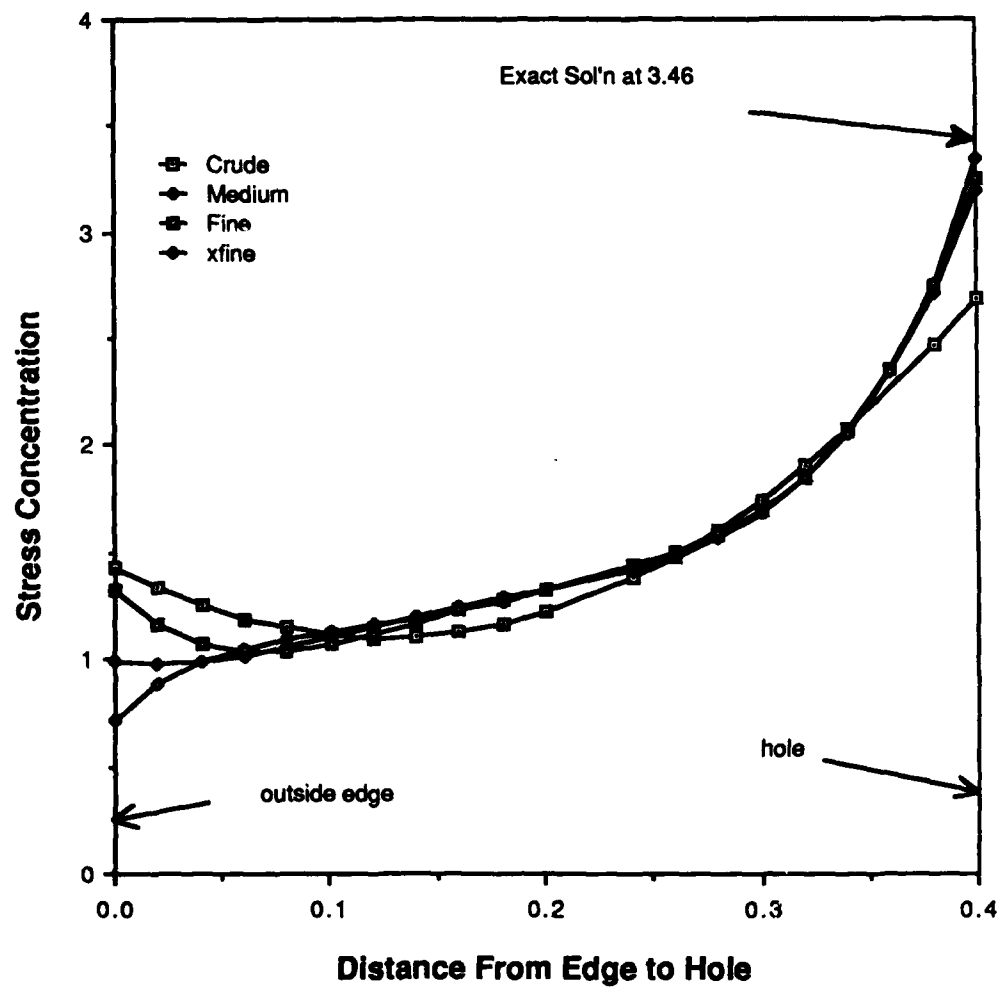
Figure 3-7. Stress Concentration Factors for Models
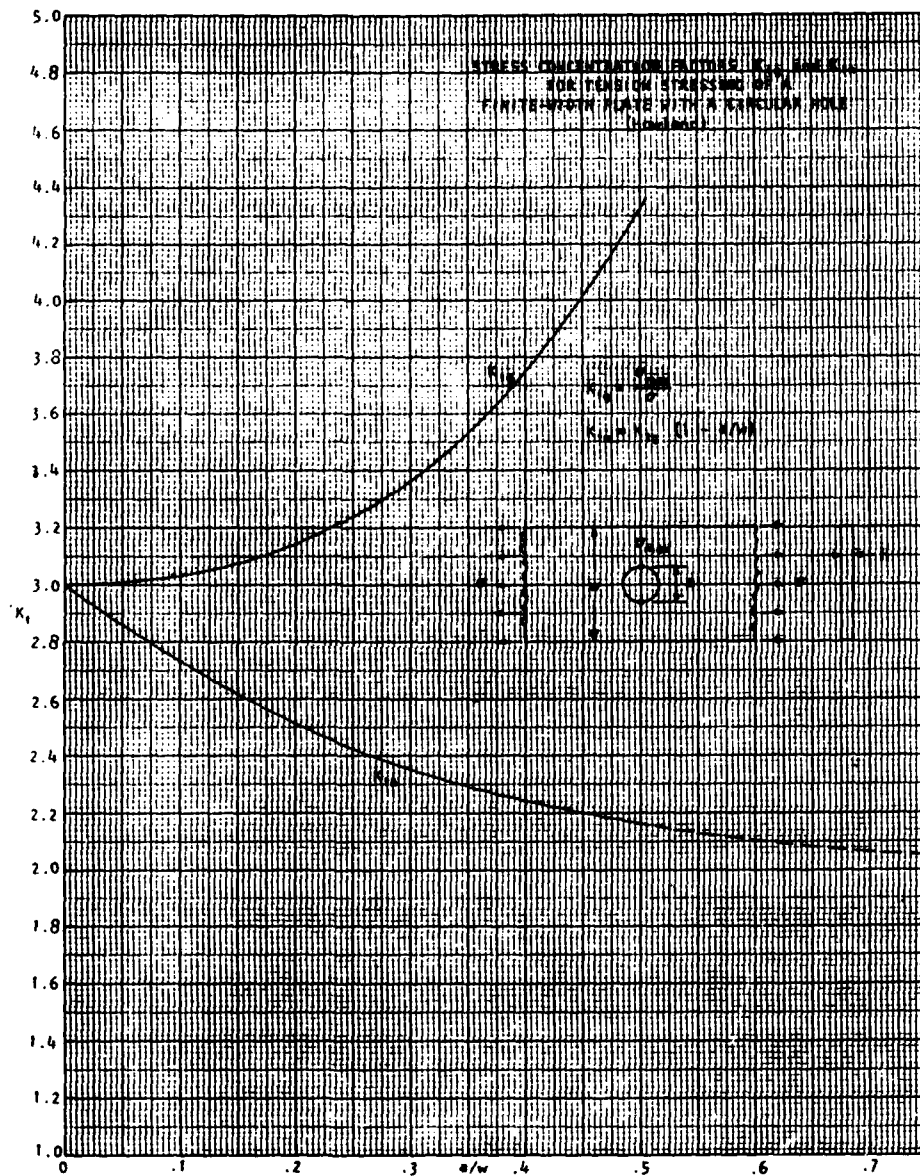
Figure 3-8.   Theoretical Stress Concentration Factors

requires roughly twice as much computer time as the preceding level. This observation will be used later to differentiate between models.

(2) <u>Ray Method</u>. For the Ray Method, the stresses along each of the "rays" shown in Figure 3-9 were plotted for each of the three remaining models. The assumption was made that the
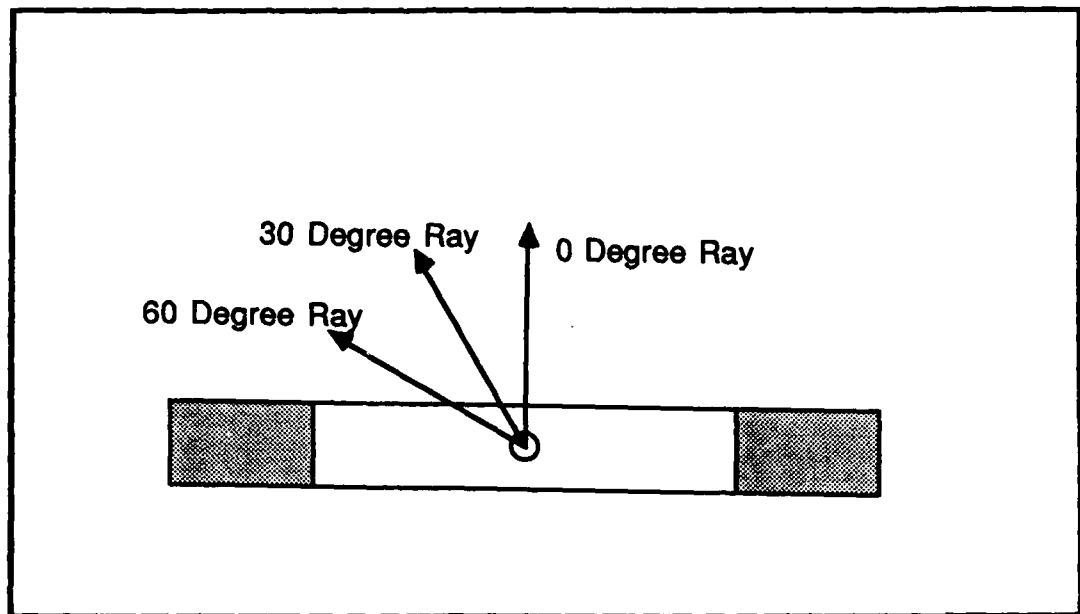
Figure 3-9. Rays Extending From Hole

most refined grid (the Extra Fine Grid) would provide the most accurate results. Therefore, significant variation between the plots for the lesser refined meshes was used as justification for removing the mesh as a candidate for use with the non-linear version of the finite element program.

Separate plots (See Appendix B) were created for each of the rays corresponding to the three stress

components (sigma x corresponds to the stress in the load

direction, sigma y corresponds to the stress in the

transverse direction, and sigma xy corresponds to the shear

stress) for a total of nine plots. The stresses on the

0-degree ray was plotted directly from the data from the

finite element program. Data for both the 30 and 60 degree

ray stress plots were interpolated using a two dimensional

Kriging algorithm. The plots for sigma x, sigma y, and the

0 degree sigma xy failed to show any significant differences

in the models. Both the 30 and 60 degree sigma xy plots

revealed some significant differences between the medium

grid and both the fine and extra fine grids but was

inconclusive. To get a more complete picture of the

stresses, it was decided to plot the stress contours for each

model.

(3) Stress Contour Method. For the Stress Contour Method

the stress contours for each of the models was plotted.

Again, the stresses from the Extra Fine Grid were assumed to

be the most accurate. The stress contours were plotted using

Surfer, a software package that also uses a two dimensional

Kriging interpolation algorithm. Samples of these plots are

in Appendix B. As with the Ray Method, results from the

sigma x and sigma y stress contours was inconclusive in

terms of removing a particular model from contention. When

comparing the shear stresses, however, significant

variations were apparent in the Medium Grid model. The

shear stress contours for both the Fine Grid and Extra Fine

3-13

Grid models compared quite well. Based on the results from plotting the stress contours the Medium Grid model was removed from consideration for use in the non- linear program.

(4) Conclusions From Finite Element Model Selection
The three methods used to differentiate between models revealed apparent shortcomings in both the Coarse Grid and Medium Grid Models, shortcomings that were not revealed in the two remaining models. A factor that was mentioned but not utilized previously was the amount of computer time required to run each of the data files with the linear version of the program. The Fine Grid model required 29.761 CPU seconds whereas the Extra Fine Grid model required 63.902 CPU seconds. For a linear program this may not be significant, but because of the incremental and iterative nature of the nonlinear program, the difference in the amount of processing time was considered significant. Because the results of the three methods was comparable for both the Fine and Extra Fine Grid models and the processing time was so much lower for the Fine Grid model, the Fine Grid model was selected for use with the nonlinear version of the finite element program.

D. Nonlinear Analysis

The nonlinear analysis of this model was conducted using a CRAY mainframe operated through a CYBER mainframe. This arrangement provided a faster (and cheaper) process than the CYBER mainframe alone. The purpose of this section is to

3-14

discuss how these computers were utilized and what kind of output they provided.

The incremental approach (as described in Chapter II) required multiple computer runs. These runs were routed from the CYBER mainframe to the CRAY mainframe where the program was executed. Although the CRAY performed the executions at a higher cost per second than the CYBER, using the CRAY saved money by reducing the execution time. Once a run was completed, the CRAY routed the output files back to the CYBER. This cycle of starts and restarts was continued until the model failed [9].

Each run consists of a specified number of load increments. These load increments were imposed by displacing the free end of the specimen by a prescribed amount. The initial displacement was determined by using a tenth of the experimental failure load as a force increment and making a test run of PLSTREN. The average of the resulting initial nodal displacements at the free end of the specimen was taken as the initial incremental displacement. Since the increment is adjusted by the program, increment sizes are not critical.

The output consists of three files which are updated at the end of each increment. These files contain the following:

(1) Tape 3, unformatted output that contains all of the displacements, stresses, strains, elastic constants, and energy levels from the last increment accomplished so that the incremental process can be restarted from the current

increment,

(2) <u>Tape 6</u>, the input data from the data file and the output containing displacements, stresses, strains, energy levels, and the order of failing elements for each increment along with information on the convergence of the solution, and

(3) <u>Tape 9</u>, total displacements at the end of the increments which can be plotted to show the deformed shape of the model at any increment.

An example of this data is included in Appendix A for the loading of a single four ply element to failure.

IV. Experimentation

The purpose of experimentation in this thesis was to provide a basis of comparison for the analytic results. Experimentation was conducted through the Structures Division of the Air Force Flight Dynamics Laboratory (FDL) at Wright-Patterson AFB, Ohio.

The three objectives for the experimentation conducted in this thesis were:

(1) to provide basic property data of Gr/PEEK at 250 F for the computer analysis,

(2) to determine the ultimate strength of the Gr/PEEK specimens,

(3) and to provide partially yielded specimens to study failure progression.

All specimens were tested at 250 F. This chapter describes the procedures and test apparatus used to accomplish these objectives. A complete list of all materials and equipment used is in Appendix D.

A. Specimen Fabrication

The Gr/PEEK specimens were fabricated from panels procured from the Fiberite Corporation, a subsidiary of Imperial Chemical Industries of Great Britain. The dimensions of the panels are listed in Table 4-1. The process used to fabricate specimens from these panels included C-scans to check for preexisting flaws, cutting the panels into subpanels, attaching tabs to the subpanels, and cutting the specimens from the subpanels.

Table 4-1. Gr/PEEK Dimensions

Laminate Type	Ply Lay-up	Size
Unidirectional	[0]	10" X 14"
Unidirectional	[90]	10" X 14"
Angle-Ply	[±45]	16" X 16"
Quasi-isotropic	[0/±45/90]	16" X 16"

To determine if any flaws existed in the panels, a through ultrasonic C-scan was conducted on each panel by the Non-Destructive Branch of the Air Force Materials Laboratory. No significant flaws were found.

After the C-scan, the panels were cut into subpanels by the AFIT Model Shop. The subpanels were cut so that the tabs could be attached to several specimens at the same time. The tab material consisted of 1/16 inch G-10 glass/epoxy (0/90 woven) and were attached to the specimens using an adhesive that requires curing in an autoclave.

Finally, the tension and compression specimens were cut out of the tabbed subpanels. The widths of the basic property specimens were based on ASTM standards and as such varied with ply lay-up. The tensile specimens are shown along with their respective dimensions in Figure 4-1. The geometry for the compression specimens was based on the Rolfes compression fixture. The compression specimens are depicted in Figure 4-2.

4-2
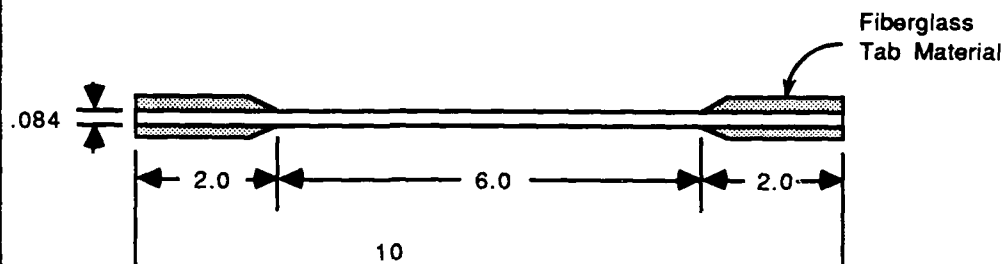
(a)   Profile View (typical)
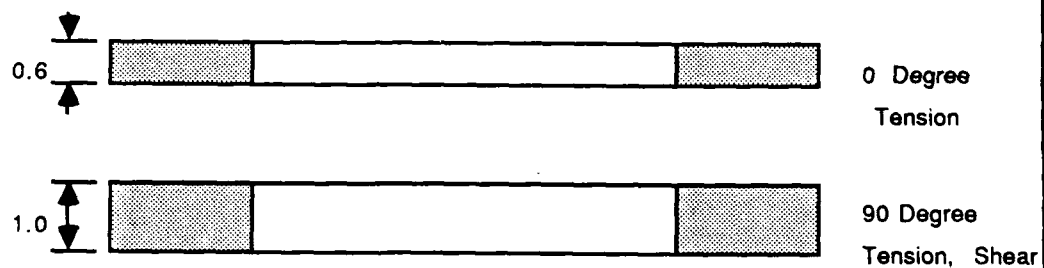
(b)   Basic Property Tension Specimens
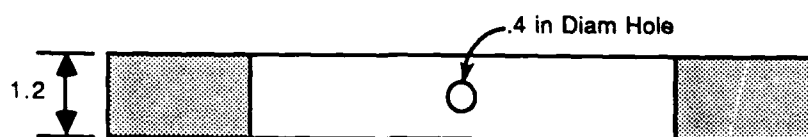
(c)   Ultimate Tension Specimens

Note: All dimensions in inches

Figure 4-1. Tension Specimens
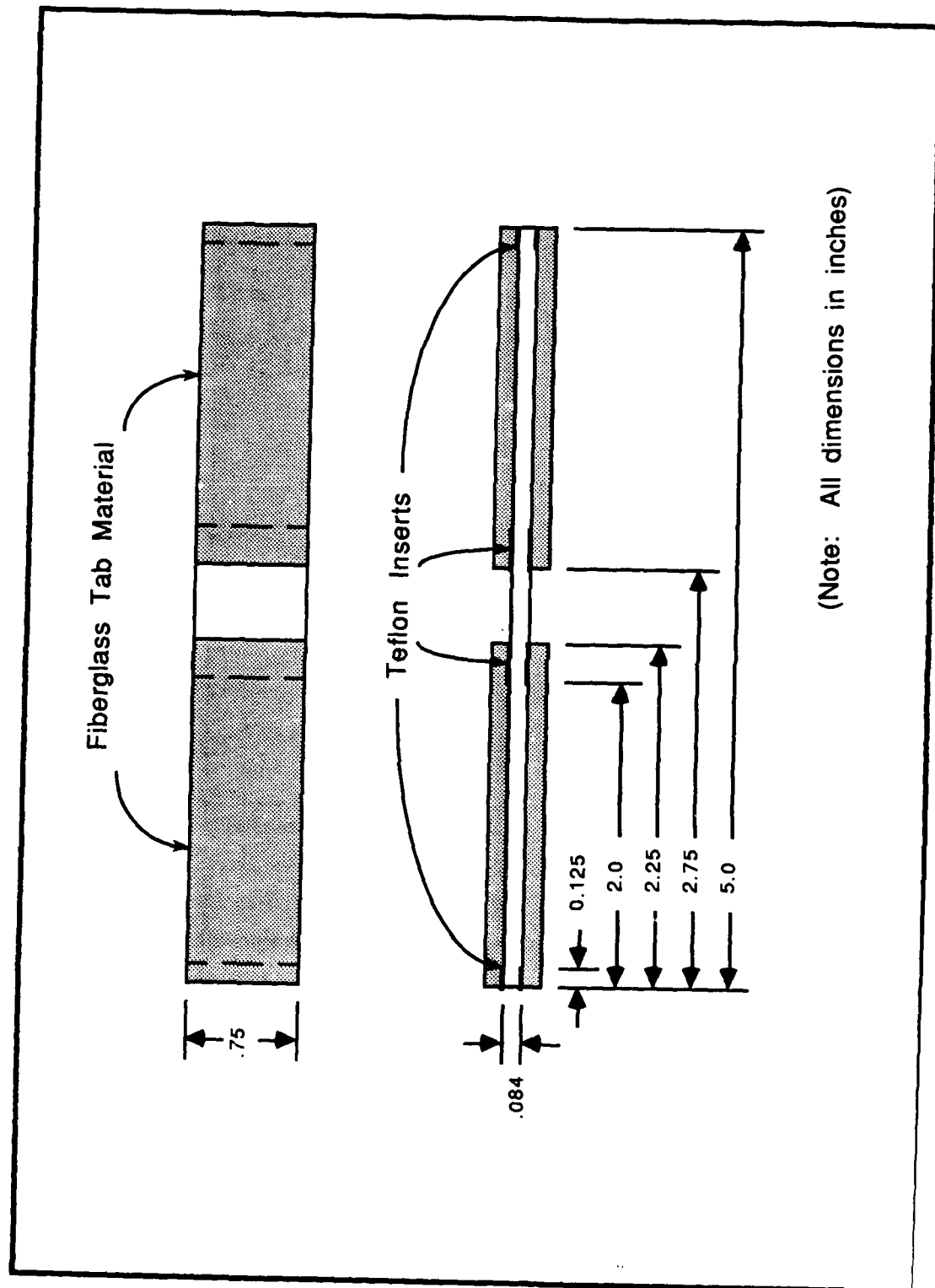
Figure 4-2. Compression Specimens

B. Specimen Instrumentation.

   After the specimens were fabricated, they were
instrumented with strain gages. Strain gage rosettes (as
depicted in Figure 4-3) were used on the tension,
compression, and other specimens to provide the longitudinal,
shear, and transverse strains. "Stacked" rosettes were used
near the holes because the strain components were required in
a small area. The gages or rosettes were placed on both
sides of the specimens at each location for two reasons. The
primary reason for using two gages was that if one gage
failed, the test would still yield usable data from the
second gage. The second reason
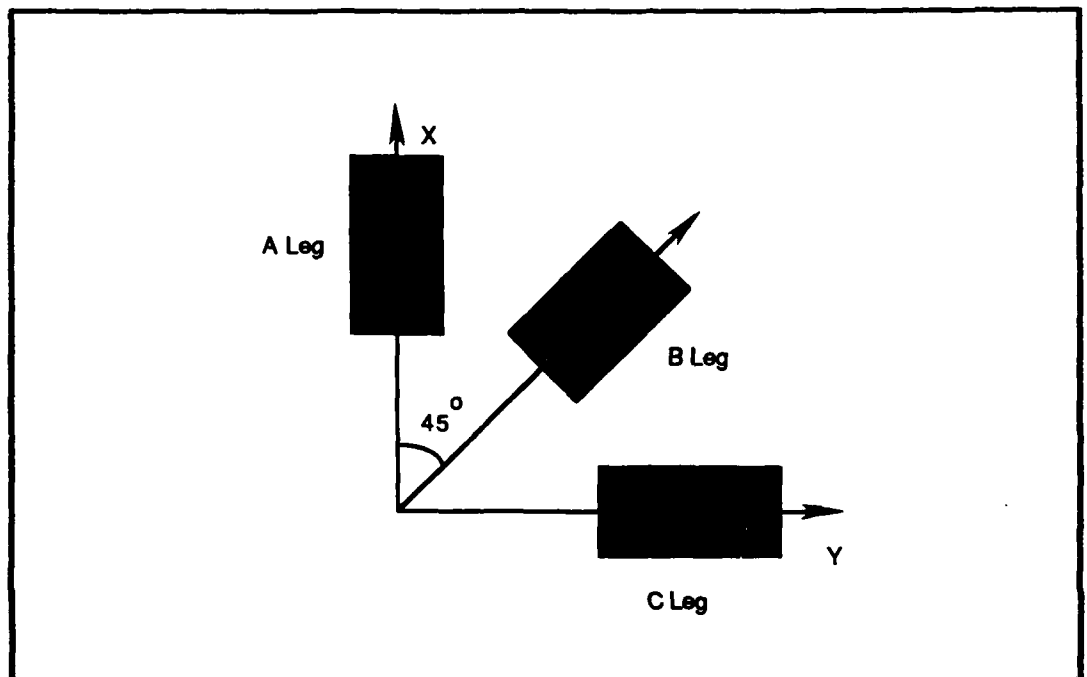
Figure 4-3. Strain Gage Rosettes

was that if both gages worked the strain could be taken as the average of the two, to detect and to mitigate any misalignments of the gage or specimen (in the Instron).

The location of each gage varied with the type of testing to be conducted. For the basic property tests (both tension and compression), all of the gages were located at the center of the specimen. For the ultimate tensile specimens, two sets of rosettes were attached to the specimens: one set (the stacked rosettes) at the hole and one set at a "far field" location as depicted in Figure 4-4. The percent of ultimate tensile specimens were gaged as depicted in Figure 4-4 except that no stacked rosettes were used.
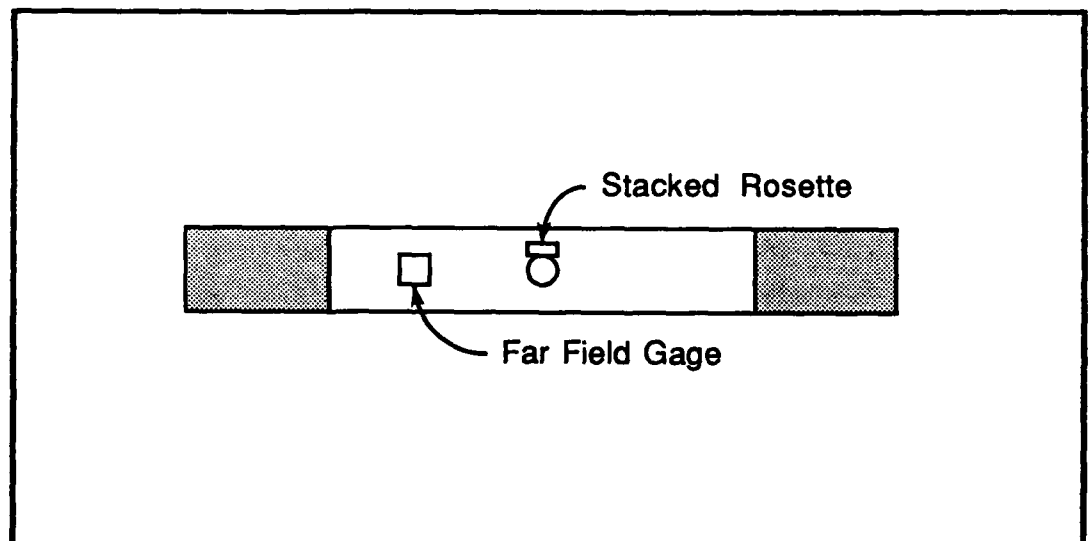
Figure 4-4. Ultimate Tension Specimen Gages

The raw data from the gages on the basic property shear specimens required a conversion for shear strain and stress.

The stresses and strains were converted using the equations

$$\gamma_{12} = \varepsilon_A - \varepsilon_C \tag{47}$$

where ε_A and ε_C are the axial and transverse strains recorded from the respective rosette legs, and

$$\tau_{12} = \frac{P}{2\ b\ d} \tag{48}$$

where P is the end load, b is the width, and d is the thickness. The assumption used for these calculations is that the fibers retain their $\pm 45^\circ$ orientation. Rotation of the fibers, or "scissoring", results in error creeping into the solution through the transformation matrix.

During the course of testing, it was apparent that strain gages alone were not sufficient to measure strain in specimens containing $\pm 45^\circ$ fibers. These ply lay ups resulted in extremely high strains. The high strains coupled with the high temperature resulted in the strain gage adhesive failing and allowing the gage to peel off the specimens. The type of gage adhesive used was Micro Measurements M-Bond 200, an adhesive that is typically good to 300 F in normal applications. No other adhesive is currently available that provides the necessary adhesion at high temperatures without affecting strain measurements. Consequently, two additional specimens were prepared in an attempt to measure strains

optically.

A basic property shear specimen was prepared for optical strain measurements by making an "X" in the center of the specimen as depicted in Figure 4-5. This technique was used successfully in an in-house effort by AFWAL/FDSCA to record shear strain and is used here for one sample only as an estimation of the magnitude of the strains in the basic property shear specimen. The legs
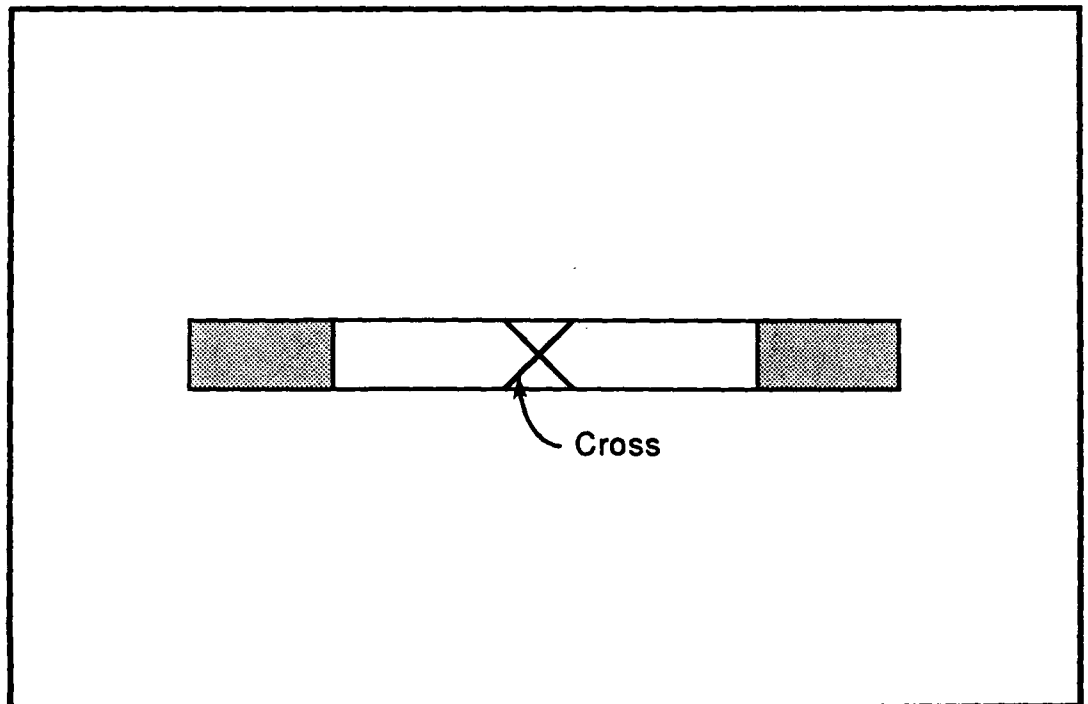
Figure 4-5. Specimen with "X"

of the "X" were coincident with the fiber direction, therefore indicating fiber rotation during loading. Photographs of the "X" and a voltmeter indicating load were taken at the start of testing and at regular intervals until

failure. Slides of these photographs were projected onto a
piece of paper so that the angle for each interval could be
measured. This angle was used to determine the strain using
the equation

$$\phi_{12} = 2 \, \gamma_{12} \qquad\qquad (49)$$

where ϕ_{12} is the change in angle from the previous
photograph. The shear strain was then correlated with the
appropriate load and stress for the G_{12} curve.

A $[\pm45]_{4S}$ ultimate failure specimen was prepared for
optical strain measurements by applying a grid of dots on one
side of the hole as depicted in Figure 4-6. This technique
is a crude variation of that used in Reference 6 for
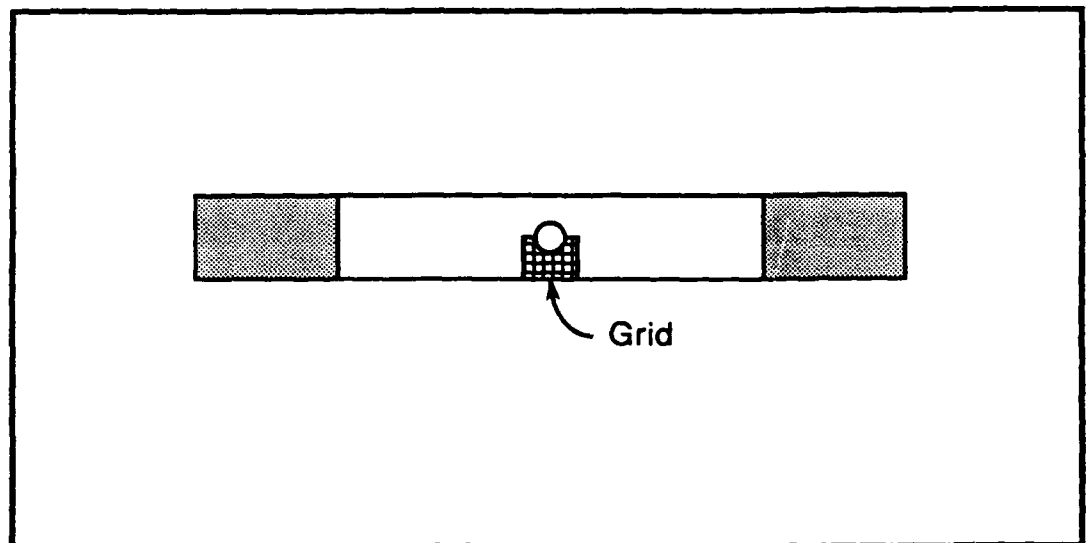
Figure 4-6. Specimen with Grid

measuring crack growth. As with the basic property specimen,
only one specimen was prepared in an attempt to measure the
magnitude of the strains. The background for the grid was
flat white latex. This grid was applied by taping a stainless
steel mesh to the specimen and marking through the grid onto
the specimen with a black felt tip marker. Photographic
resolution was essential for these measurements, so the camera
lens was located 4 in from the specimen. This precluded
getting the load from the voltmeter in the photograph.
Consequently, photographs were taken at 20 s intervals so that
load from the strip chart could be correlated with a
particular frame. The only dots actually measured formed one
line in the load direction and one line in the transverse
direction. The movement of the dots was measured using a
digitizer (see Appendix D for description). The slides were
blown up to 8 in by 10 in prints to facilitate making these
measurements. These measurements required use of a reference
scale in the field of view of the photograph. This was
provided by a small ruler attached to the upper jaws and
extending through the heat chamber on one side of the
specimen. Both longitudinal and transverse strain were then
calculated using

$$e = \frac{\delta L}{L} \qquad (50)$$

where:

e = strain in the x or y direction

δL = change in the length in the x or y direction

L = original length in the x or y direction

This strain was then correlated with the load indicated on the strip chart for the stress-strain curve.

Table 4-2 contains a list of the specimens that were prepared and tested for this study including the number and type of gage (if applicable) attached to the specimen.

C. Test Apparatus.

The test apparatus used used to test the specimens consisted of an Instron universal test machine, a data collection system, and a heating fixture. The Instron and the data collection system were identical for all testing. Separate heating fixtures were developed for tension and compression testing.

A 20 kip Instron was used to load the specimens in either tension or compression. The specimens were all loaded at a constant rate of 0.05 inches per minute to minimize the viscoelastic effects. The Instron also provided a strip chart of load versus time using a 20 kip load cell (consisting of permanent strain gages).

The data collection system consisted of a system to record the strain gage data, devices to facilitate testing, and video equipment. The system to record the strain gage data was used throughout testing. The rest of the equipment was used as required.

Table 4-2. Experimental Specimens

Specimen Type	Number of Specimens	Gages
0° Tension	6	2 of (a)
0° Compression	8	2 of (b)
90° Tension	8	2 of (a)
90° Compression	8	2 of (b)
Shear	1	2 of (c)
	1	2 of (d)
	5	2 of (e)
	1	None (Cross)
$[0]_{16}$ with hole	3	2 of (a) & 2 of (f)
	5	None
$[90]_{16}$ with hole	3	2 of (a) & 2 of (f)
	3	None
$[\pm45]_{4S}$ with hole	3	2 of (a) & 2 of (f)
	4	None (1 with grid)
$[0,\pm45,90]_{4S}$ with hole	3	2 of (a) & 2 of (f)
	3	None

(a) CEA-03-125UR-350   (d) PAHE-03-125RB-350

(b) CEA-03-062UR-350   (e) PAHE-03-062RB-350

(c) PAHE-03-250RB-350   (f) WK-08-060WR-350

The system used to record the strain gage data was connected to a FDL VAX. A data file was created for each test that included the strain of each gage, the load applied, and the time. This data was later used to either create the stress-strain plots or to assess the failure progression of the specimens. Additionally, the system recorded data from three thermocouples attached to the specimen. These thermocouples were attached using alligator clips and rubber pads to protect the gages. They were typically an inch apart along the length of the specimen with the center thermocouple at the center of the specimen. The data from the thermocouples was used to verify that the temperature of the specimen was (250 ± 5) F.

Separate heat fixtures were developed for use on the tension and compression specimens. This was primarily due to the nature of compression testing and the need for a device to restrain the compression specimen from buckling.

The heat fixture for the tension specimens is shown in Figure 4-7. Figure 4-7 (a) depicts the individual components, (b) depicts the assembled enclosure, and (c) is a photograph of the enclosure installed on the Instron. Heat was supplied using a hot air gun controlled by a rheostat on the handle. The heat enclosure was fabricated from clear materials so that videos could be taken of the failure progression. The circular chamber was fabricated from acrylic tubing and the flat pieces were fabricated from Lexan. Note that the top and bottom slots are taped off allowing only enough room for
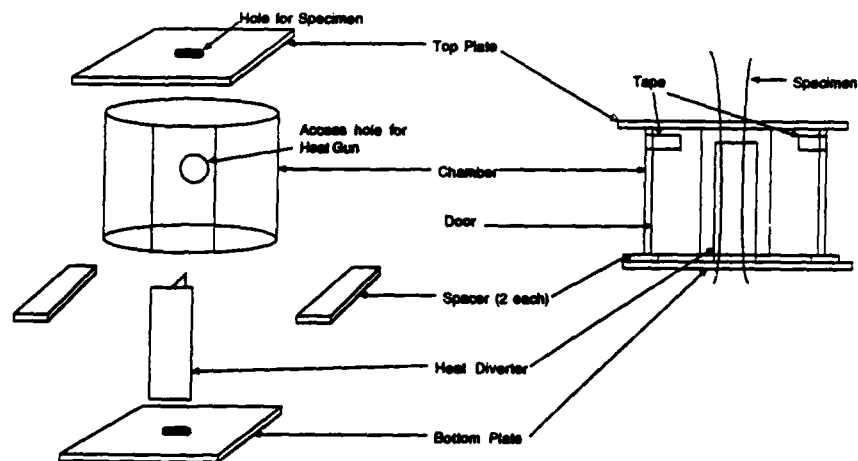
(a) Heat chamber parts   (b) Heat chamber
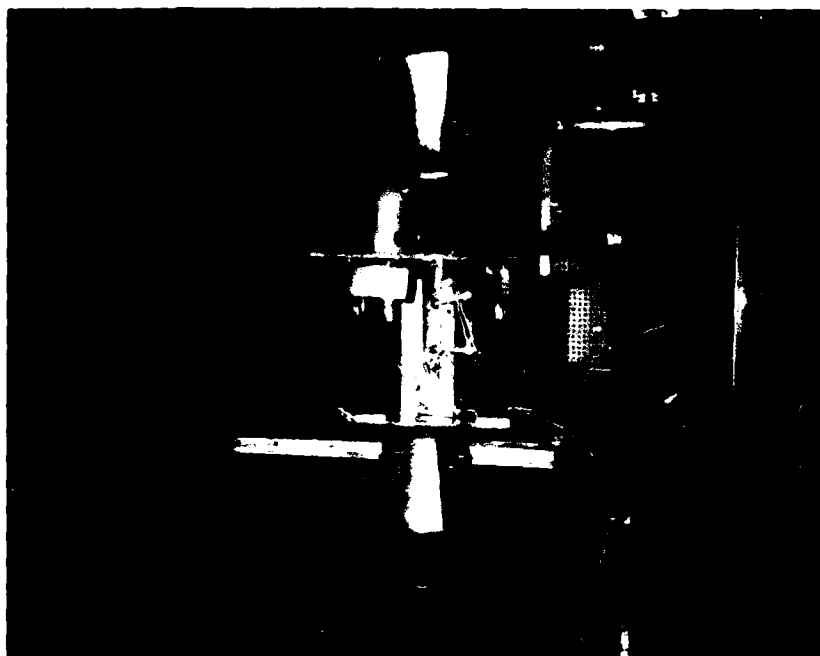
(c) Installed heat chamber

Figure 4-7. Tension Configuration

the specimen. This was necessary to preclude hot spots from developing on the specimen as the hot air was vented from the chamber. The heat diverter was installed between the hot air gun and the specimen to distribute the heat in the enclosure more evenly. Composites such as Gr/PEEK transfer heat in the matrix direction much more slowly than in the fiber direction. Consequently, even heating of the specimen through the thickness required even heating through the enclosure. The spacers at the bottom of the chamber provide the exhaust for the hot air. This fixture worked well because it was easy to fabricate, easy to assemble for each test, and was able to control the specimen temperature to (250 ±5) F.

The heat fixture for the compression specimens is shown in Figure 4-8. The compression fixture used for this testing was a Rolfes fixture. This relatively massive fixture was too large to heat in an enclosure using a hot air gun. Since the unsupported portion of the specimen was so small, we tried to heat just that portion. This rather simplistic set up was settled upon after many attempts to develop a fixture using one heat gun failed (miserably). Using one hot air gun, the temperature difference on either side of the specimen varied from 50 F to 100 F, depending on the configuration. Using two hot air guns, one on either side of the Rolfes fixture, the temperature could be controlled to within 5 F any where on the untabbed portion of the specimen. The temperature of the specimen is controlled by simply
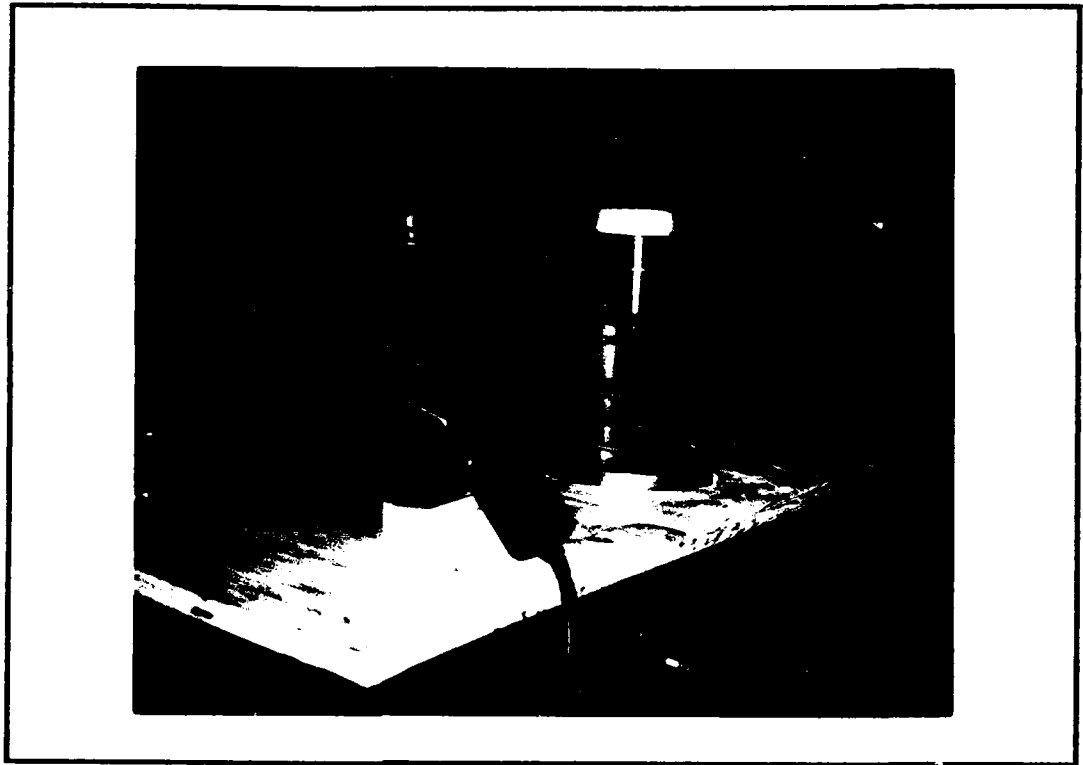
Figure 4-8. Compression Configuration

moving the heat guns toward or away from the Rolfes fixture,
as appropriate. This fixture provided excellent control of
the temperature because adjustments could be closely
correlated with the distance of the gun from the specimen.

Devices used primarily to facilitate testing included a
digital thermometer and a digital voltmeter. The digital
thermometer was used to monitor the temperature of the
specimen either inside or just above the heat enclosure.
Monitoring the temperature inside with the digital
thermometer made temperature adjustments much easier and

4-16

faster than using the VAX output. Early in the testing, monitoring the temperature on the specimen just above the enclosure was necessary to verify that the temperature was not greater than 250 F. During the initial check out of the heat enclosure the specimen failed just outside the enclosure, presumably because the slot was permitting too much heat out in the vicinity of the specimen resulting in a hot spot. This situation was resolved by taping the slot closed (except for the specimen) using a filament reinforced tape and venting the air out the bottom of the enclosure by inserting spacers between the circular chamber and the bottom plate (see Figure 4-7). The slot resulting from taping the hole closed was just large enough for the cross section of the specimen and effectively sealed the top and bottom plates. Subsequent monitoring indicated the specimen temperature outside of the enclosure was never greater than 210 F. The digital voltmeter was set up adjacent to the specimen to indicate the applied load. This was primarily used in conjunction with the video camera so that when the tapes were viewed the applied load could immediately be associated with a failure phenomenon.

The video equipment used consisted of both a normal speed and a high speed video camera. As the high speed camera was available for a limited time frame, one of each of the types of samples were taped first using the normal speed camera. From these tapes, specimens were selected where use of the high speed camera was deemed necessary.

4-17

V. Results and Discussion

The purpose of this chapter is to present and discuss the experimental and analytic results from this thesis. This material is presented in two sections; results of basic property tests and results of ultimate strength tests. The results of basic property tests contains all of the basic property curves derived for Gr/PEEK at 250F along with a discussion of how the tests progressed. The ultimate strength tests contain the stress strain curves for a point near the hole from both experimental and analytic techniques. In both sections, stress strain curves are used as a basis for comparing experimental and analytic results. The stress-strain curves for experimental results were derived from the experimental load and the strain. The load data was either recorded from the data collection system on the VAX, the load meter next to the test fixture, or the strip chart from the Instron, as described in Chapter 4. This load was converted to a stress by dividing by the area of the specimen. The strain was recorded by either the data collection system for the strain gages or one of the optical techniques, as described in Chapter 4. For the analytic results, all stresses were obtained from the output file from PLSTREN. The nominal stresses were determined by converting the stresses at each of the elements at the fixed end of the model to loads, summing the loads across the end of the model, and dividing the end load by the area of the specimen. The strains were

calculated by PLSTREN for each of the elements. Included in
this section is a discussion of the progression of failure
using the partially failed specimens and the analytic results
for comparison. Data collected from the high speed video
camera and other techniques is included as necessary.

A. Results of Basic Property Tests

The nonlinear material properties for Gr/PEEK at 250 F
were derived using the raw data from the basic property tests.
These tests are discussed in detail in Chapter 4. The
nonlinear finite element program requires the basic properties
in tabular format. This was accomplished by recording
stresses from each curve at specific strain intervals using a
digitizer (see Appendix D) and averaging the stresses at each
strain interval. Poisson's ratio required an additional
processing step since the axial and the transverse strain are
required at equivalent stresses. For ν_{12}^{t} and ν_{12}^{c}, tabular
stress-strain (ϵ_1 and ϵ_2) values were used with a program based
on the Lagrangian interpolation function to determine strains
at equivalent stresses. These strains were used to calculate
Poisson's ratio as described in Table 2-1. The tabular basic
properties including Poisson's ratio are included in Appendix
C. This tabular data was used to generate the curves depicted
in Figures 5-1 through 5-5, 5-13, and 5-14 primarily as a
visualization. The room temperature curves are included from
Reference (9) as a comparison. In general, the specimens
tested that were fiber dominated (E_1^{t} and E_1^{c}) resulted curves

that were more nonlinear than at room temperature. The remaining matrix dominated specimens resulted in curves that were much more nonlinear than at room temperature.

(1) 0 Degree Tension Specimen Tests. The first 0° tension specimen failed outside of the heat enclosure, probably because the hot air inside was vented where the specimen entered the enclosure causing a "hot spot" on the specimen. The enclosure was modified so that the hot air was vented away from the specimen and the slots in the enclosure for the specimen were taped closed. None of the remaining specimens failed outside the enclosure. When the stress strain curves for each specimen were plotted there was no discernible difference between the first specimen and the remaining specimens. Therefore, the data from the first test was not significantly corrupted and was used with the remaining data for the basic properties. The failure of the specimens occurred perpendicular to the fibers, but since there was no stress concentrator, the location of the failure was fairly random. The resulting stress strain curve was essentially a linear curve. Note that the curve at 250 F represents a material that is actually stiffer than at room temperature. Since this a fiber dominated phenomenon, the stress strain curves should actually be very similar. Any differences would be the result of the behavior of the carbon fibers which should be minimal. This anomaly is probably due to the relatively small number of specimens tested at each
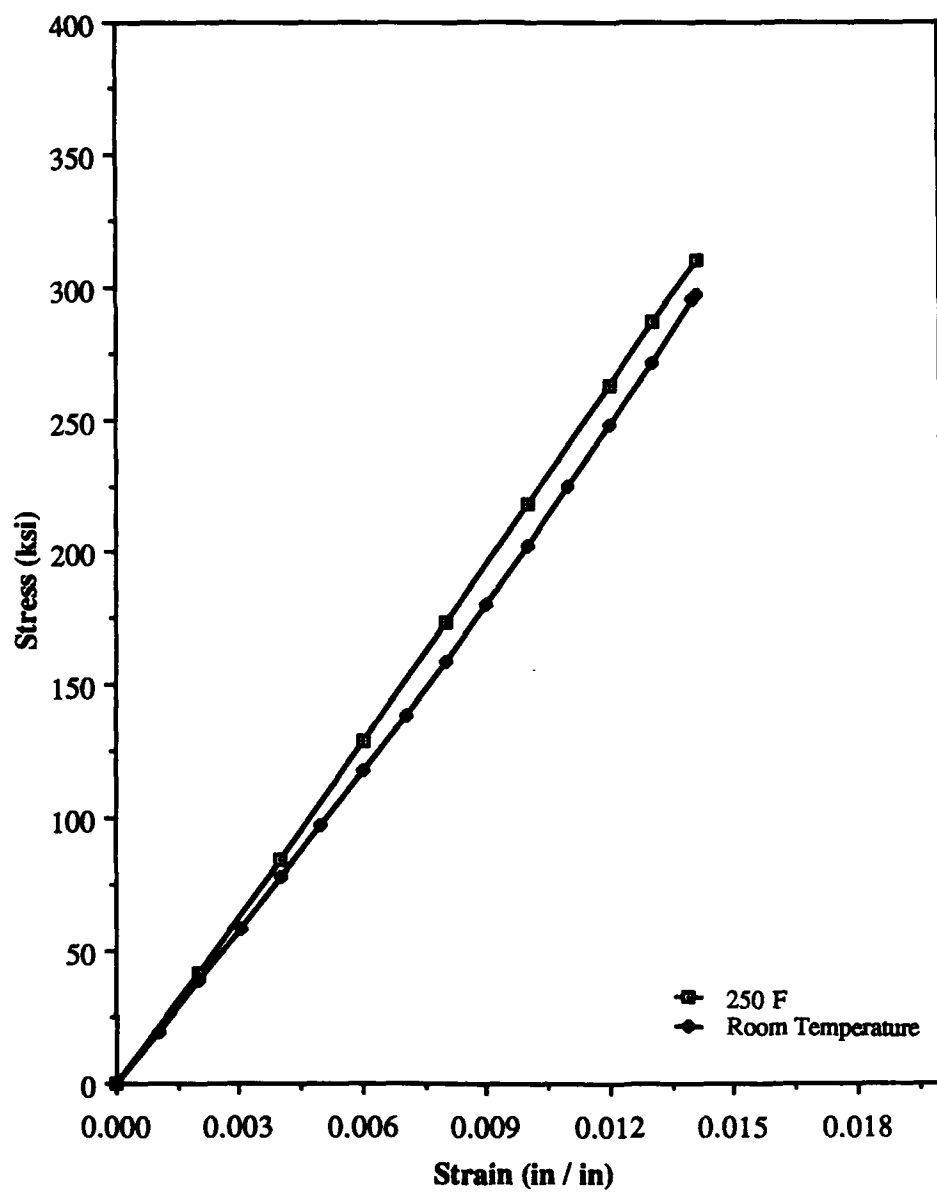
5-3

Figure 5-1. E_4^t Curve

temperature. If a statistically sufficient number of specimens had been tested at each temperature, the curves would probably been identical.

(2) 90 Degree Tension Specimen Tests. The 90° tension specimens all failed within the heat enclosure with failure loads within a 14 lb range. The resulting curves were significantly more nonlinear than either the 0° tension specimen or the corresponding 90° specimens tested at room temperature. This was expected because the 90° specimens are matrix dominated. Failure of these specimens was parallel with the fibers with little or no damage away from the actual failure.

(3) 0 Degree Compression Specimen Tests. The first two 0° compression specimens tested failed below expected levels and at significantly different values. We concluded that the tabs must have slipped even though in post test inspections no tab slippage was obvious (we later determined that the tabs readhered while the specimen cooled in the test fixture). A different tab adhesive (see Appendix D) was used to attach tabs to the first specimen tested and the specimen was retested. The failure was about at the expected value and resulted in a clean break of the specimen. Therefore, all of the remaining specimens were retabbed using the new tab adhesive. None of the tabs on the remaining specimens slipped. The stress strain curve for the 0° compression specimens at 250 F were identical to the room
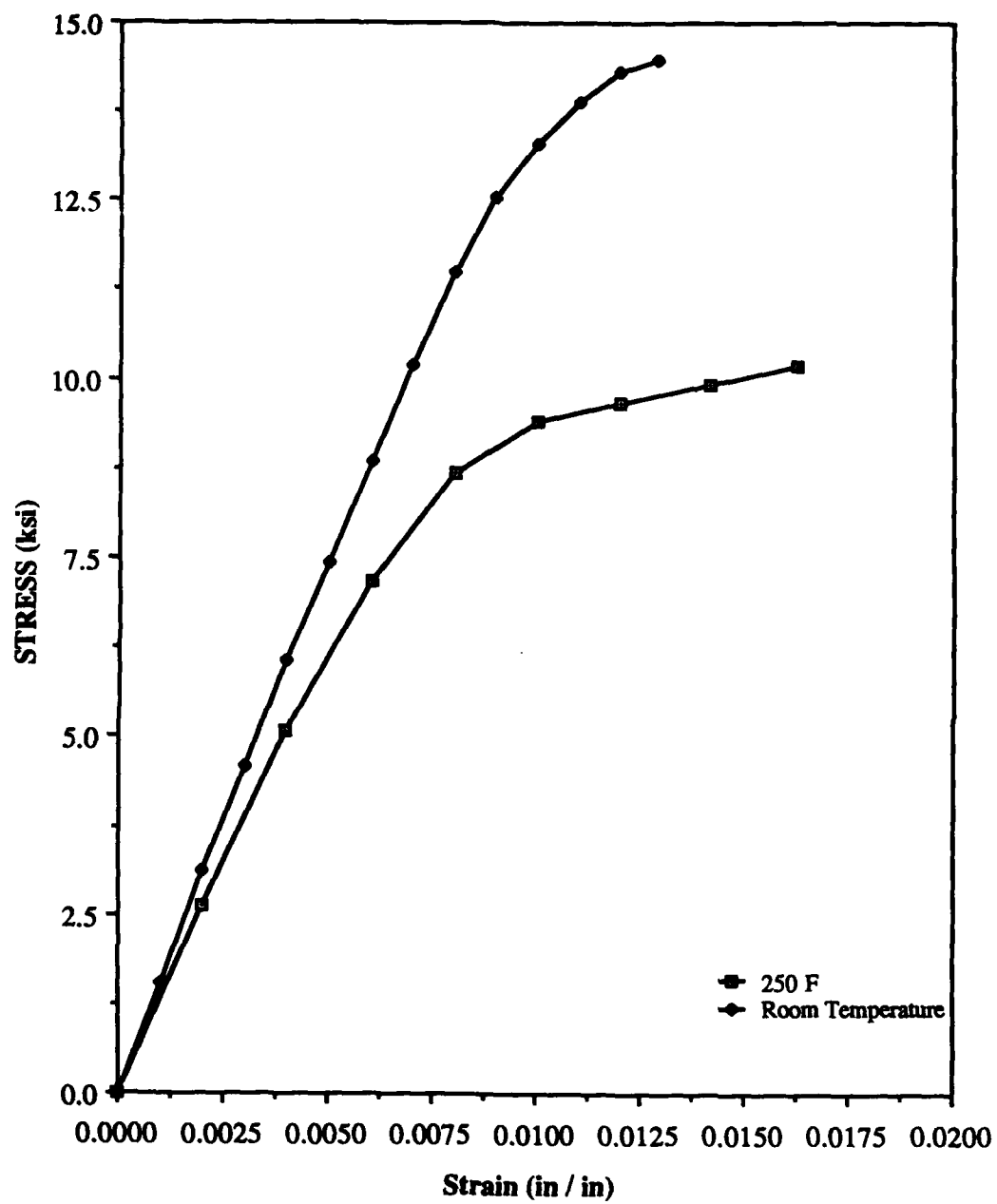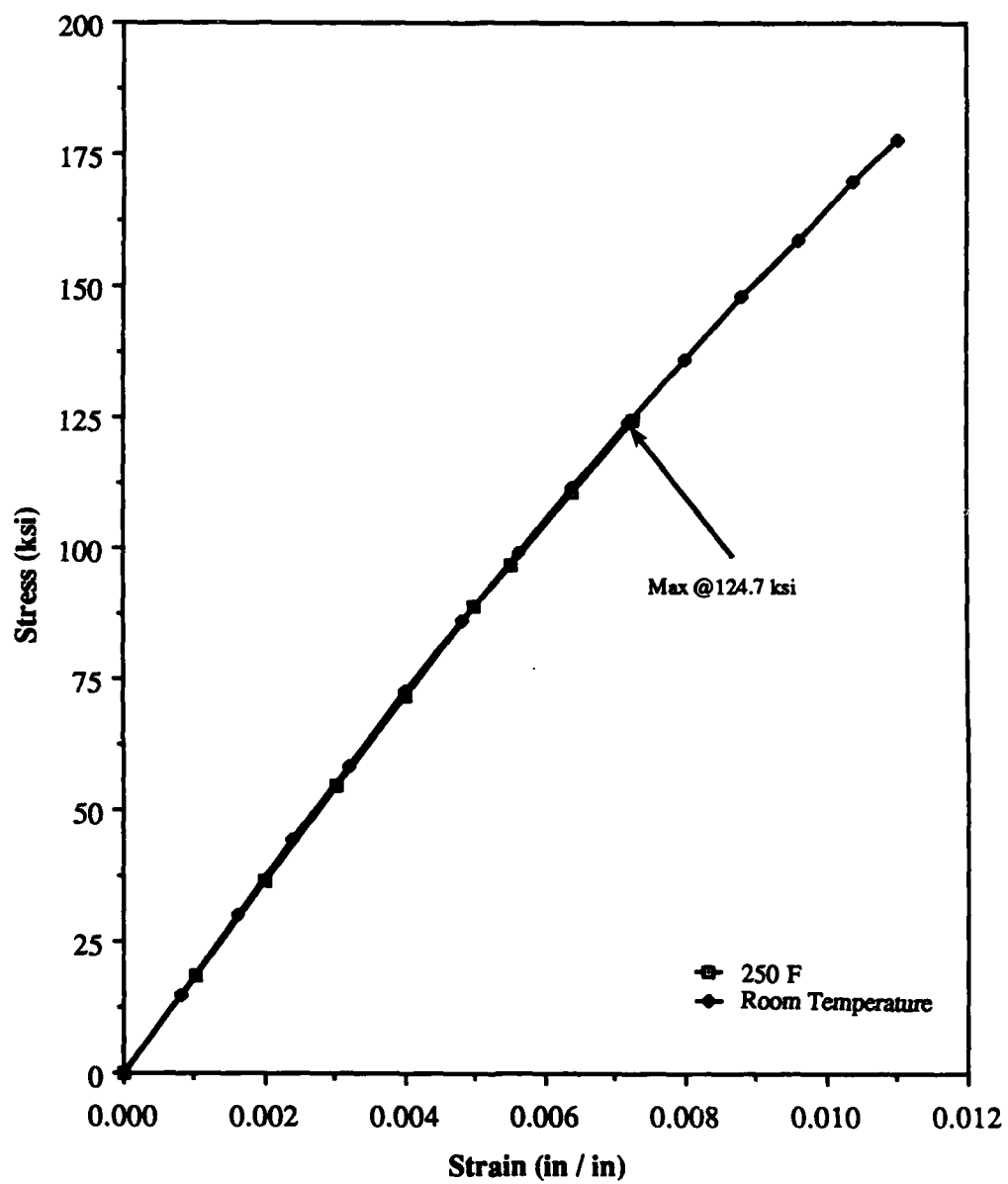
5-5

Figure 5-2. E_2^t Curve

Figure 5-3. E_1^c Curve

temperature specimens except that the 250 F specimens failed
at much lower stresses. The similarity in the curves resulted
from the fiber dominated ply lay up of the 0° compression
specimens. The lower ultimate failure resulted from the
inability of the heated (and consequently weakened) matrix to
restrain the fibers in compression.

(4) 90 Degree Compression Specimen Tests. After having
worked out the tab slippage problem with the 0° compression
specimens, all of the 90° compression specimens failed
without any problems. Being a matrix dominated ply lay up,
the stress strain curve was substantially more nonlinear
than the room temperature stress strain curve.

(5) ±45 Degree Shear Specimen Tests. Several problems
developed in testing the $\pm 45^\circ$ shear specimens because of the
high strains and the high temperature. These specimens
deformed in the load direction as much as 40% of the
original length before failure. One major problem
was that the high elongation gages on the shear specimens
would not stay attached until the specimen failed. The first
specimen was tested with 0.25 in wide, high elongation gages
(Electrix Industries PAHE - 03 - 250RB - 350 LEN) but the
gages failed before more than 3% of the total elongation was
reached. After using .125 in wide gages (Electrix Industries
PAHE - 03 - 125RB - 350 LEN) with only marginally better
results, .0625 in wide gages (Electrix Industries PAHE - 03 -
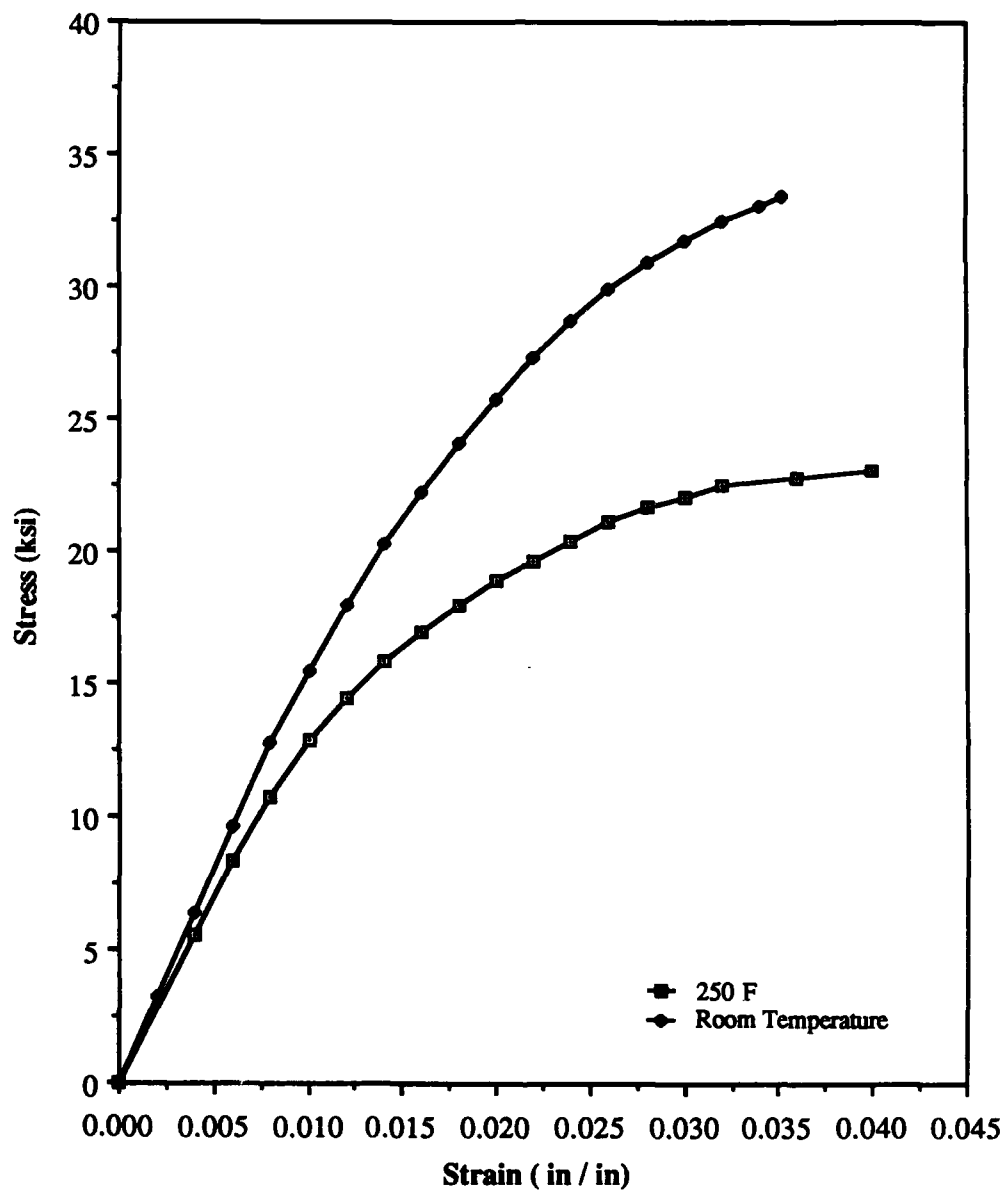062RB - 350 LEN) provided the best results. The gage backing

Figure 5-4. E_2^c Curve

on the .0625 in wide gages began peeling off at about 8

percent elongation. After the gage backing began peeling off,

the legs of the gage would fail one at a time until all the

legs were gone (by 12 percent elongation). A significant

amount of the deformation was due to the scissoring of the

fibers (the rotation of the fibers in line with the load).

As discussed in Chapter 3, this scissoring effect induces

error into the data because of the change in angle of the

fibers. To determine the magnitude of the error with respect

to the load, a shear specimen was marked with an X

corresponding to the fibers and slides were taken of the

specimen and a voltmeter as the specimen was tested. The

voltmeter was connected to the leads of the strip chart and so

indicated the same load as the strip chart. A sample of these

slides are included in Figures 5-6 through 5-9. Figure 5-6

also contains an illustration of the contents of the

photographs in Figures 5-6 through 5-9. A completely failed

specimen is shown in Figure 5-10. The change in angle (shear

strain) was measured for each slide and plotted versus the

load and the error due to scissoring in Figure 5-11. Shear

strain is plotted on the left vertical axis versus shear

strain and the error is plotted on the right vertical axis

versus shear strain. For example, if you were interested in

the error associated with a 10 ksi load you would first read

the strain associated with a 10 ksi load (.1) then read the

error associated with that strain (2 %). The maximum load,

where the gages would measure strain, was 1100 to 1500 lbs. This corresponds to 5 to 10 degrees of fiber rotation and 2 to 3 percent error as defined by the fiber rotation discussed in Chapter 4 and plotted in Figure 5-11. Any data collected beyond this point is suspect because the error increases substantially, as depicted in Figure 5-11.

Figure 5-5. G_{12} Curve
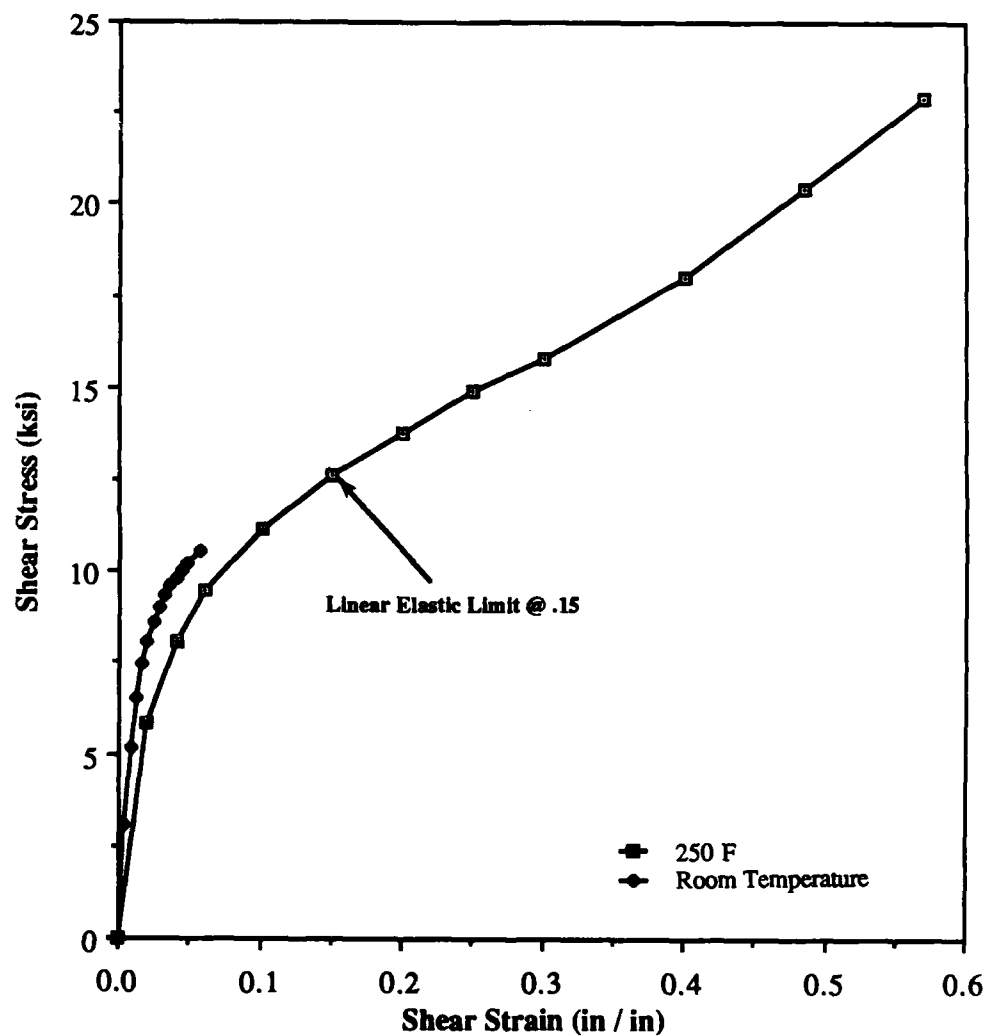
Tape Securing Door
Tape securing fixture to upper jaws
Top Plate
Thermocouples (secured with pad and alligator clip)
Specimen With Cross
0.010
Voltmeter
Access door (overlap over Chamber)
Resette
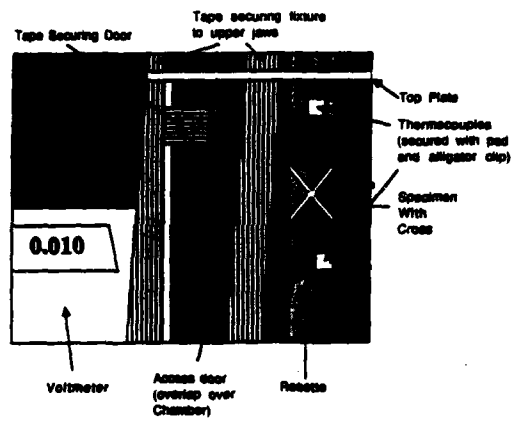
(a) Illustration

(b) Photograph

Figure 5-6.   Cross at 0 Load

Figure 5-7. Cross at 2300 lbs Load

Figure 5-8. Cross at 2400 lbs Load

Figure 5-9. Cross at 4100 lbs Load
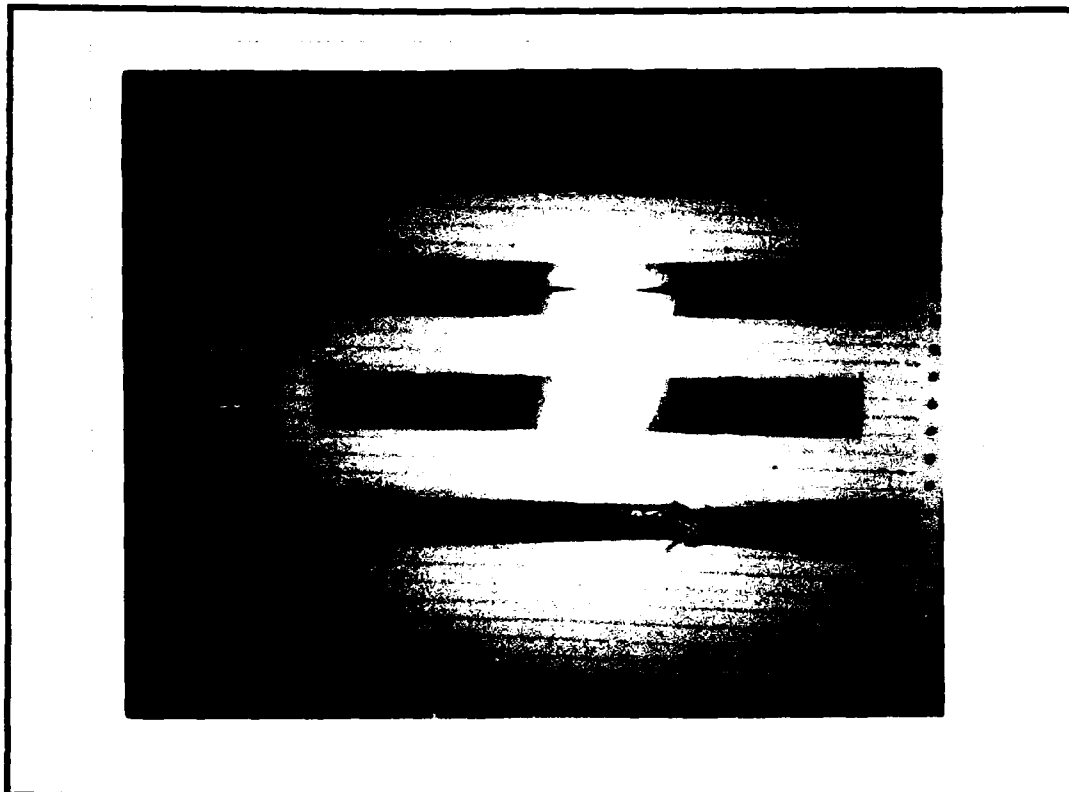
Figure 5-10. Failed Shear Specimen

This was fortunate because any strain measurements at higher
stresses can not be made using strain gages.

To assess how accurately the cross painted on the
shear specimen measured shear strain, the cross shear strain
was plotted with the shear strain measured with the strain
gages in Figure 5-12. The cross shear strain agreed quite
well with the strain gage data until .15 in/in. This point
corresponds to where significant error is introduced into
the strain gage data because of the scissoring of the fibers.
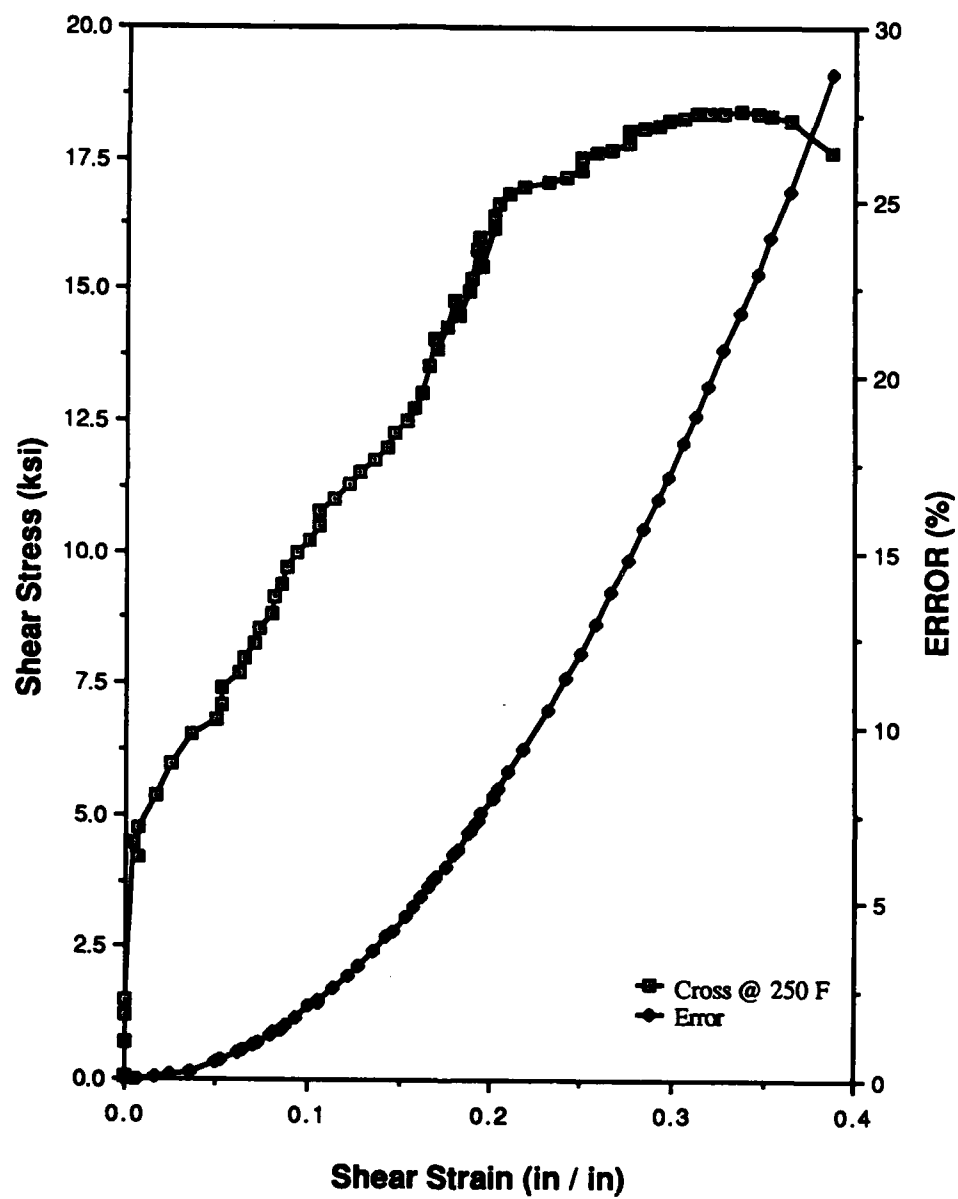
Figure 5-11. Shear vs Error
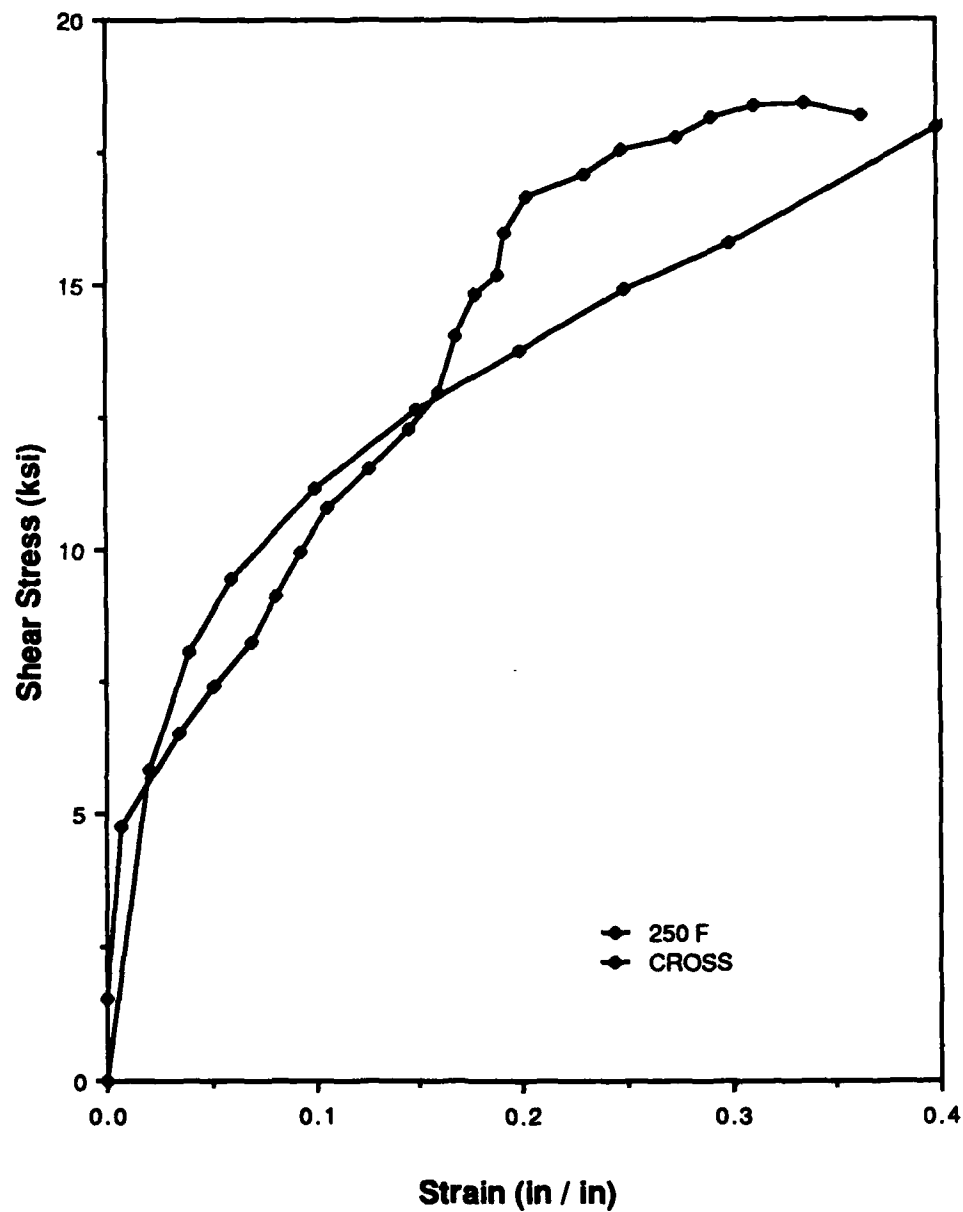
Figure 5-12. Comparison of Data From Gages and Cross

(f) <u>Poisson's</u> <u>Ratio</u> <u>Curves</u>. As discussed in Chapter 4, the Poisson's ratio curves were derived from E_1^t and E_1^C. These curves are shown in Figures 13 and 14.
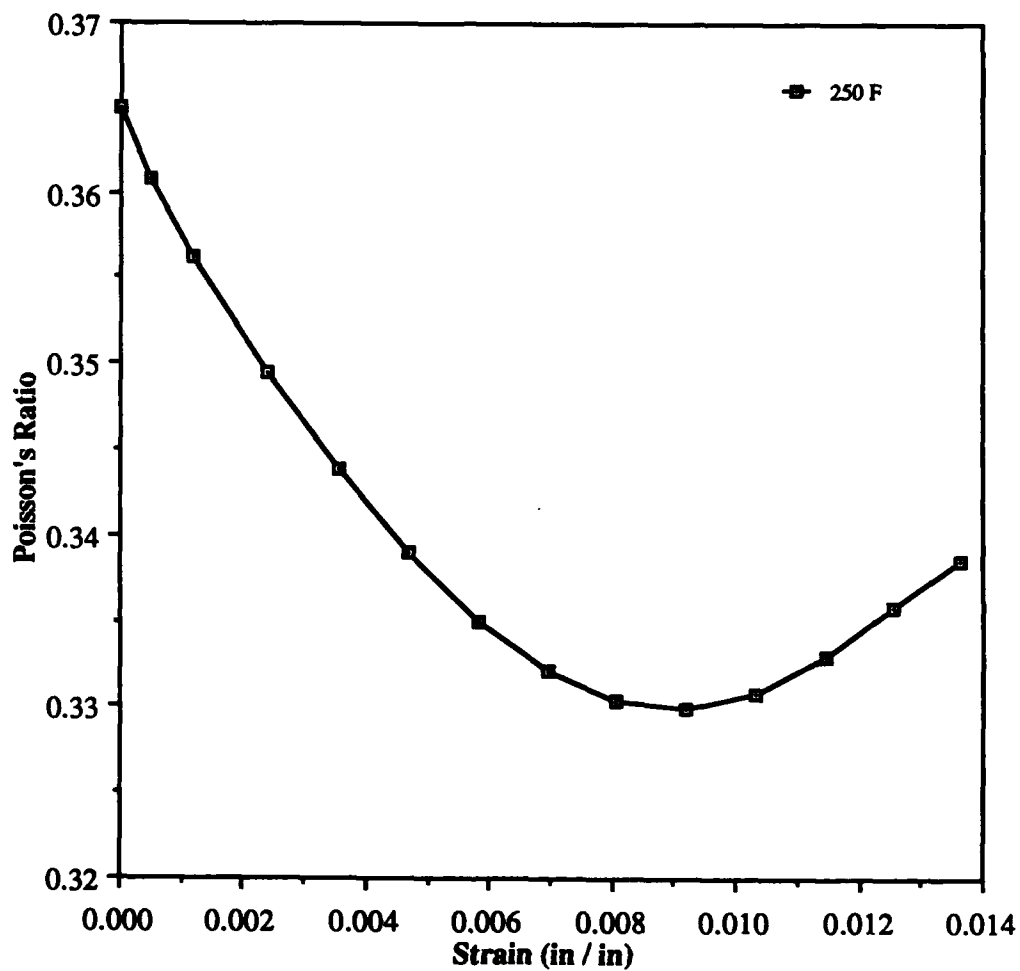
Figure 5-13. ν_{12}^t Curve
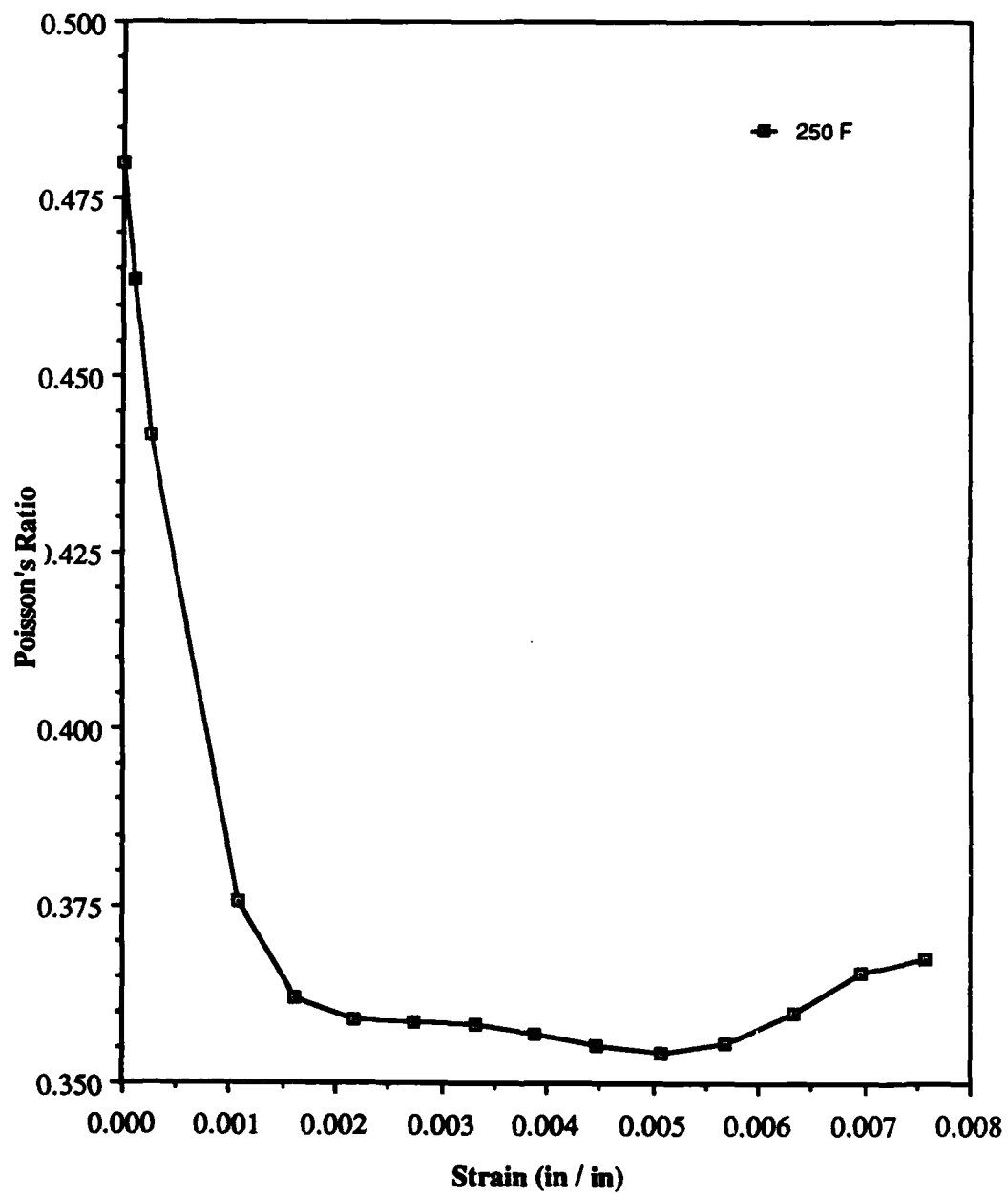
Figure 5-14. ν_{12}^c Curve

Having the tabular basic properties, the only remaining material parameters required for PLSTREN are the initial elastic constants. These constants are provided in Table 5-1 for both 250 F and room temperature as a comparison.

Table 5-1. Elastic Engineering Constants

Constant	Room Temperture	250 F
E_1^t	19.5×10^6 psi	20.9×10^6 psi
E_1^c	18.75×10^6 psi	18.4×10^6 psi
E_2^t	1.55×10^6 psi	1.31×10^6 psi
E_2^c	1.60×10^6 psi	1.40×10^6 psi
G_{12}	$.8125 \times 10^6$ psi	$.292 \times 10^6$ psi
ν_{12}^t	.305	.365
ν_{12}^c	.34	.480

B. **Results of Ultimate Tensile Strength Tests**. This section contains all of the results from the study of the progression and ultimate failure of the test specimens. There are four sections, each corresponding to the different ply lay-ups studied. Each of these subsections compares and contrasts the experimental and analytic results from this study. The

5-21

stress-strain curves and the ultimate strength of each of the four ply lay-ups was derived by testing three specimens to failure. Equipment set-up and specimen geometry are described in Chapter 3. The data collected from these tests included: stress-strain data from both the stacked rosettes at the hole and the far field gages near the tabs, regular speed video, and high speed video.

(1) [0] Ultimate Tension Specimens With Holes. A total of five [0] specimens were tested: three with gages attached and two without gages. Two problems with this testing were discerning what constituted failure in these specimens and getting good pictures of the failure with the video camera.

The failure of the $[0]_{16}$ specimens was very similar to the type of failure observed at room temperature [9]. The behavior of these specimens was repeatable to a certain point, then varied from specimen to specimen. This point corresponded to an instantaneous (but only partial) unloading indicated on the strip chart. When the specimens were inspected immediately after the unloading, splitting had propagated the length of the specimens as depicted in Figure 5-15. The resulting specimen was actually three distinct specimens not affected by any stress concentrations from the hole. Consequently, this unloading was defined as failure and the resulting stress strain curves are depicted in Figure 5-16.
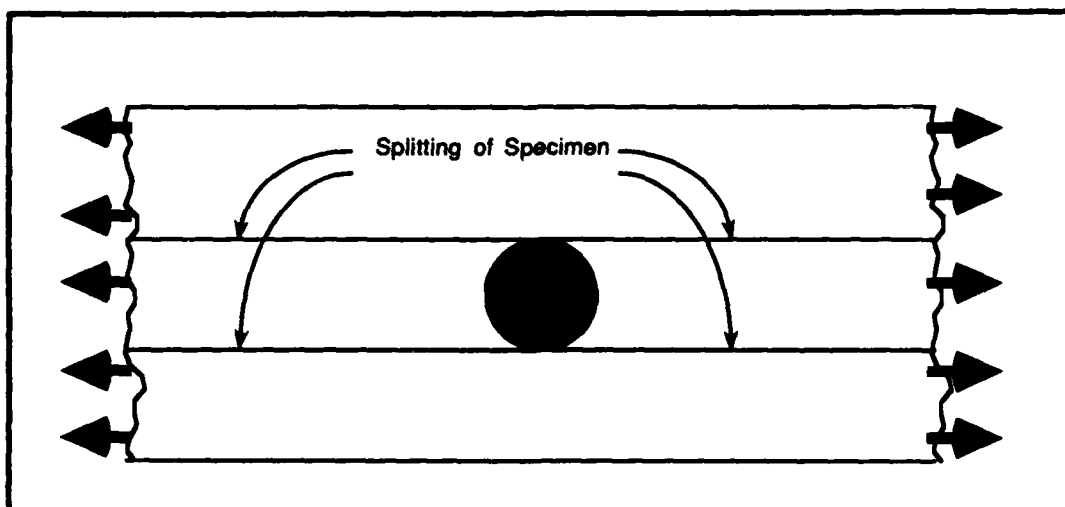
Figure 5-15. Splitting of 0° Specimens

The analytic stress strain curve for a point coincident with the experimental results is also in Figure 5-16. The predicted failure from the nonlinear FE code was 17% lower than experimental. The slope of the transverse strain is fairly well correlated with experimental but the longitudinal strain is not. The splitting of the specimen experimentally is caused by the material on the side of the hole attempting to neck. This necking is what initiates the crack in the matrix in the direction of the fibers. The model chosen to analyze the specimen is poorly suited to replicate this phenomena. To verify this, the model depicted in Figure 5-17 was constructed. Note that all of the elements are oriented in the direction of the fibers and that the elements around the hole are not nearly as refined as the original model.

5-23
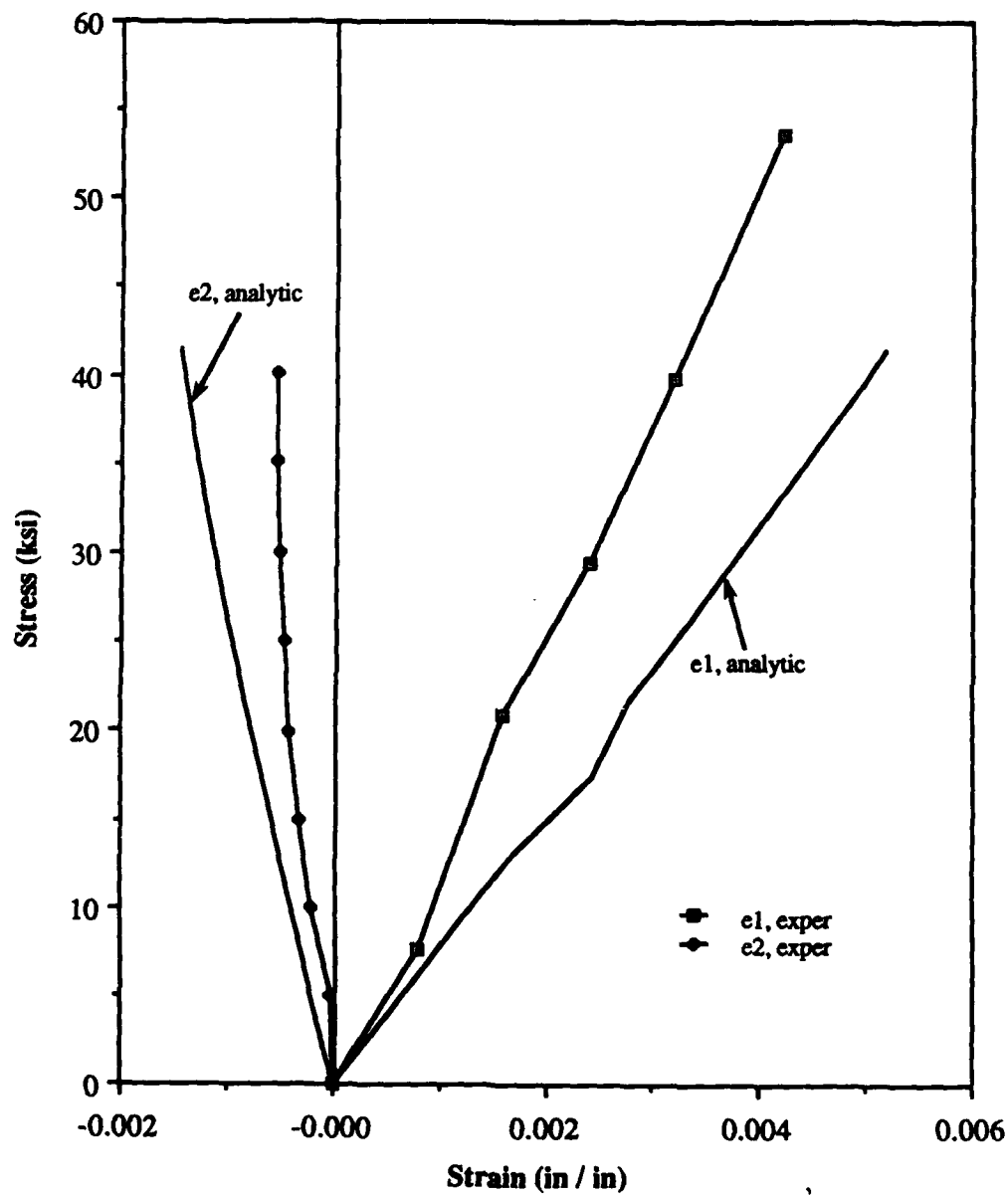
Figure 5-16. Stress Strain at Hole, [0]₁₆
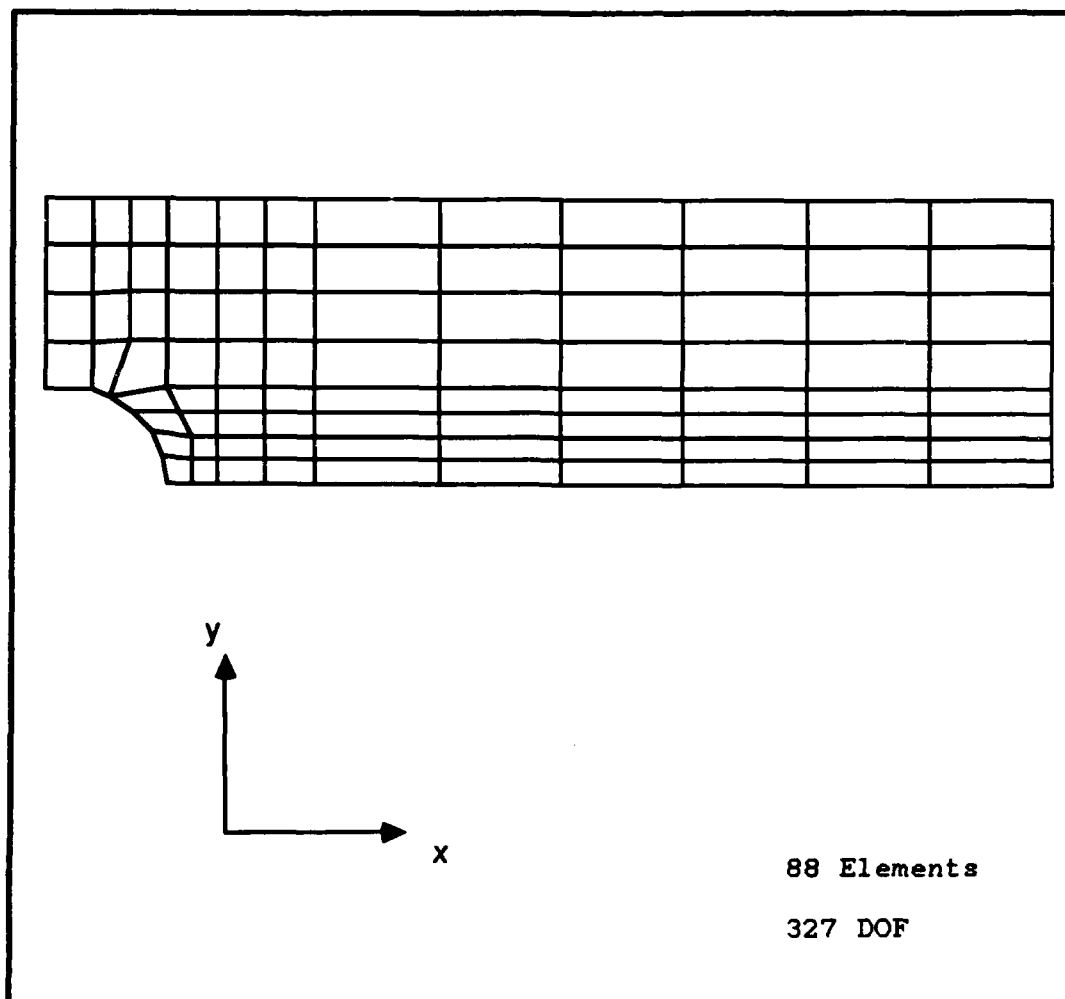
Figure 5-17. New $[0]_{16}$ Model

The resulting stress-strain curve for longitudinal strain is shown in Figure 5-18 for both models and experimental data. Note that even though the element refinement at the hole is not as good as the original model, the new model predicts failure only 3% higher than experimental and the predicted stress-strain curve is substantially closer to experimental.
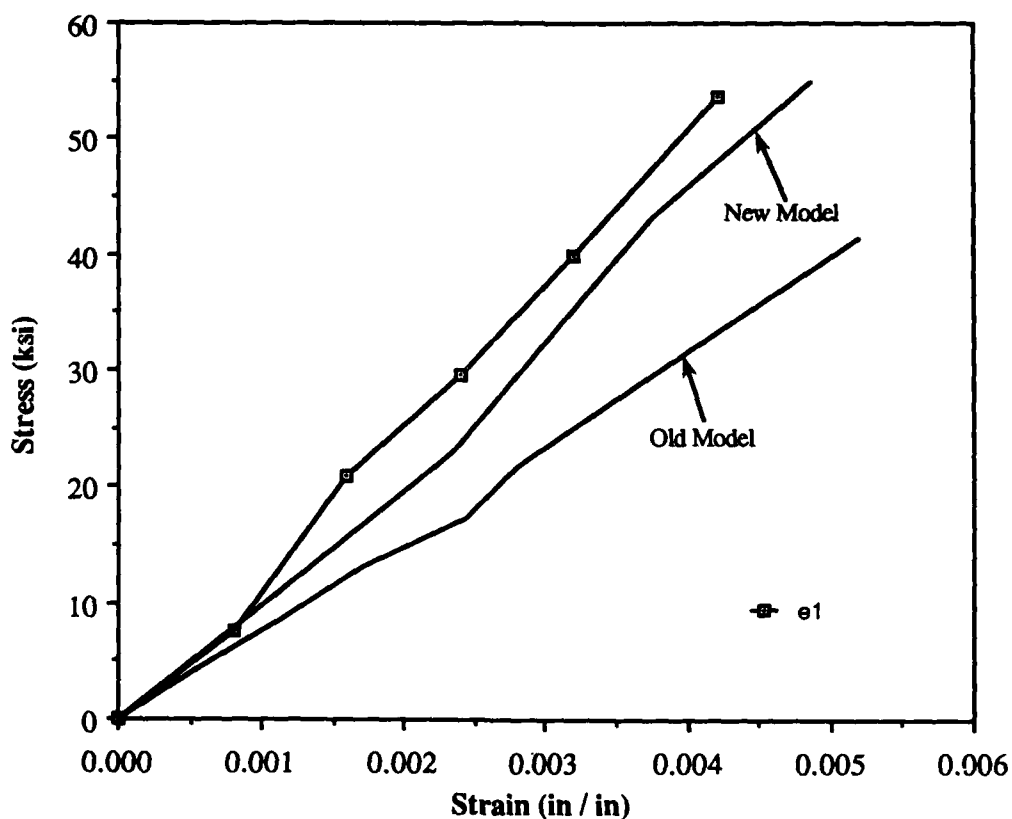
Figure 5-18. Comparison of New [0] Model

The progression of failure in these specimens was not very revealing because failure occurred so rapidly. As shown in the stereo x-rays in Figures 5-19 through 5-21, there is no preliminary indication of failure at any load level. This phenomenon is replicated in the progression of failure predicted by the FE model, as depicted in Figure 5-22. Once failure begins in this ply lay-up experimentally, the specimen fails completely. In the model, the progression of

5-26

failure occurs in each iteration while the stresses are distributed to surrounding elements after an element has failed. This translates as catastrophic failure of the model. Unfortunately, this unloading model is too drastic and results in gross failure of elements that do not accurately depict the mode of failure. For the original model, this catastrophic failure occurs at 82.7 of the ultimate tensile (UT) strength of the specimen determined experimentally. This same type of catastrophic failure can be shown for the new model, except at 103 % of UT.
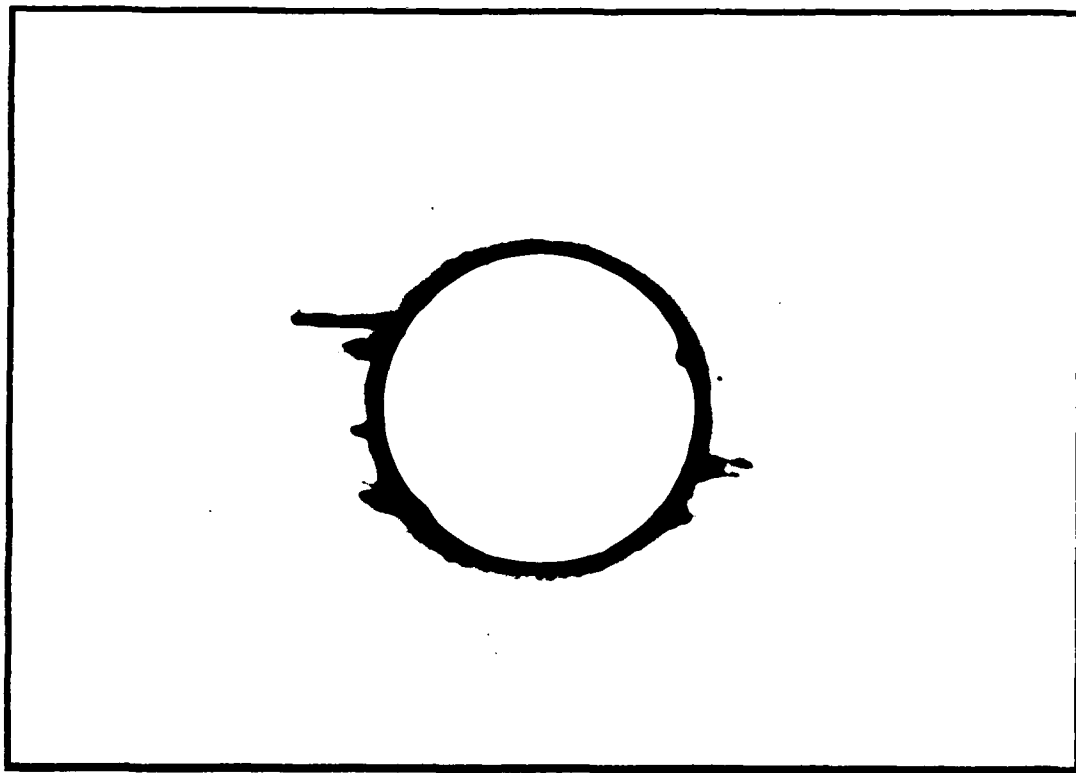
Figure 5-19. Stereo X-Ray at 75% UT, $[0]_{16}$
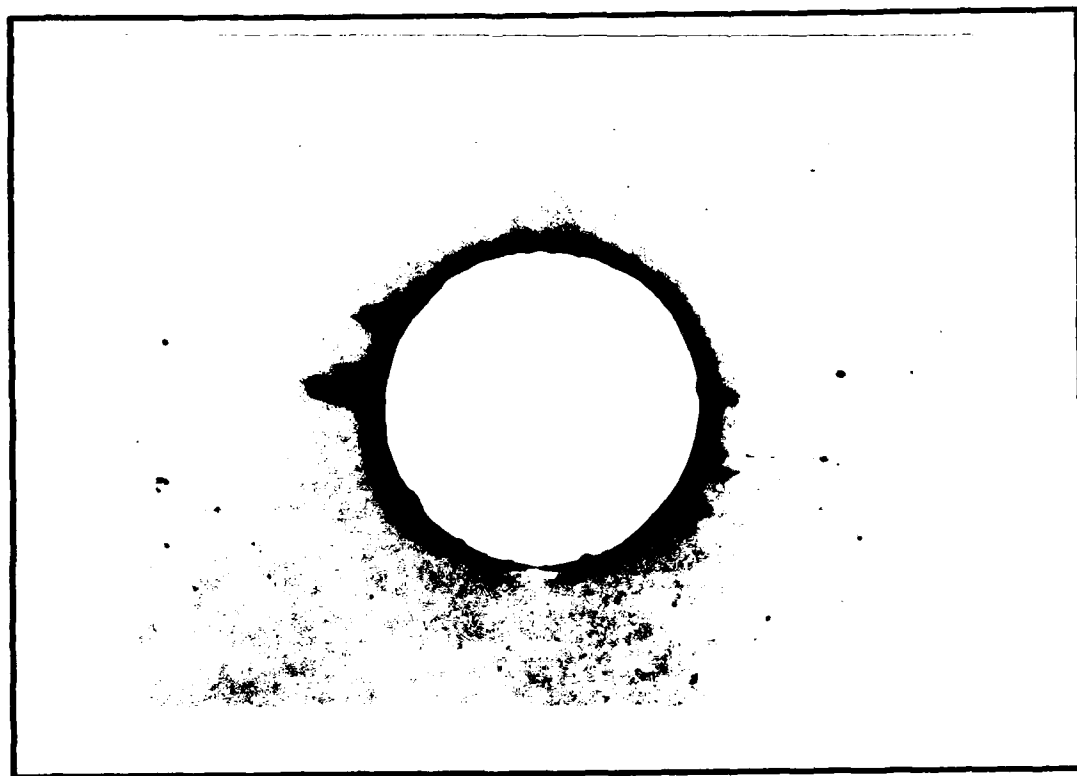
Figure 5-20.   Stereo X-Ray at 85% UT, [0]$_{46}$
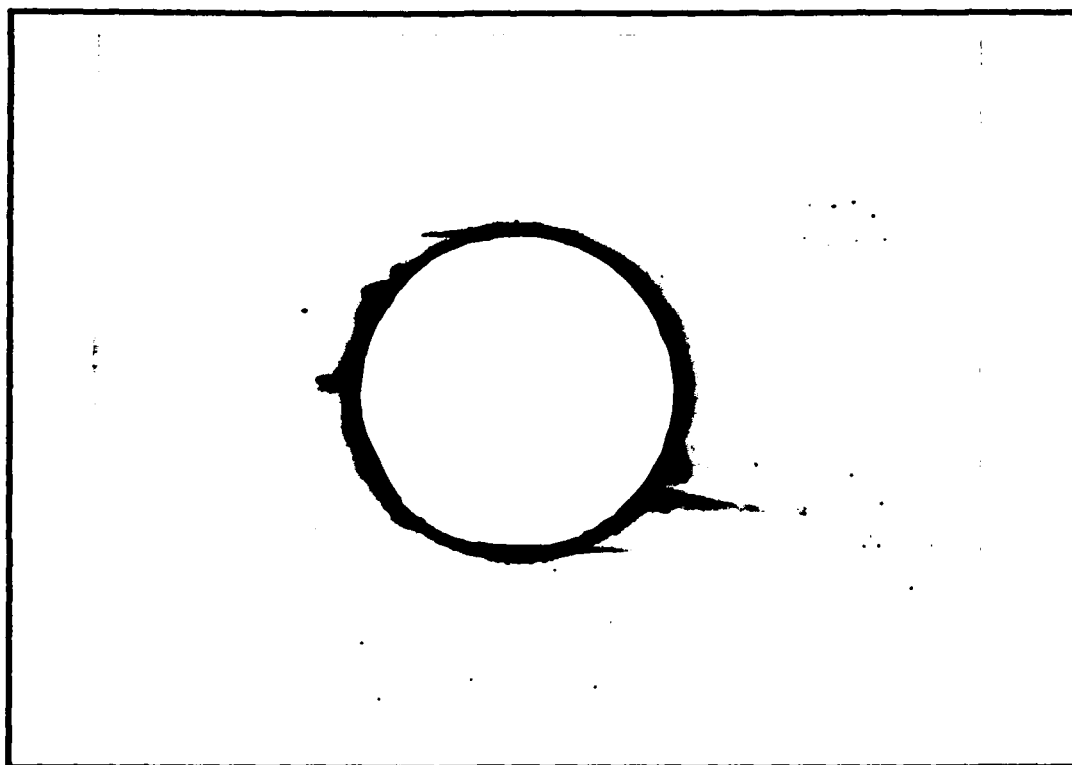
Figure 5-21.   Stereo X-Ray at 95% UT, [0]$_{16}$

Note: All failed elements are blacked out. All
elements failed at 82.7 % of UT.

Figure 5-22.   Failure Progression, $[0]_{16}$

An excellent technique for analyzing failure of the
specimen was monitoring the deformation of the model
incrementally. This was accomplished by transferring the
tape 9 file from the CYBER to the FDL VAX and plotting (and
saving) the deformed shapes on a McIntosh computer. The
program used to plot the deformed shapes was able to amplify
the dimensions of the deformations to accentuate movement.
All deformations shown in this thesis were multiplied by 10.
These deformed shapes could be regenerated at any time for

comparison. Figure 5-23 contains samples of these deformed shapes starting from the first increment.

Failure of these specimens occurred when cracks propagated the length of the specimen, but the only visible indication of this failure was an instantaneous reduction of load on the strip chart. Attempts to film the phenomenon with both the regular and high speed video were not successful because of the speed and nature of the failure. The speed of the crack propagation dictated a high frame rate on the high speed video. These high frame rates are at the expense of photographic resolution. When failure occurred the poor resolution and the nature of the failure resulted in videos where the crack propagation could not be discerned.

(2) 90° Ultimate Tensile Strength Specimen. The stress strain curve of the element near the hole was derived by testing three specimens. Unlike the 0° specimen, failure of these specimens was easy to discern and to videotape.

The stress strain curve recorded from the stacked rosettes is in Figure 5-24. The correlation between both experimental and analytic stress strain curves was excellent. There was essentially no difference until 75% of UT and was less than 8% off at the worst case (at failure).

Progression of failure occurred very rapidly with these specimens, as with the $[0]_{16}$ specimens. However there is an indication that failure is about to occur. The stereo x-rays

5-31
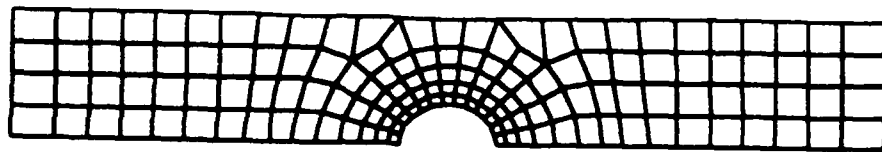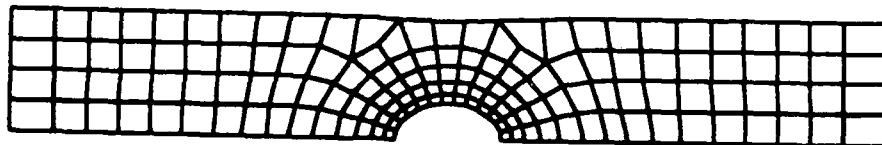
Model at 7.3% UT

Model at 76.5% UT
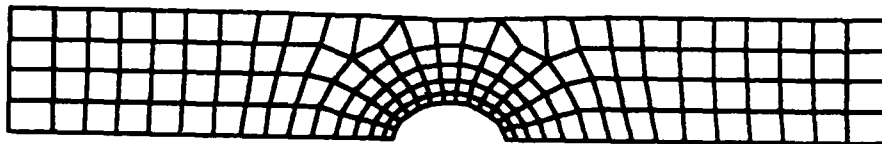
Model at 82.7% UT
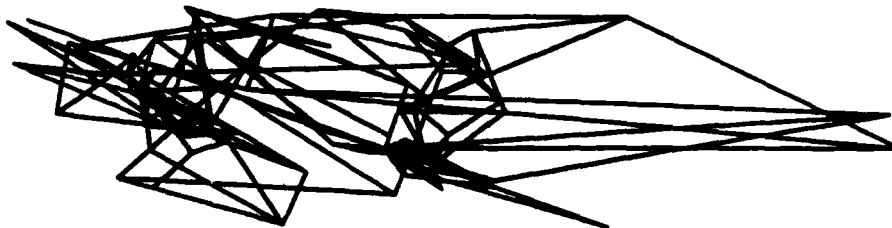
Model at 85.4% UT

Note: all deformations shown at 10X actual except 85.4% UT model

Figure 5-23. Deformed Shape of $[0]_{16}$ Model
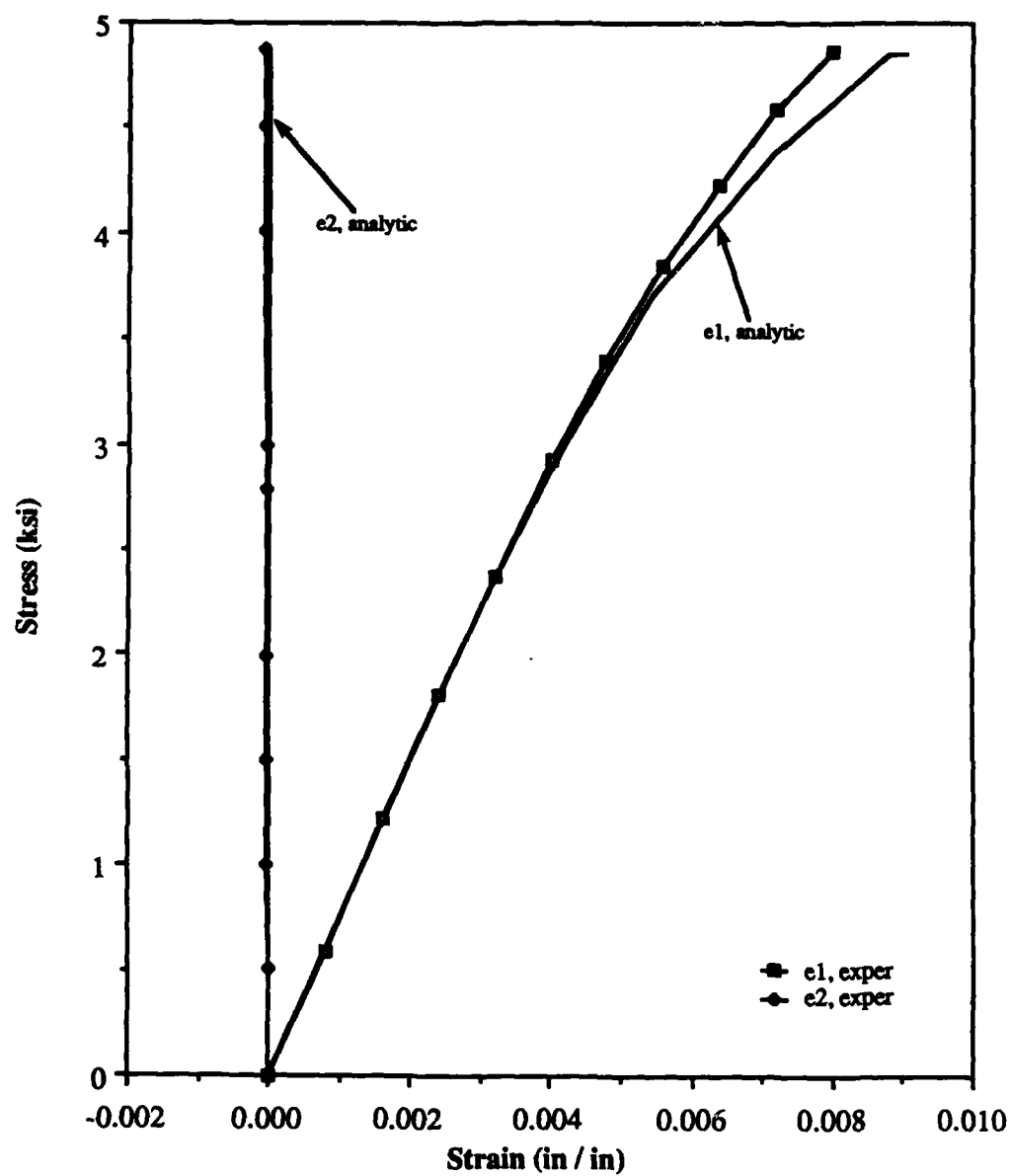
Figure 5-24. Stress Strain at Hole, $[90]_{16}$
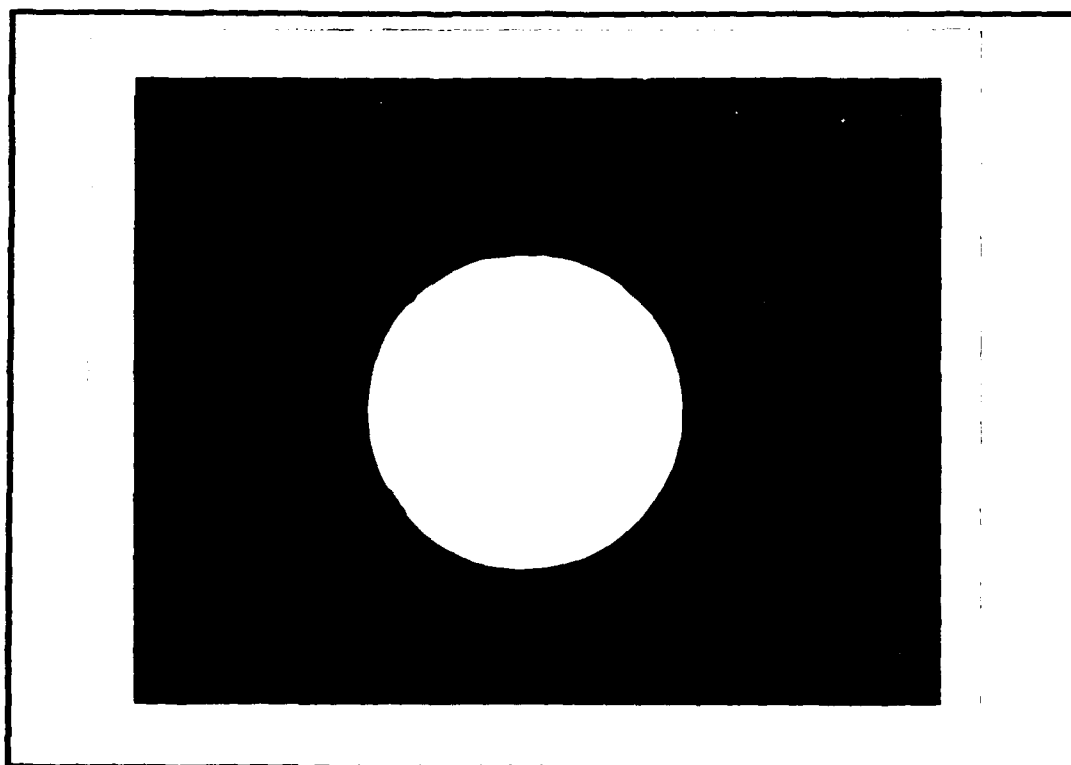
Figure 5-25. Stereo X-Ray at 70% UT, [90]₁₆
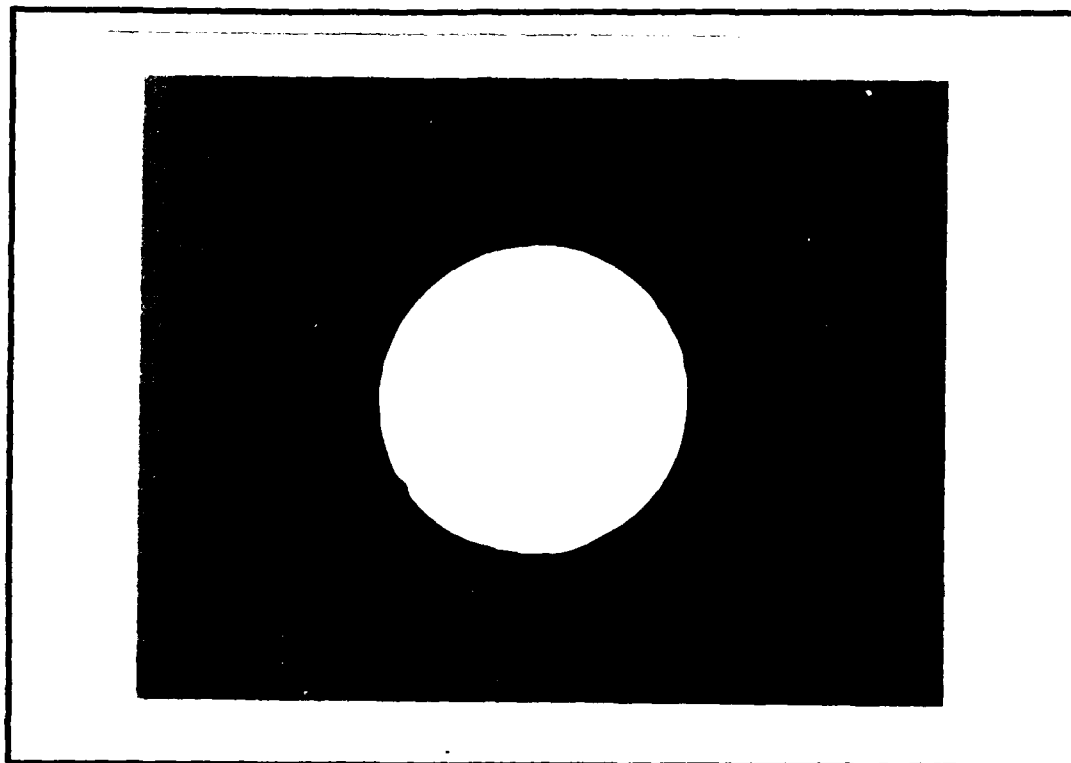
Figure 5-26.   Stereo X-Ray at 80% UT, $[90]_{16}$
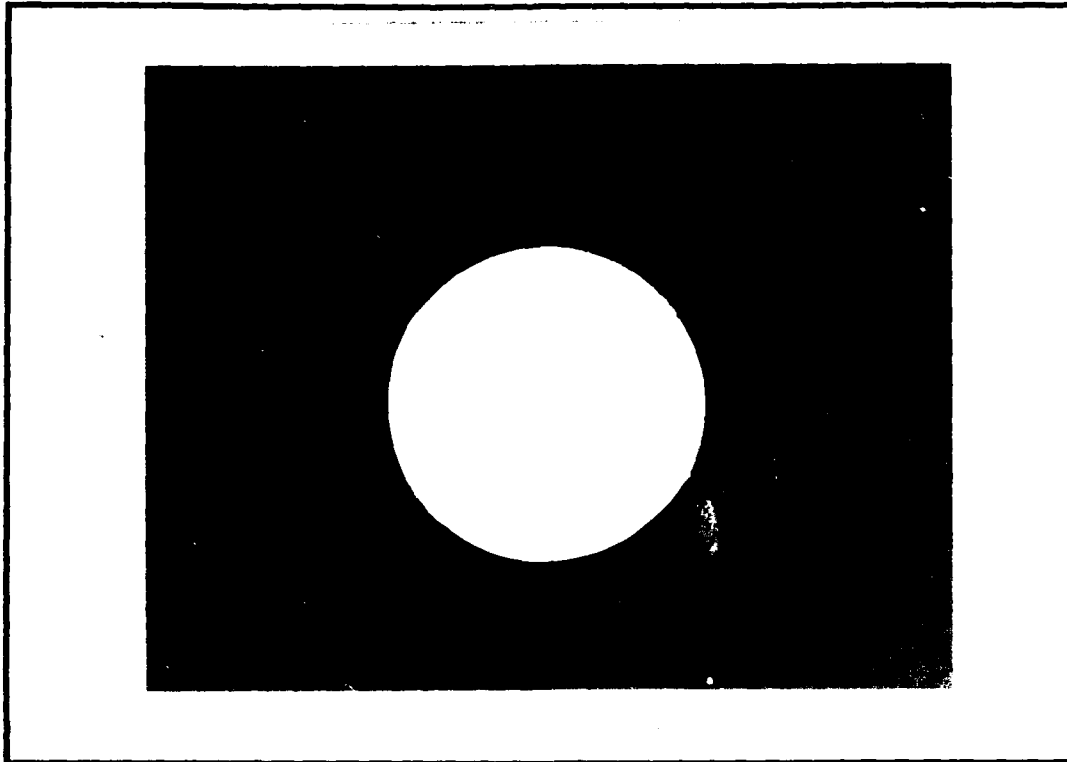
Figure 5-27. Stereo X-Ray at 90% UT, $[90]_{16}$

for specimens at 70%, 80%, and 90% of ultimate failure are
shown in Figures 5-25 through 5-27. Although there are no
damaged areas at 70% or 80%, there is an area at 90% that
indicates that failure is about to occur. Note that the
damaged area is isolated to one side of the specimen. The
damage zone did not correlate that well with the zone
predicted analytically. Consequently, the model was
reevaluated using the tangent modulus unloading scheme. Both

of these predicted failure zones are in Figure 5-28. The
instantaneous unloading predicts a substantial amount of
damage early in the loading and primarily in the load
direction. According to the stereo x-rays, this is not
appropriate. The negative tangent modulus unloading scheme
predicts some initial failure just prior to complete failure,
which is appropriate.

As with the $[0]_{16}$ specimens, the deformed shapes of the
model were viewed after each increment. Samples of these
deformed models are included in Figure 5-29. The deformed
shapes don't indicate failure as clearly as with the $[0]_{16}$
specimen, but the solution fails to converge after 105.9% of
UT which was taken as failure.

The high speed video of the specimen failure
demonstrated how rapidly failure occurred. The failure of
the first two specimens was missed for a variety of reasons,
including the inherent unreliability of the high speed video
camera and the exceptionally small time window for the high
frame rate desired (at 2000 fps only 30 s of tape is
available for any single tape). The failure of the third
specimen was taped at 1000 frames per second (fps) but this
proved to be too slow because all that could be seen during
replay was before and after images. A fourth specimen
(ungaged) was taped at 3000 fps to try and get better
results. Still shots of these images are included in Figure
5-30 through 5-32. Figure 5-30 also contains an illustration

5-37

of the photographs in Figures 5-30 through 5-32. At this
frame rate the camera is recording three distinct images per
frame so even though the frames are at 1000 fps, the images
are recorded at 3000 fps. These images do seem to show the
opening of the crack, but the poor photographic resolution at
this frame speed hinders any quantitative analysis.

These photographs in Figures 5-30 through 5-32 require
some explanation. As depicted in the illustration, the image
actually contains three specimens per photograph. Vertical
lines were painted on the specimen using a silver paint pen in
an attempt to make measuring the velocity of the crack easier.
The horizontal lines are tape drop outs. Quite often tape
drop outs occur because the high speed tape recorder does not
have an erase head so tapes must be erased using a tape
degausser. The drop outs are a result of incomplete
degaussing. The numbers surrounding the image contain
information such as the test number and date. The upper right
hand corner contains the time measured in milliseconds. The
shiny surface in the picture is the aluminum heat reflector
reflecting the light. The diagonal line on the right side of
the specimen is the thermocouple attached to the specimen
using an alligator clip. The first image in which any
activity can be seen is the second image of Figure 5-30. A
very slight opening appears on the left side of the specimen.
This opening progresses through the remaining images until the
specimen is completely open in the last image of Figure 5-32.

Percent of UT

■ 90.5
● 94.5
▲ 95.1

(a) Instantaneous Unloading

Percent of UT

■ 90.5
● 105.9
▲ 107.6

(b) Negative Tangent Unloading
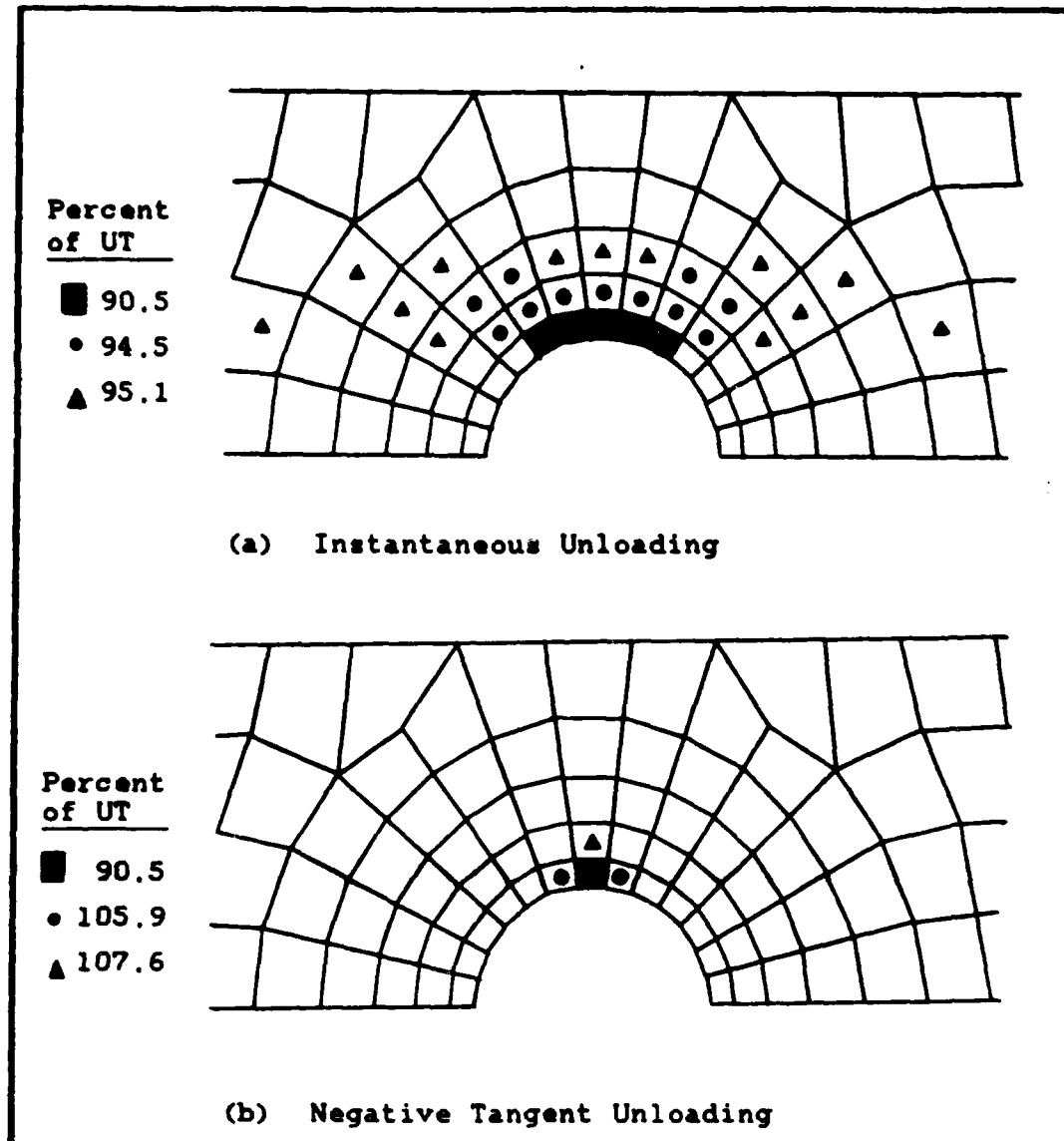
Figure 5-28. Failure Progression, $[90]_{16}$
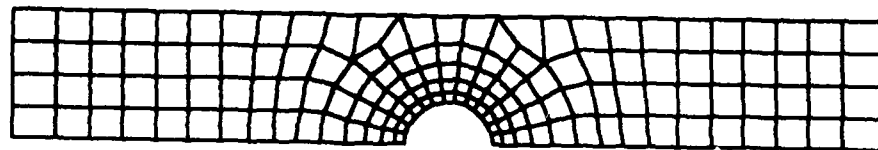
Model at 0 Load
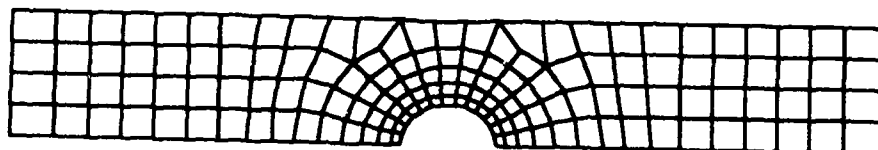
Model at 90.5% UT
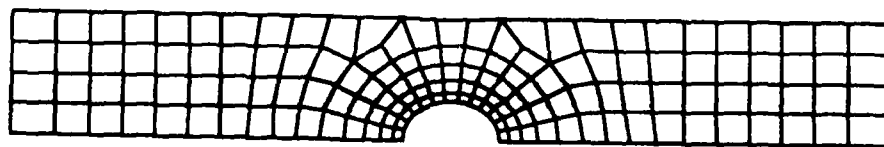
Model at 105.9% UT
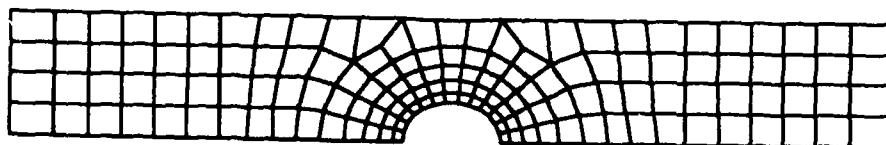
Model at 107.6% UT

Note: all deformations shown at 10X actual

Figure 5-29. Deformed Shape of [90]$_{16}$ Model
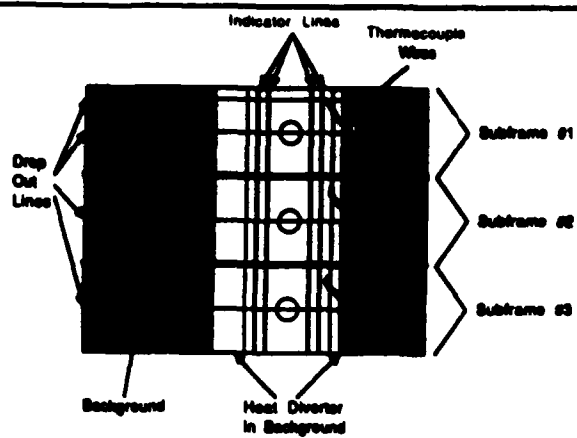
(a)   Illustration
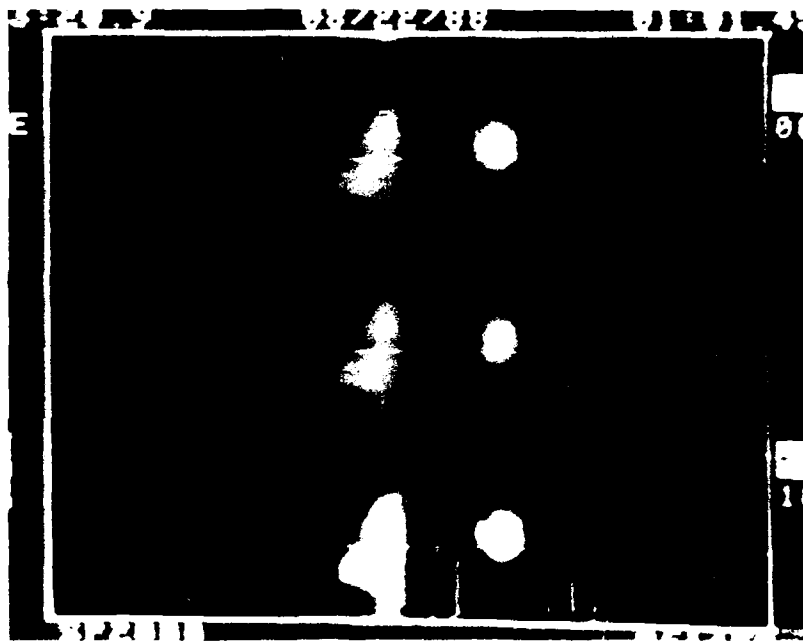

(b)   Photograph

Figure 5-30.   High Speed Video Images, Frame 1 - [90]$_{10}$
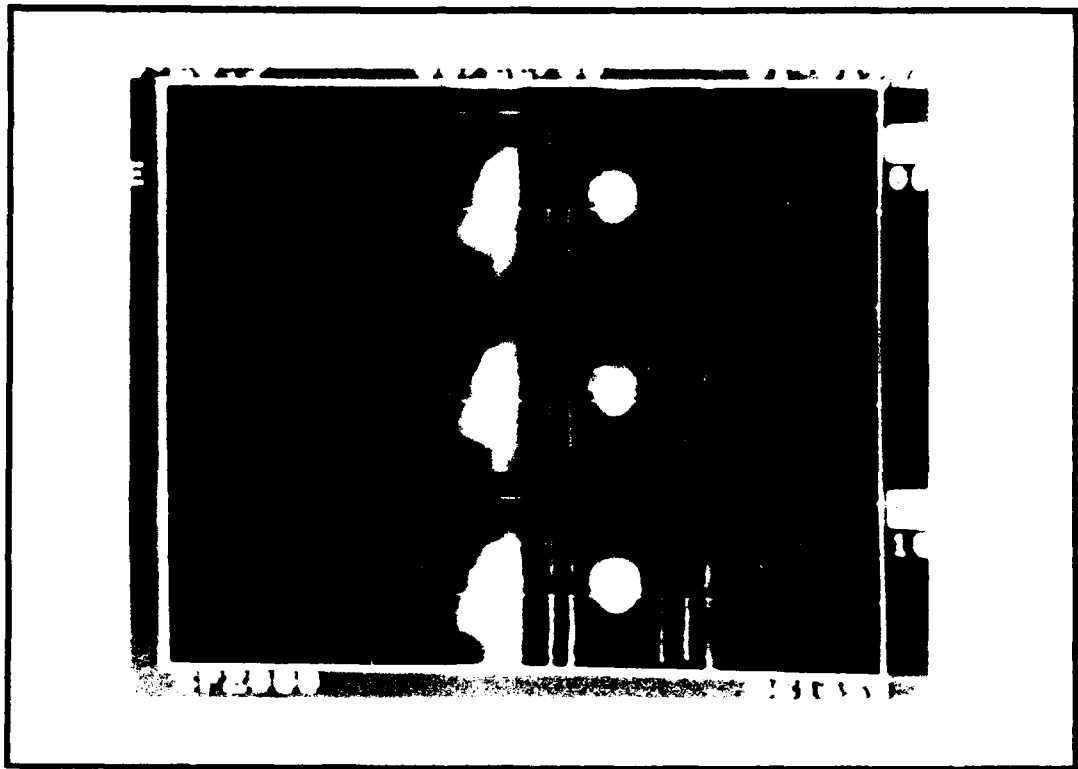
Figure 5-31.   High Speed Video Images, Frame 2 - [90]₁₆
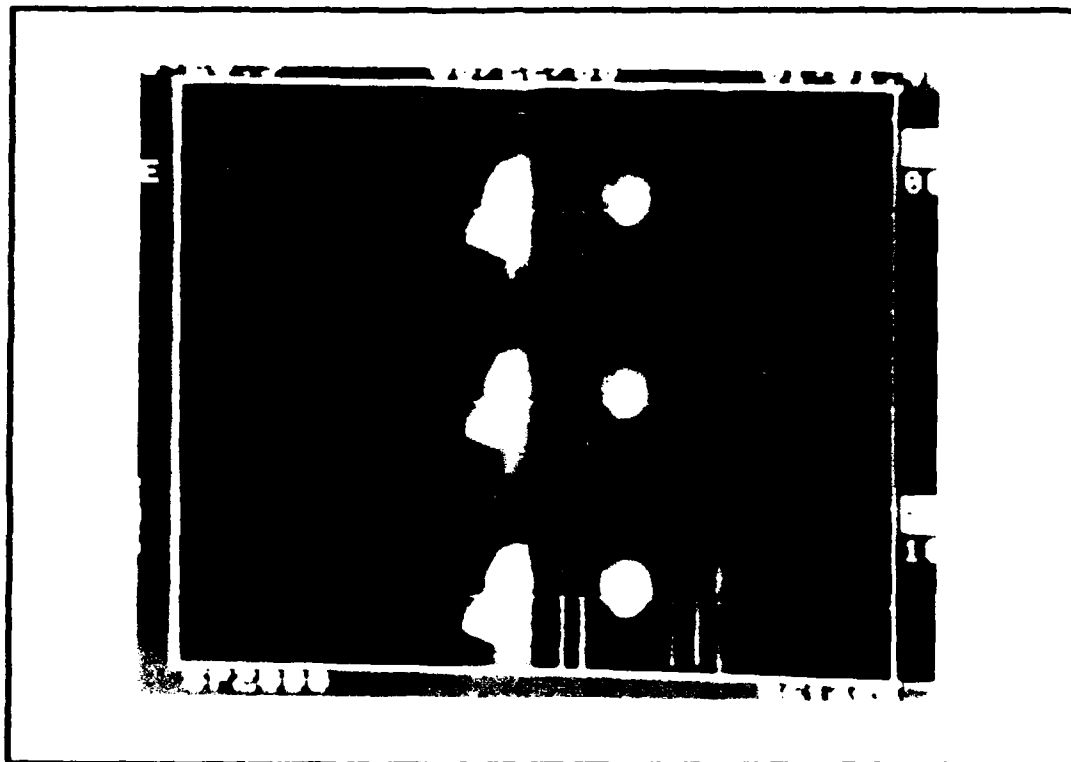
Figure 5-32. High Speed Video Images, Frame 3 – [90]$_{16}$

(3) ±45° Ultimate Tensile Specimen Tests. Three ±45°
specimens were tested to derive the stress strain curve of
the element near the edge of the hole. As with the basic
property shear specimens, the high strains for this ply lay-up
were too high for the gages to measure, as the rosettes at
the hole came, unglued at 25% of UT. For this reason, an
optical strain measuring technique was used as described in
Chapter 4. The stress-strain curve for both types (from
gages and the optical technique) of experimental data is in
Figure 5-33 along with the analytic stress strain results.
There is fairly good correlation between both experimental
techniques and the analytic results at lower load levels. At
higher loads, only experimental data from the optical optical
technique (one specimen only) is available and it reflects
substantially higher strains than are predicted analytically.
This difference is due to both the nonlinear strains and
possibly other sources. The nonlinear strains are very
apparent in the photographs taken for this technique. Figures
5-34 through 5-36 contain 4 in by 5 in samples of the
photographs used for these measurements. Figure 5-34 is taken
prior to any loading. Figures 5-35 and 5-36 are taken at 1350
lb and 1900 lb, respectively. Because the hole deforms
symmetrically, the center of the hole is used as a reference
for measurements. Note the movement of the hole. In Figure
35 the bottom of the hole has moved from 43 mm to 46 mm. In
Figure 36 the bottom of the hole has moved from 46 mm to 50mm.
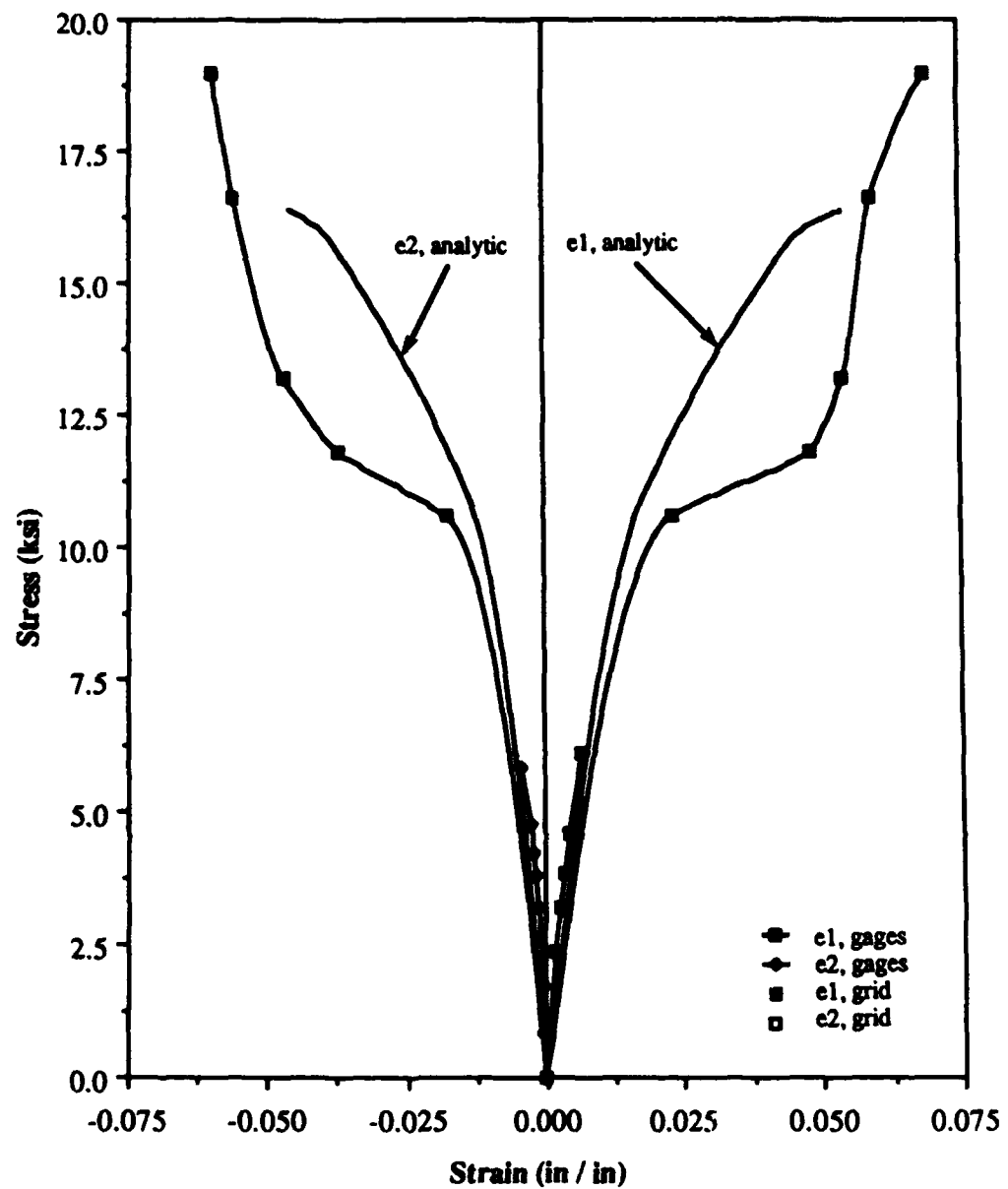
Figure 5-33.   Stress Strain at Hole, [±45]₄ₛ

The ruler was used as a reference for dimensions. The space
opening up between the ruler and the specimen was caused
primarily by the heat enclosure pushing the ruler out of
position and not just a result of the specimen necking. To
mitigate any errors in measurements, each of the dots used was
measured three times with the digitizer (see Appendix D). The
average of the three measurements was used to calculate strain
as described in Chapter IV. These strains are plotted in
Figure 5-33. For the basic property shear specimen, a
simple error analysis based on the rotation of the fibers
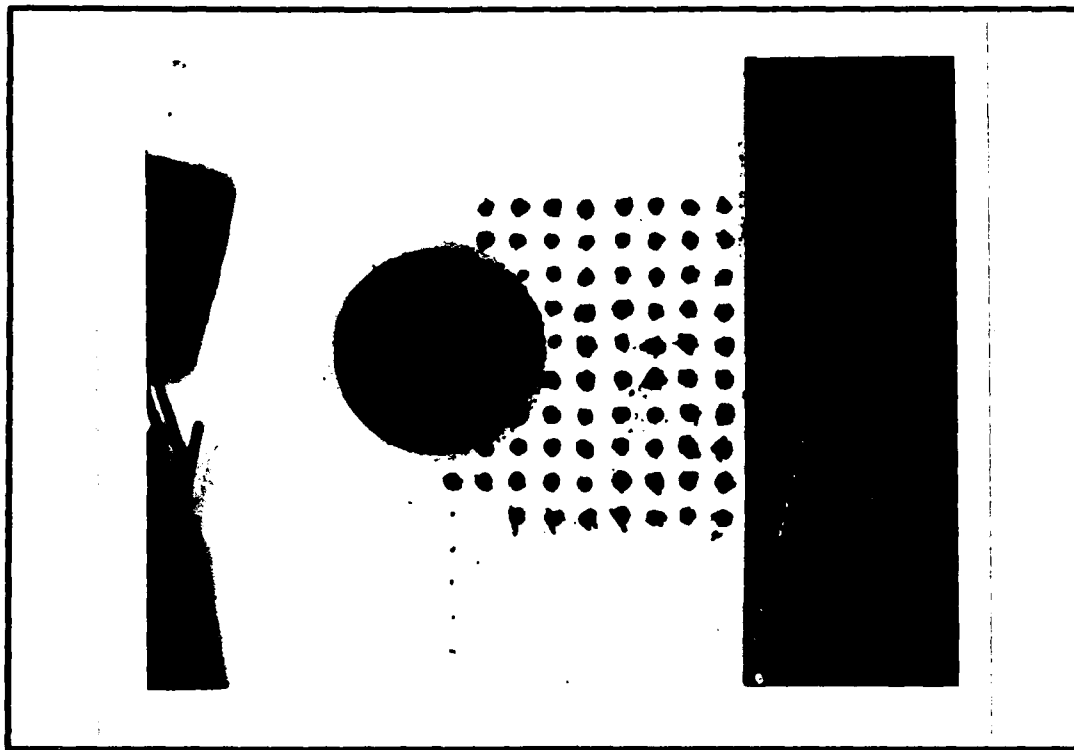
Figure 5-34. Grid at 0 Load, $[\pm 45]_{16}$

provided insight into how much error was induced by the fiber
rotations. That error analysis was based on the assumption
that the fibers retain their $\pm 45^\circ$ orientation. Error was
induced by the effect of the rotating fibers on the
transformation matrix. This is difficult to duplicate for
these specimens because the geometry is not uniform and the
amount of rotation seen in the fibers is dependent on
location.
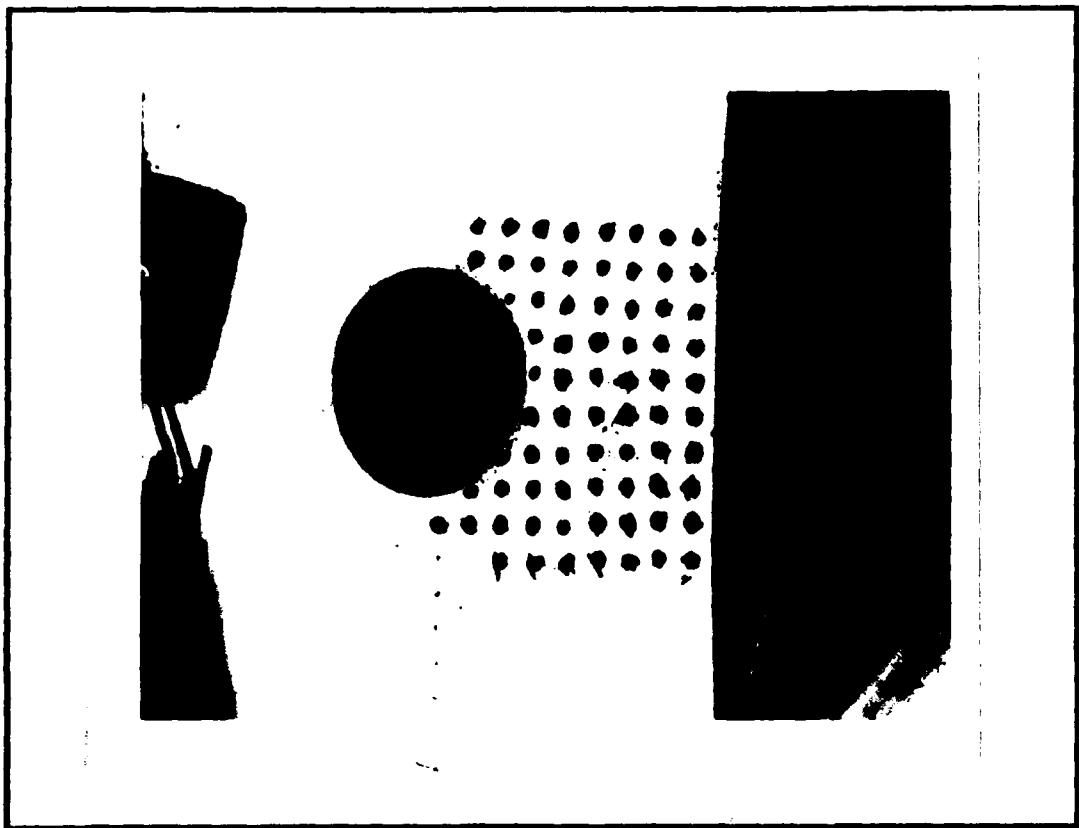
Figure 5-35. Grid at 1350 lbs, [±45]$_{4s}$
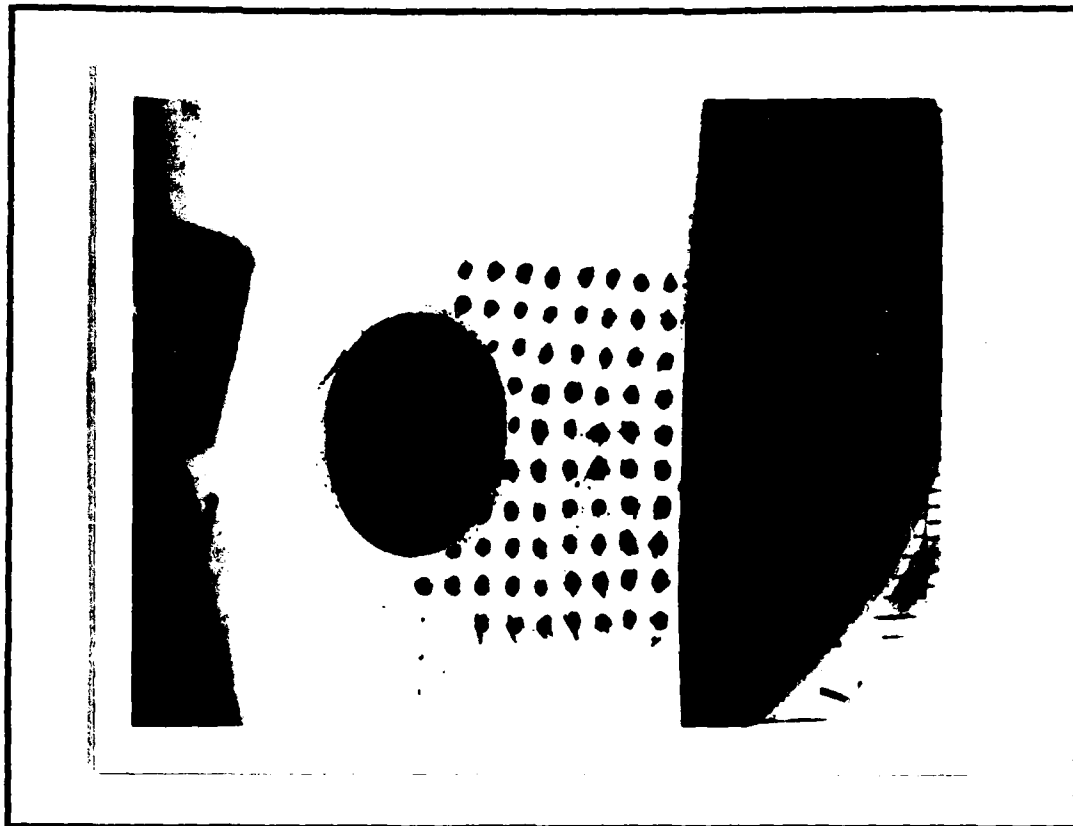
Figure 5-36. Grid at 1900 lbs, [±45]$_{4S}$

Another possible source of error was discovered accidentally while recording failures using the high speed video camera. Due to scheduling conflicts, the high speed video camera was only available for two weeks. The gaged [±45]$_{4S}$ specimens were not available during this time, so failures of ungaged specimens were filmed. At the film speed selected, only three minutes of tape could be recorded at any one time. If at the end of the tape the specimen failure had

not occurred, the Instron was stopped, a new tape was loaded, and the test was resumed. This took about 20 seconds. The first specimen test was halted three times to exchange tapes. Figure 5-37 is a copy of the strip chart of load versus time recorded by the Instron. After the test was complete, one of the observers noted that the specimen had appeared to unload itself each time the test was halted. This unloading varied from about 7% at 1400 lbs to 12% at 2050 lbs. The Instron is a screw driven machine that loads specimens by displacement so it is unlikely that the source of unloading was the Instron. Another possible source of unloading could have been the tabs or grips, but if the tabs or grips had slipped no additional loading would have been possible. The only credible source of unloading had to be the specimen itself, due to viscoelastic (time dependent) effects. This phenomenon was apparent at relatively low loads (65% of UT), and similar results were obtained for the remaining specimens. Since there is no creep data available for this material at this temperature (and since investigating the effects of creep is beyond the scope of this study) it is difficult to determine the overall effect that creep has on the results. It is conceivable that the assumption of minimum viscoelastic effects is probably not a good assumption for specimens with $\pm 45^{\circ}$ fibers.

The progression of failure occurred at a relatively slow pace with the fibers allowing the hole to elongate

5-49
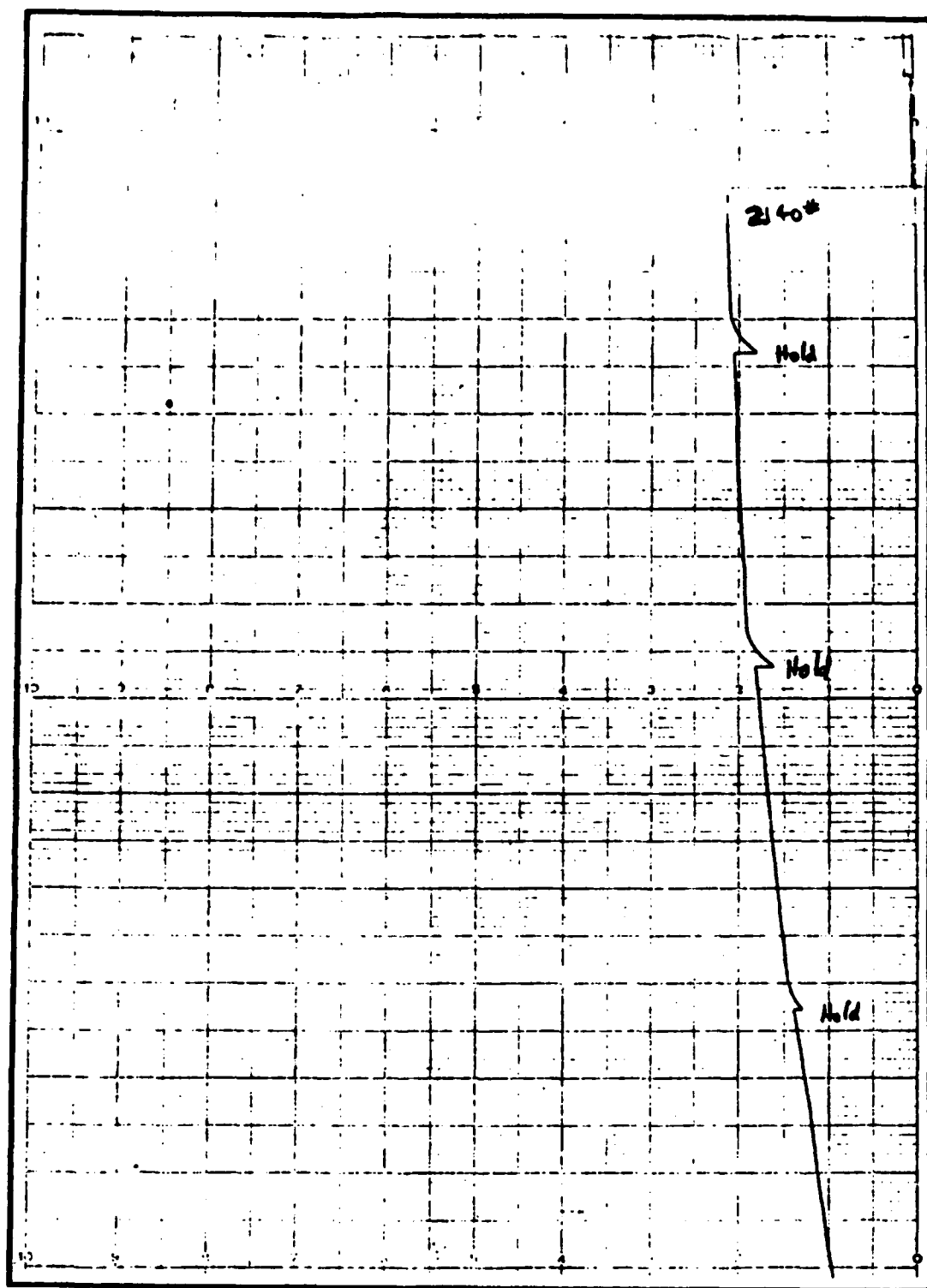
Figure 5-37. Instron Strip Chart Plot of [±45]$_{4s}$ Specimen

substantially before failure. The failure zone appeared as a V shaped area on either side of the hole as shown in the stereo x-rays in Figures 5-38 through 5-40. This failure zone was replicated quite well analytically as shown in Figure 5-41. As with the previous ply lay-ups, the failure of elements became rather random beyond a certain point. After the 100.9% of UT shown in Figure 5-41, elements began failing at a number of locations. The incremental displacements were again used to plot the deformed models. Samples of the deformed models are included in Figure 5-42. The deformed models below the 100.9% level show a significant amount of necking but, compared to experimental results, this is reasonable. After this level, the models show that the elements on the side of the hole actually swell, which is not reasonable. The solution at this point is not converging and any additional results are not useful.

(4) Quasi-isotropic Ultimate Tensile Specimen Tests. Three $[0/\pm 45/90]_{2s}$ specimens were tested to derive the stress strain curve for the element near the edge of the hole. Progression of failure was not instantaneous like the unidirectional specimens and not nearly as gradual as the $[\pm 45]_{4s}$ specimens. A ragged failure zone appeared adjacent to the hole just prior to failure that was observed in both the stereo x-rays and the high speed video and seemed to be predicted analytically.
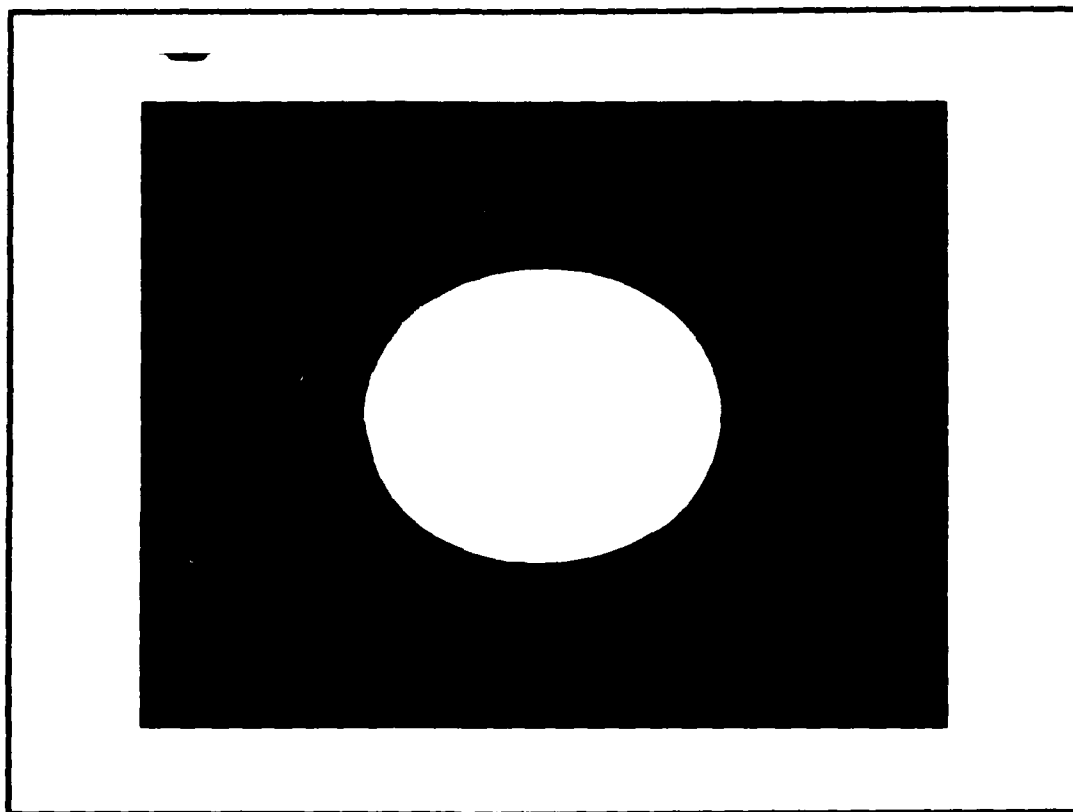
Figure 5-38. Stereo X-Ray at 75% UT, [±45]₄ₛ
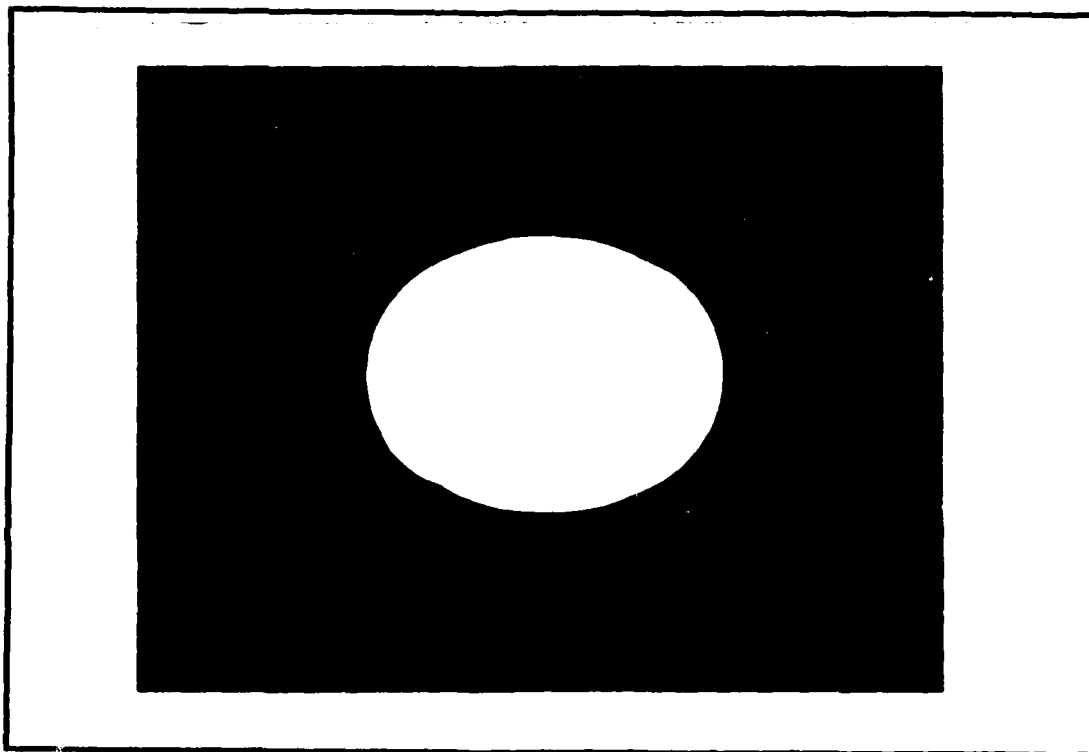
Figure 5-39. Stereo X-Ray at 85% UT, [±45]_{4s}
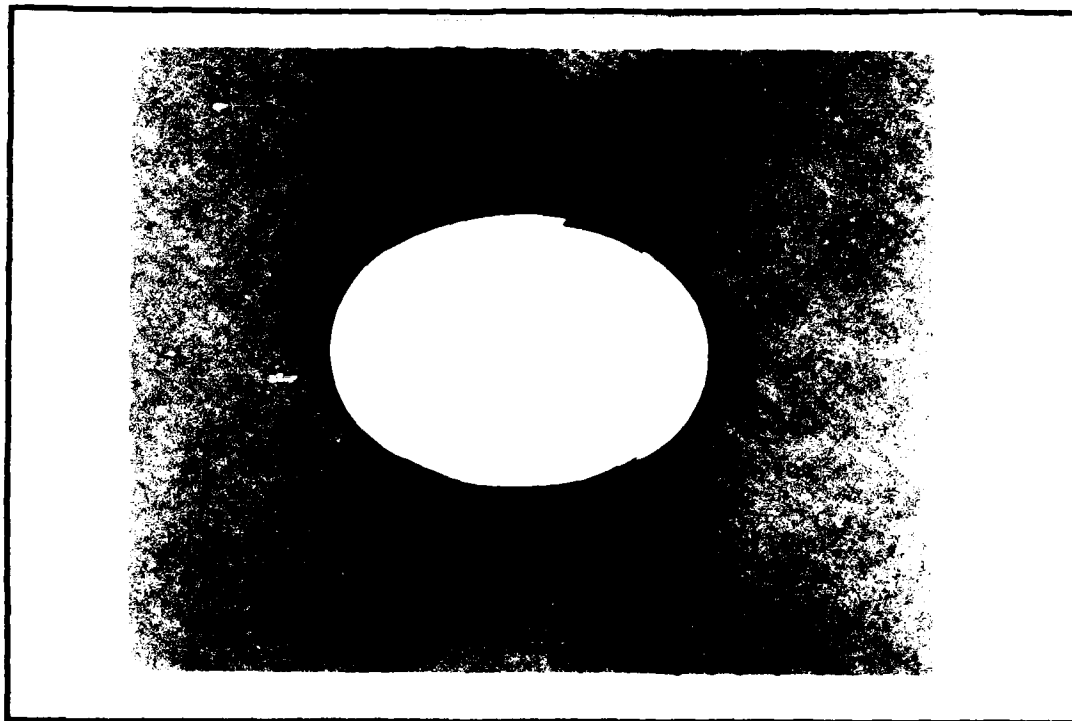
Figure 5-40. Stereo X-Ray at 95% UT, [±45]$_{4S}$
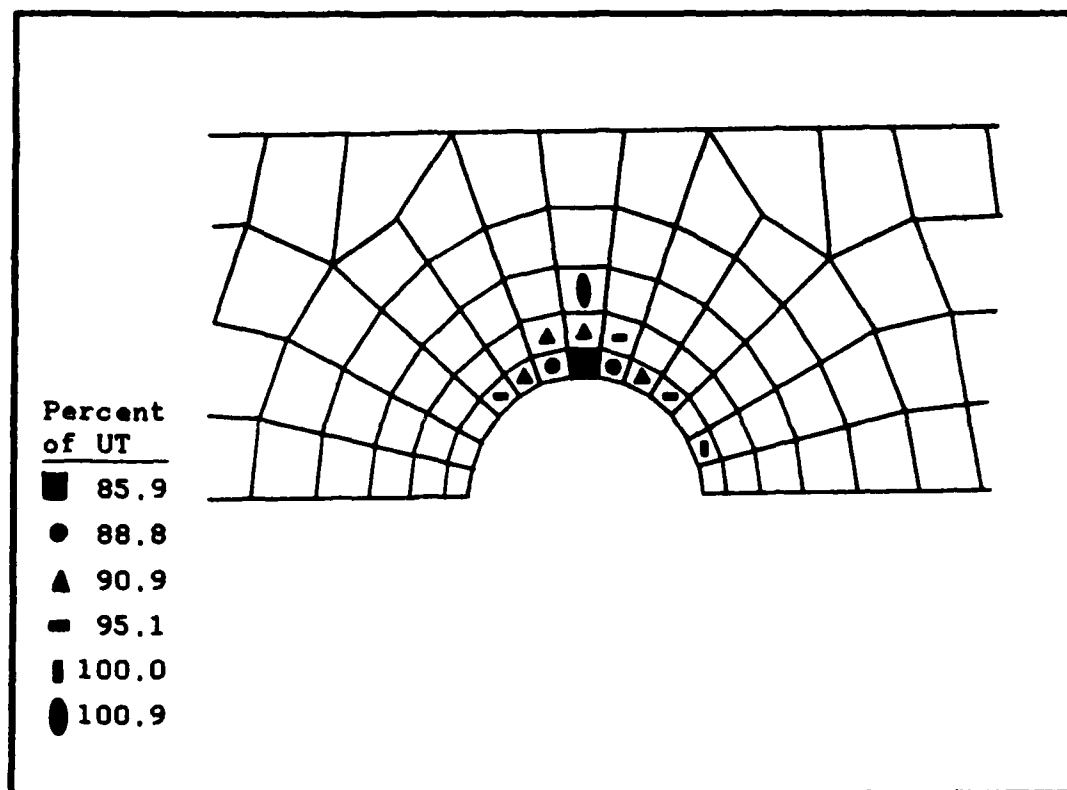
Figure 5-41. Failure Progression, $[\pm 45]_{4s}$
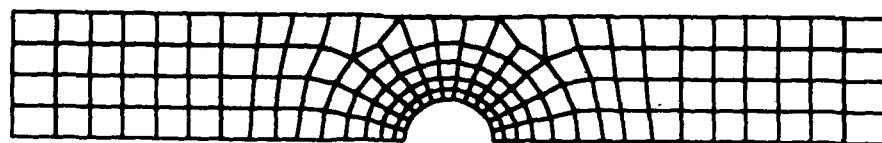
Model at 0 Load

Model at 55.0% UT
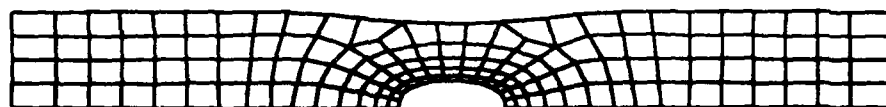
Model at 100.9% UT

Model at 111.3% UT

Note: All defformations shown at 10X actual

Figure 5-42. Deformed Shape of [±45]₄ₛ Model

The stress strain curve for the experimental data is in Figure 5-43 along with the analytic results. As with the [±45]$_{4s}$ specimens, the stacked rosettes at the hole would not stay adhered for the duration of the test. Time constraints precluded the development or use of optical techniques that were used for the [±45]$_{1s}$ specimens. As indicated in Figure 5-43, correlation between experimental and analytic results is better for the longitudinal strain (el) than for the transverse strain. Just prior to failure of the gage the curves appear to be diverging. This is either due to degraded performance of the rosette, the same creep effects in the ±45° plies that were discussed in the preceding section, or the initiation of the geometric nonlinearities caused by the rotation of the ±45° fibers. Since no comparable experimental data was collected using the optical techniques, it is difficult to determine the source of the error.

The progression of failure was much slower than for the unidirectional specimens. The stereo x-rays in Figures 5-44 through 5-46 indicate that very little damage is apparent in the specimens until 95% UT. However, the failure of elements depicted in Figure 5-47 indicates that substantial failure of elements occurs as low as 60% of UT. The 90° plies are completely failed at 83% of UT. The stereo x-rays fail to indicate any of this damage because most of it occurs below the surface of the material. Figure 5-48 indicates when all

5-57

plies of a given element have failed analytically. The
failure progression predicted in Figure 5-48 compares quite
well with the experimental results.
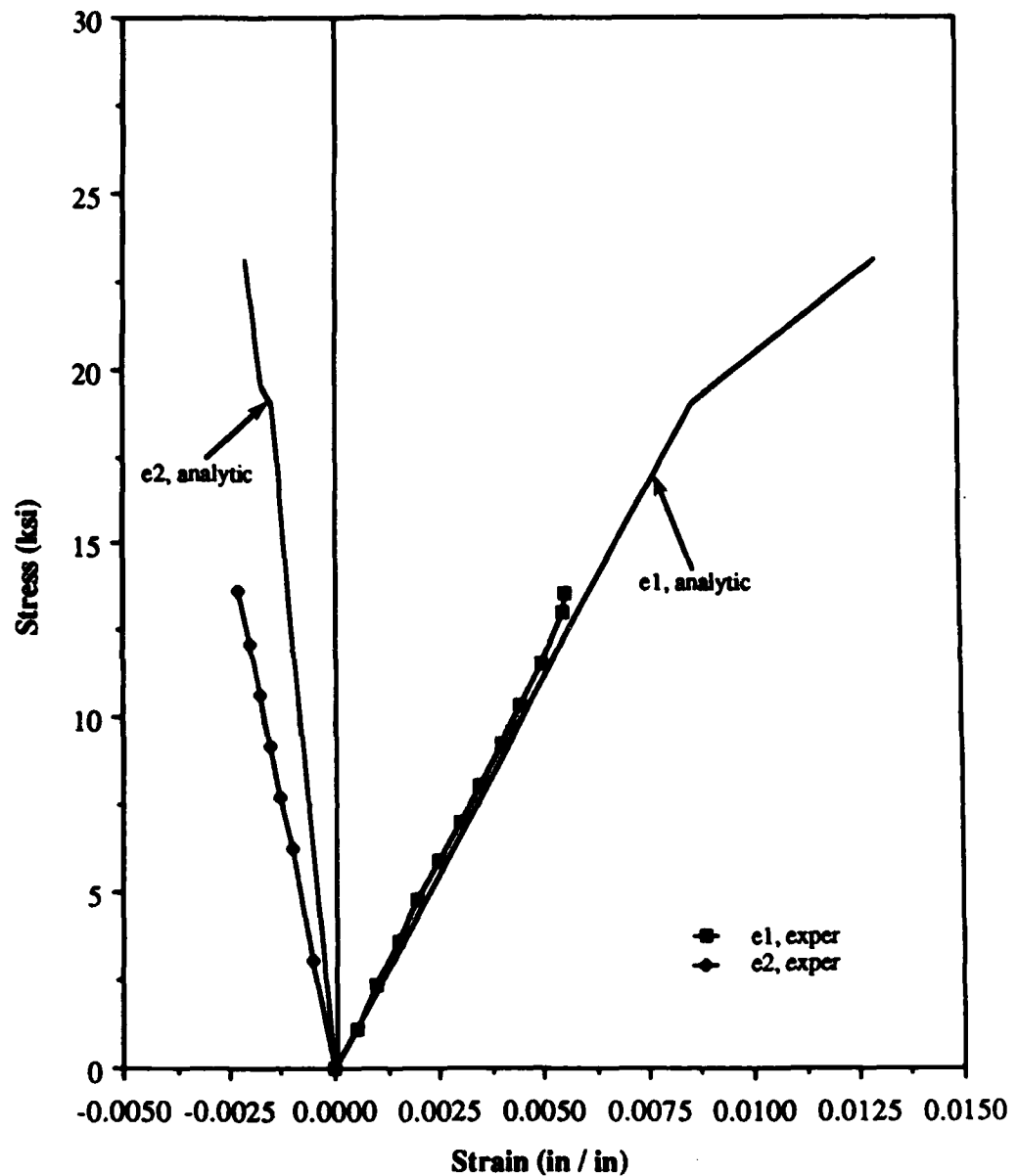
Figure 5-43. Stress Strain at Hole, $[0, \pm 45, 90]_{2s}$
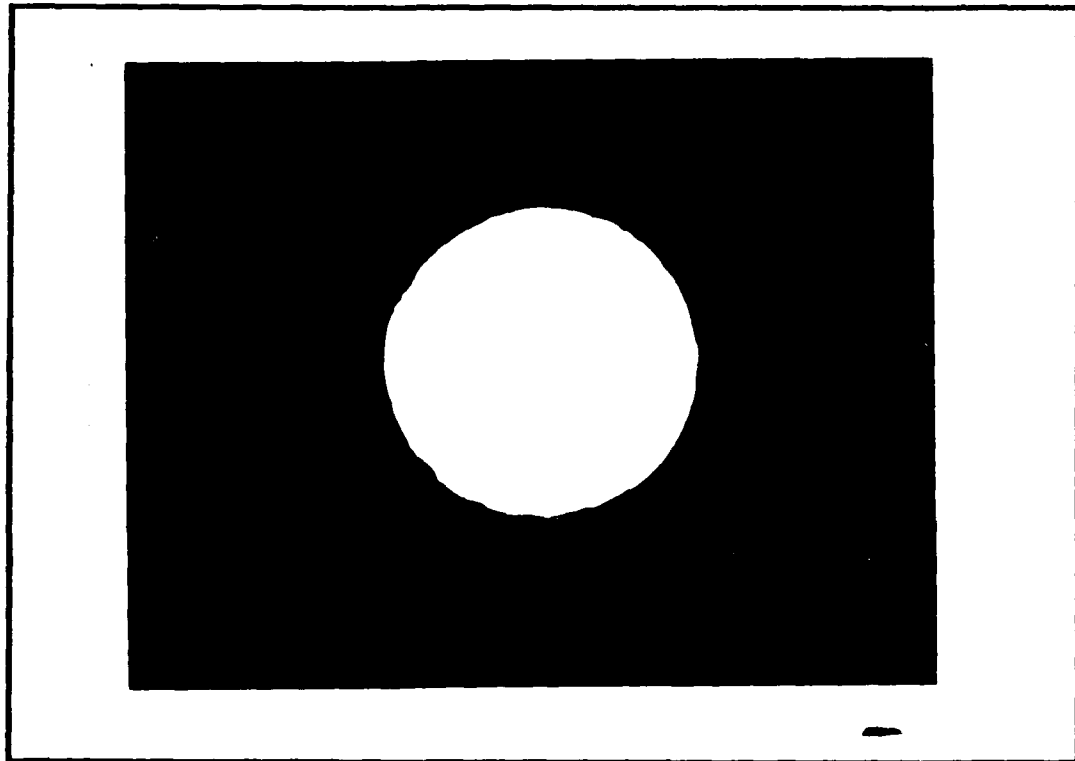
Figure 5-44. Stereo X-Rays at 75% UT, $[0,\pm45,90]_{2s}$
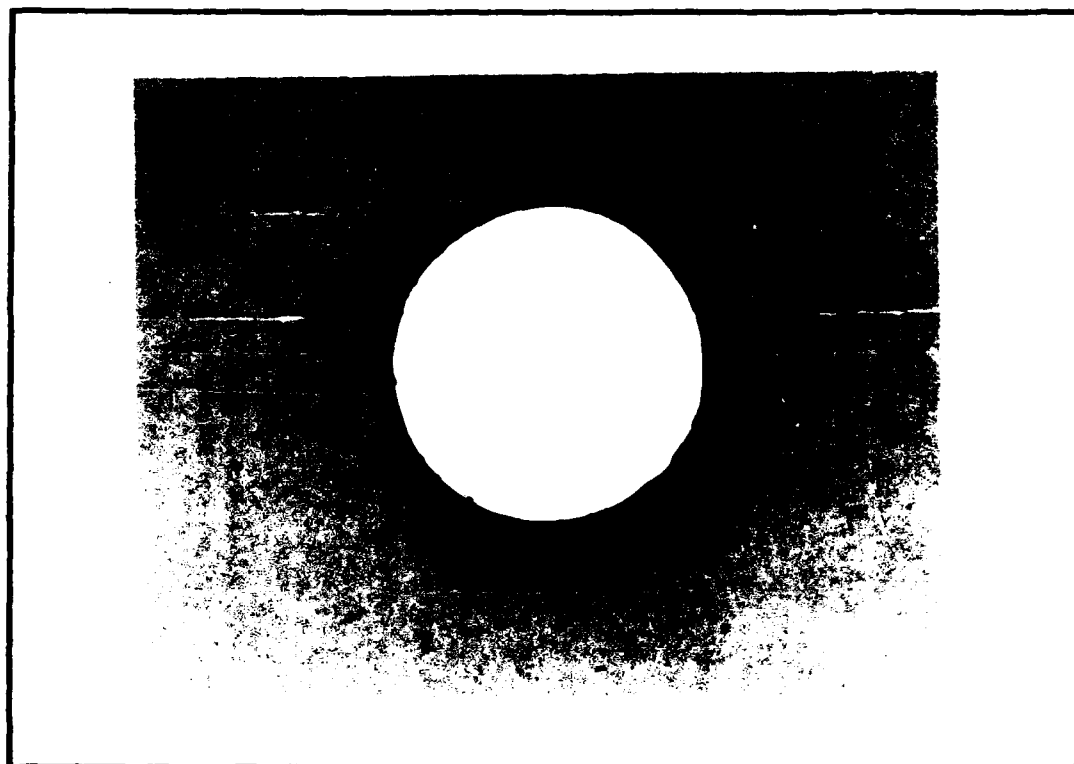
Figure 5-45. Stereo X-Rays at 85% UT, $[0, \pm 45, 90]_{2s}$
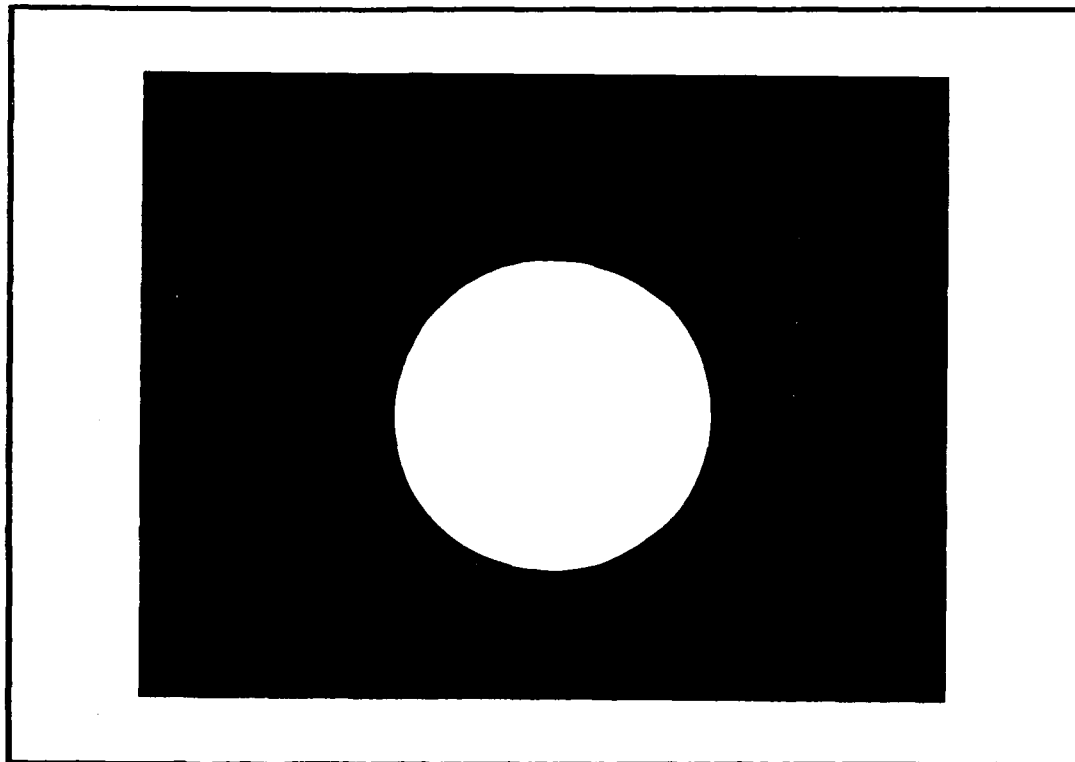
Figure 5-46. Stereo X-Rays at 95% UT. $[0,\pm45,90]_{2s}$
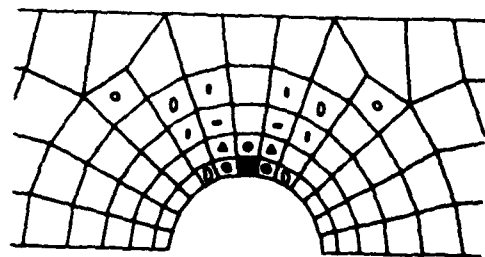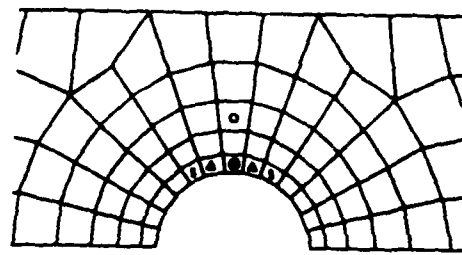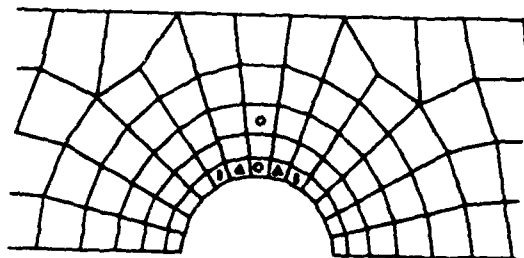
(a) 0° Plies

(b) + 45° Plies

(c) -45° Plies
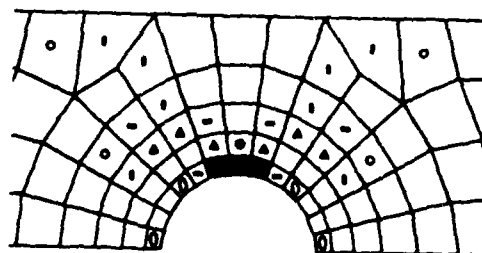
(d) 90° Plies

Percent of UT

- ■ 57.3
- ● 64.9
- ◖ 72.2
- ▲ 83.0
- ╎ 83.0
- ◖ 92.5
- ○ 106.2

Figure 5-47.   Failure Progression by Ply, [0,±45,90]$_{\text{2s}}$
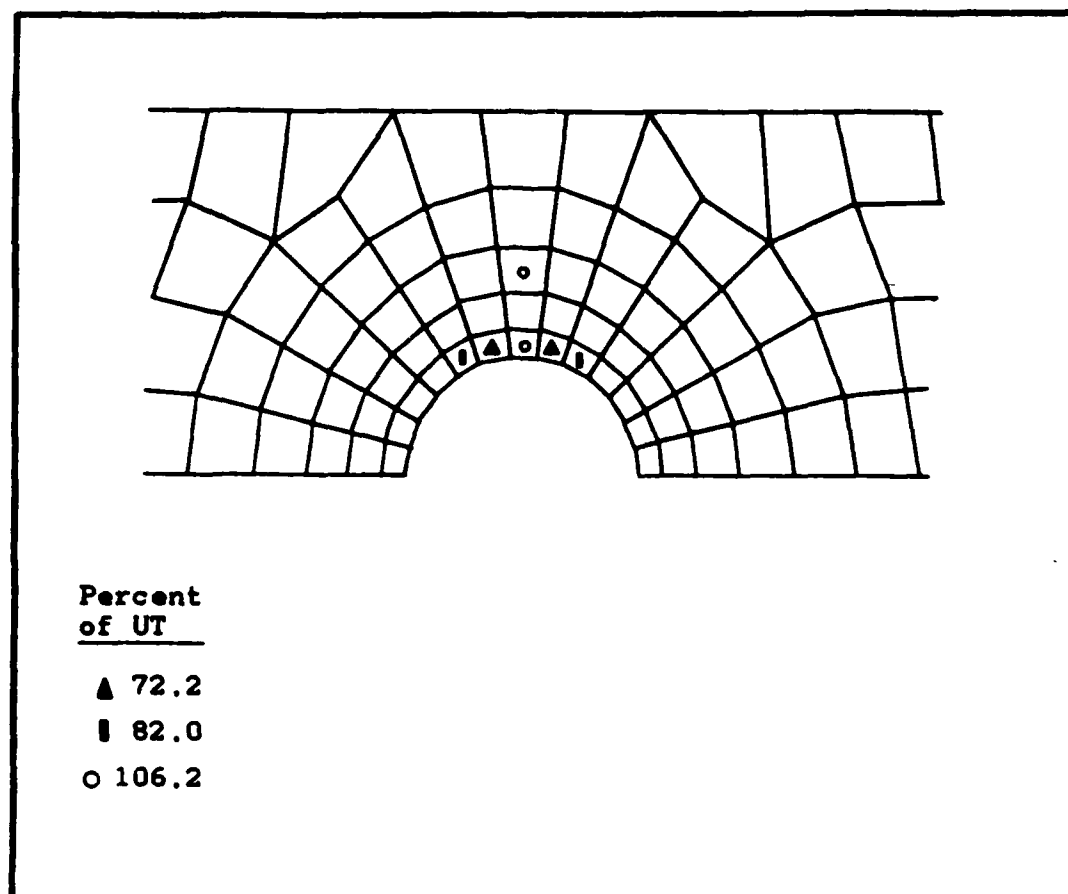
Figure 5-48. Failure Progression, $[0,\pm45,90]_{2s}$

As with the previous ply lay-ups, determining where the model actually failed required monitoring the deformed shape of the model. Figure 5-49 contains samples of the deformed shapes of the model. The progression of deformation is similar to to the $[\pm45]_{4s}$ except the deformations are not as large. The models continue to neck until the 106.2% of UT increment where elements in the specimen deform into shapes that are unrealistic. This corresponds to the increment where

5-63
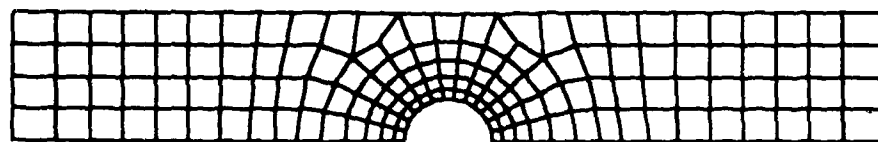
Model at 0 Load
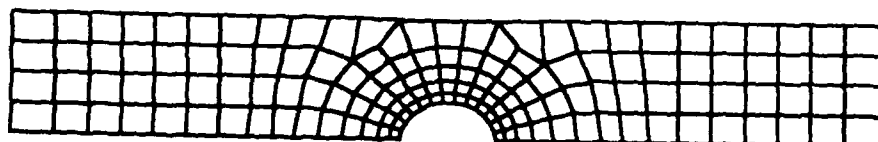
Model at 57.3% UT
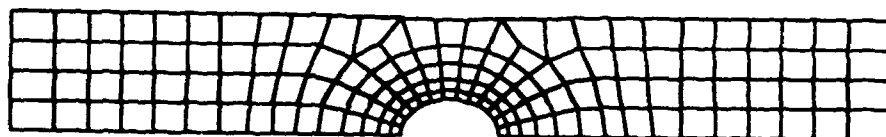
Model at 92.5% UT
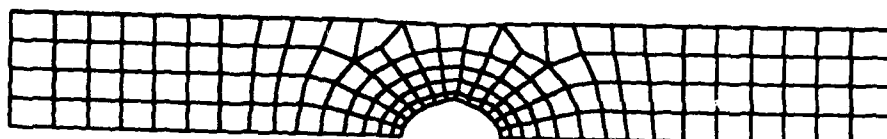
Model at 106.2% UT

Note: all deformations are 10X actual

Figure 5-49. Deformed Shape of [0,±45,90]$_{2s}$ Model

the solution ceases to converge. Any results after this point are not significant.

The failure of two specimens was recorded with the high speed video, one at 1500 fps and one at 2000 fps. Both recordings revealed progression of failure similar to that shown in the stereo x-rays and the failure of elements in Figure 5-47. In these tapes, the hole developed a ragged "tear" at the side of the hole and perpendicular to the load. This tear was similar in length to the failure zone predicted in Figure 5-47 and the crack shown in the stereo x-rays.

VI. Conclusions

In Section V a substantial amount of information is presented from studying the failure characteristics of Gr/PEEK at 250 F. There are a number of conclusions that can be drawn from this information. This section presents the conclusions of this study in three subsections: basic property derivation conclusions, failure from a stress concentrator conclusions, and general conclusions.

A. Basic Property Derivation Conclusions. The following conclusions were drawn from the derivation of the basic properties of Gr/PEEK at 250 F.

1. The material response of the matrix dominated ply lay-ups of Gr/PEEK at 250 F are extremely nonlinear, much more so than for Gr/PEEK at room temperature or Gr/Ep.

2. The material response of the fiber dominated ply lay-ups of Gr-PEEK at 250 F is essentially linear and very similar to that of Gr/PEEK at room temperature. The primary difference is that in compression, the matrix is weakened by the heat and is incapable of restraining the fibers at 250 F as at well room temperature.

3. Selection of the tab adhesive for the compression specimens is much more critical than for the tension specimens, probably because the tabbed area is so much harder to isolate from the heat. The same tab adhesive that worked successfully for every tension test conducted for this study failed for each of the two compression tests it was used for.

4. The gages on the basic property shear specimens would

not stay adhered to the specimens until failure of the specimen. The problem is a combination of high temperature and high strain cause the adhesive to yield and the gage backing to peel. The data collected from the cross was well correlated with the gages for the duration gage data was available. Presumably the additional data collected from the cross is also accurate. This indicates the these measurements are a viable technique for making shear measurements. However, the error analysis revealed that any data collected above .15 in/in has substantial error due to the rotating of the fibers. Consequently, the data collected from the strain gages was sufficient for use as a basic property curve.

5. Use of the digitizer for reducing the basic property curves to one "best fit" curve was a very accurate and very quick technique. Use of a digitizer for deriving the Poisson's Ratio curves is nearly mandatory when derived from these basic property curves. The measurements that must be taken from the respective curves are extremely tedious by hand and must be very accurate. The width of .5 mm pencil lead can create substantial error. This is complicated by the fact that the curves produced by the FDL VAX software from the raw data are automatically scaled to maximize the resolution. This quite often results in scales that are at odd intervals. Using a digitizer makes these measurements accurately and fairly quick irrespective of how hard the measurements are to read or how arbitrary the scales are

created.

6. The heat fixture used for the compression testing was very convenient and reliable. The only drawback was that once the test was complete, the Rolfes fixture was extremely warm and required 10 to 15 minutes to cool before it could be disassembled. This is probably unavoidable.

7. Determination of the behavior of Gr/PEEK using the basic properties is obviously temperature dependent, especially in matrix dominated ply lay-ups. If basic property curves were determined at several intermediate temperatures experimentally, basic property surfaces could be constructed. These surfaces could be used to analytically predict the behavior of models at any temperature. The limiting case for high temperatures is probably 250 F. Viscoelastic effects are already apparent at 250 F and as the temperature approached glass transition (approximately 300 F) the viscoelastic effects would increase substantially.

B. <u>Failure</u> <u>From</u> <u>A</u> <u>Stress</u> <u>Concentrator</u>. The following conclusions were drawn from the experimental and analytic failure of the four ply lay-ups.

1. The experimental and analytic results for the $[0]_{16}$ ply lay-ups compared very well. The stress-strain relationship predicted analytically was very close to experimental, especially for the new model with appropriately oriented elements. The propagation of failure predicted analytically using the instantaneous unloading scheme (based on the original model) revealed catastrophic failure of most

of the elements. There are two possible problems that caused this: either the instantaneous unloading model is inappropriate or the geometry of the model was inappropriate. Time constraints did not permit resolving this problem.

2. The experimental and analytic results for the $[90]_{16}$ ply lay-ups was excellent. The stress-strain relationship predicted analytically was almost identical to experimental. The propagation of failure analytically using the instantaneous unloading scheme was revealed some of the same problems indicated in the $[0]_{16}$ specimens. Even though failure of the specimen was predicted at the correct level, the failure zone was grossly exaggerated. The predicted failure zone using the negative tangent modulus was much more appropriate even though the failure did not propagate very rapidly.

3. Based on the discussions in 1. and 2., instantaneous unloading is probably too drastic a modeling scheme for unloading. It appears that the surrounding elements are incapable of assuming the stresses from the initially failed elements and the failure propagates radially outward. Ideally, an unloading scheme for unidirectional specimens would permit the initial failures observed in the $[90]_{16}$ specimens and then transition to rapid unloading in the direction of the fibers. The current technique of unloading stresses onto all of the surrounding elements appears to propagate failure radially outward from the initial failure instead of along the fibers.

4. The experimental and analytic results for the $[\pm 45^\circ]_{4s}$ specimens was good for the available data. The analytical stress-strain relationship was very close to experimental for the data collected from gages. The stress-strain data at higher strains was collected using an optical technique and was not nearly as well correlated. This could be either because the optical technique requires refinement or because the geometric nonlinearities (which were not accounted for analytically) were too substantial to ignore. The progression of failure using the negative tangent modulus was well correlated to the failure observed experimentally in the stereo x-rays. The failure appeared as a V open toward the hole both experimentally and analytically.

5. The viscoelasticity observed during the testing of the $[\pm 45]_{4s}$ specimens was significant even at moderate load levels. This is an aspect of Gr/PEEK for which very little research has has been accomplished and an area that definitely needs attention.

6. The experimental and analytic results for the $[0,\pm 45,90]_{2s}$ specimens was good for the available data. The analytical stress-strain relationship was very close to experimental for the data collected from gages. No stress-strain data at higher strains was collected using the optical technique because of time constraints. The progression of failure predicted analytically was very similar to that observed in the stereo x-rays, especially when

6-5

considering the failures through the thickness.

7. Determining failure of an element was specifically determined by the program. Determining failure of the model took a little more insight. In the case of the $[0]_{16}$, failure was determined when the shear quantity of failed elements indicated failure. This was also the case for the $[90]_{16}$ using instantaneous unloading. When considering the $[90]_{16}$ model with negative tangent unloading, failure was determined as when the failure zone had moved beyond the initial stages. For both the $[\pm 45]_{4S}$ and $[0,\pm 45,90]_{2S}$, determination of total failure relied on monitoring the deformed shape and the ability of the solution to converge. For both ply lay-ups illogical deformed shapes (swelling instead of necking) occurred at the same time the solution had trouble converging. This was considered as failure. Using the illogical deformed shapes as the basis for failure yielded failure loads that compared well with those determined experimentally.

C. General Conclusions. The following conclusions are of a general nature and, although related directly to the study, did not apply to any one specific aspect of the study.

1. The heat fixtures developed for the tension tests was an effective means for heating the specimens. The fixture was inexpensive, easy to fabricate, easy to assemble on the Instron, and capable of controlling the temperature of the specimen to 250 F, ±5 F. The fixture also provided a viewing area so that the failure of the specimen could be

recorded. A great deal of care should be taken to ensure even heating of the specimens. As discussed in Chapter V for the compression specimens, temperature differences across the thickness can be as high as 100 F. This condition would induce a significant amount of error if not corrected.

2. The data from the strain gages all seemed to drift significantly while the specimen was heated from room temperature to 250 F. Consequently the temperature of the fixtures had to be maintained fairly stable for at least five minutes before any test could be initiated. The process of heating and stabilizing the temperature was very time consuming taking up 30 minutes from the time the equipment was ready until the gages had stabilized.

3. The results from recording the failure with the high speed video were disappointing. The combination of poor photographic resolution, insufficient lighting, and unreliable equipment made filming the failure at high speeds valuable only in the sense that we had a reasonable estimate of how fast failure occurred. Our relatively poor results are pretty consistent with results obtained by personnel at the base photo lab who are very experienced at operating the high speed video camera. This indicates that recording the failure of these specimens optically is probably beyond current capability. The FDL is currently procuring a data collection system capable of recording up to a million samples per second. With the right transducer, this data collection system could probably provide greater insight into how rapidly

6-7

the failure of these specimens occurs.

4. In general, the two optical techniques showed a great deal of promise in measuring high strains in enclosed environments. Refinement of this technique to include automatically (as opposed to manually) recording the measurements could be very valuable. Some of the techniques considered included use of a knurled knob or a manufactured grip pattern similar to the jaws of the Instron with carbon paper to transfer a grid onto the painted surface. The technique discussed in Reference 6 using a fine nickel mesh is also viable. These techniques could be valuable in determining high strains in other adverse environments such as high humidity.

5. The strains measured optically in both the $[\pm 45]_{4s}$ basic property specimen and specimens containing a hole showed very high (nonlinear) strains and consequently the strain gages failed to stay adhered to the specimen. The strain gages for the $[0,\pm 45,90]_{2s}$ quasi-isotropic specimens also failed to stay adhered to the specimen until the specimen failed. Even though the strains for the higher load levels were not measured, its reasonable to assume that these same nonlinear strains exist in the quasi-isotropic specimens. The common thread between these specimens was the $\pm 45^{\circ}$ fibers. Consequently, any ply lay-up of Gr/PEEK containing $\pm 45^{\circ}$ fibers (in relation to the load orientation) has the potential of developing the same nonlinear strains observed in the two shear specimens.

6. In general, Dr.Sandhu's program PLSTREN predicted the
behavior of the unidirectional laminates quite well. PLSTREN
also predicted the behavior of the angle ply and
quasi-isotropic laminates well at low load levels. This
correlation did not extend to higher load levels because
PLSTREN only accounts for nonlinear material properties, not
geometric nonlinearities or viscoelastic effects. These two
effects would have to be accounted for in an analysis to
accurately predict the behavior of Gr/PEEK at 250 F when
subjected to high loads.

Bibliography

1. Awerbuch, J. and M. S. Madhukar. "Notched Strength of Composite Laminates: Predictions and Experiments -- A Review." _Journal of Reinforced Plastics and Composites_. Vol. 4, January 1985.

2. Bathe, K.J. _Finite Element Procedures in Engineering Analysis_. Englewood Cliffs, N. J.: Prentice-Hall Inc., 1982.

3. Carnahan, B., H. A. Luter, and J. O. Wildes. _Applied Numerical Methods_. New York: John Wiley and Sons, Inc., 1969.

4. Cron, Steven M. _Improvement of End Boundary Conditions for Off-Axis Tension Specimen Use_. MS Thesis, AFIT/ GAE/AA/85D-3. School of Engineering, Air Force Institute of Technology (AU), Wright-Patterson AFB, OH. _December 1985_.

5. Cook, R. D. _Concepts and Applications of Finite Element Analysis_. New York: John Wiley and Sons, 1981.

6. Czarnek, R., D. Post, and J. Lee. "Experimental Analysis of the Failure Process of a Simulated Solid Rocket Propellant." _Proceedings of the VI International Congress on Experimental Mechanics_, Vol. I (June 6-10, 1988), pp. 454-458.

7. Fiberite Corporation, a subsidiary of Imperial Chemical Industries (ICI). _APC-2 PEEK/Carbon Fibre Composite_. Manufacturers Data Sheets 1 through 8. Orange, CA, 1986.

8. Jones, R. M. _Mechanics of Composite Materials_. Washington D. C.: Scripta Book Company, 1975.

9. Martin, J. _A Study of Failure Characteristics in Thermoplastic Composite Material_. MS Thesis, AFIT/ GA/AA/88M-2. School of Engineering, Air Force Institute of Technology (AU), Wright-Patterson AFB, OH. December 1985.

10. Nahas, M. N. "Survey of Failure and Post-Failure Theories of Laminated Fiber-Reinforced Composites." _Journal of Composites Technology and Research_, Vol. 8, No. 4 (Winter 1986), pp. 138-153.

11. Peterson, R. E. _Stress Concentration Factors_. New York: John Wiley and Sons, 1974, p.150.

12. Ramey, J. E. _Comparison of Notch Strength Between Gr/PEEK (APC-1 and APC-2) and Gr/Epoxy Composite Material at Elevated Temperature_. MS Thesis, AFIT/GAE/AA/85D-12. School of Engineering, Air Force Institute of Technology (AU), Wright-Patterson AFB, OH. December 1985.

13. Rolfes, R. L. "Compressive Properties of Oriented Fiber Composites with the Prototype Compression Fixture (1983)." Technical Manual AFWL-TM-85-222 FIBC, Air Force Wright Aeronautical Laboratories, Wright-Patterson AFB, OH.

14. Rowlands, R. E. "Strength (Failure) Theories and Their Experimental Correlation." _Handbook of Composites_, G. C. Sih and A. M. Skudra, Eds. Vol. 3, Ch. 2, Elsevier Science Publishers B. V., 1985, pp. 71-125.

15. Sandhu, R.S. "Analytical-Experimental Correlation of the Behavior of 0°, $\pm 45^\circ$, 90° Family of AS/3501-5 Graphite Epoxy Composite Laminates Under Uniaxial Tensile Loading." Air Force Flight Dynamics Laboratory, AFFDL-TR-79-3064, May 1979.

16. Sandhu, R. S. "Nonlinear Behavior of Unidirectional and Angle Ply Laminates." _Journal of Aircraft_, 13, No. 2 (February 1976), pp. 104-111.

17. Sandhu, R. S. "Ultimate Strength Analysis of Symmetric Laminates." Technical Report AFFDL-TR-73-137, AD 779927, Air Force Flight Dynamics Laboratory, Wright-Patterson AFB, OH, February 1974.

18. Sandhu, R. S. "A Survey of Failure Theories of Isotropic and Anisotropic Materials." Technical Report AFFDL-TR-72-71, AD 756889, Air Force Flight Dynamics Laboratory, Wright-Patterson AFB, OH, January 1972.

19. Sandhu, R. S. and G. P. Sendeckyj. "On Delamination of $(\pm\theta_m/90_{n/2})_s$ Laminates Subjected to Tensile Loading." Technical Report AFWAL-TR-87-3058, Air Force Wright Aeronautical Laboratory, Wright-Patterson AFB, OH, July 1987.

20. Sandhu, R. S., R. L. Gallo, and G. P. Sendeckyj. "Initiation and Accumulation of Damage in Composite Laminates." Composite Materials: Testing and Design (Sixth Conference), ASTM STP 787, I. M. Daniel, Ed., American Society for Testing and Materials, 1982, pp. 163-182.

21. Sandhu, R. S., G. P. Sendeckyj, and R. L. Gallo. "Modeling of the Failure Process in Notched Laminates." Recent Advances in Mechanics of Composite Materials. IUTAM Symposium on Mechanics of Materials, (16-19 August 1982). Z. Hashin and C. Herakovitch, Eds. Virginia Polytechnical Institute: Pergamon Press, 1983, pp. 179-189.

22. Sendeckyj, G. P., M. D. Richardson, and J. E. Pappas. "Fracture Behavior of Thornel 300/5208 Graphite/Epoxy Laminates -- Part 1: Unnotched Laminates." Composite Reliability, ASTM STP 580, pp. 528-546.

23. Tan, S. C. "Tensile and Compressive Notched Strength of PEEK Matrix Composite Laminates." Journal of Reinforced Plastics and Composites. Vol. 6 (July 1987), pp. 253-267.

24. Whitney, J. M., I. M. Daniel, and R. B. Pipes. Experimental Mechanics of Fiber Reinforced Composite Materials, Society for Experimental Mechanics (SEM) Monograph No. 4, Revised Edition. Brookfield Center, CT: SEM, 1984.

25. Williams, M. L. "Structural Analysis of Viscoelastc Materials," AIAA Journal, Vol. 2, No. 5 (1964), pp. 785-808.

26. Witt, W. P. III, A. N. Palazotto, and H. T. Hahn. "Numerical and Experimental Comparison of the Notch Tip

Stresses in a Laminated Plate." AIAA _Journal_, Vol. 17,
No. 5 (1978), pp. 500-506.

Appendix A: Sample Data File and Output File For

PLSTREN

This appendix contains two parts: a sample data file for
PLSTREN and an output file from a single element in a
$[0, \pm 45, 90]_{2s}$ ply lay up. The loading and boundary conditions
of this element are depicted in Figure A-1. The first three
lines of the data file contain the control cards. The first
line is the title to be printed on the output file. In the
second and third line, zero entries indicate either options
that were not taken or values that did not apply. The second
line indicates the following:

    4 - 4 nodes

    4 - 4 elements

    1 - 1 type of material

    2 - code for anisotropic material

    1 - code for nonlinear analysis

The third line indicates the following:

    1 - code for negative tangent ply failure scheme

    15 - maximum number of increments allowed

    4 - last element represented in output (per increment)

    0 - first element in output

    4 - number of elements deep

    50 - processing time limit (CPU sec)
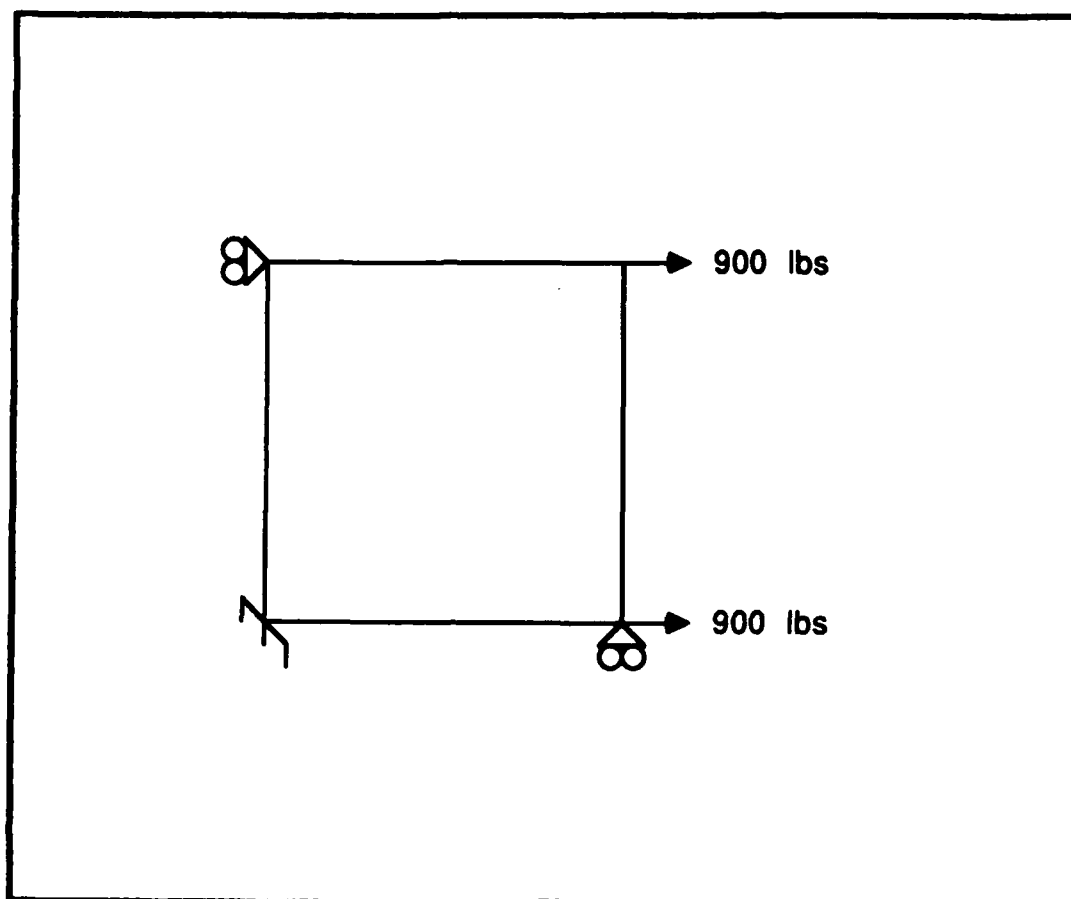
Figure A-1. Single Element Model

Lines 4 through 7 contain the information for each node.
Each line contains the node number, boundary condition code,
x and y coordinates, x and y loads (or displacements), and
the temperature. The eighth line contains the ply
orientation, the ninth line contains the ply thickness, and
the tenth line contains the material type for each ply.
PLSTREN uses line eight through ten for automatic numbering of
elements. Lines 11 and 12 contain the element information.
Each line contains the element number, node numbers,

material type, ply orientation, and ply thickness. The remaining information are the nonlinear material properties. Lines 13 and 14 contain the material number (1) and the number of tabular values provided for each of the 7 material properties. All of the remaining lines, except the last, contain the tabular material properties for Gr/PEEK. The last line contains the initial elastic modulii for Gr/PEEK.

In the output file, PLSTREN first prints out the information read from the data file. This allows the user to check the appropriateness of the data file because this information is written before the program runs (and has an opportunity to bomb). The remaining information is the incremental output. First the ITERATION CONTROLS are printed. These indicate how the solution converged. Then the nodal displacements are printed. Finally, the Stresses, strains, and energy ratios for each element are printed. For each element, the first and second lines represent the stresses and strains. The third line contains the longitudinal, transverse, and shear strain energy ratios and the total energy ratio.

Failure of an element is indicated when the the total energy ratio of an element exceeds 1.00. PLSTREN indicates which elements have failed and in what order by printing a flag on the energy line. This is shown in increment 4 for element 4, increment 6 for element 1, and increment 11 for elements 2 and 3.

COMPOSITE (0/.45/-45/90) ELEMENT *** NON-LINEAR DATA FILE ***

```
                                                  2   0   0   0   1
    4    4    1    0    0         50    0         0   0   0   0
    1   15    4                                   0   0   0
    1   11    0    0.0   1.0    0.0              900.      0   0   0
    2   10    0    1.0   1.0    0.0              900.
    3    0    1.0   1.0    0.0
    4    1    1.0   1.0   -45.    90.            .0210
                                   .021          .0210
    0.        45.
   .021        .021    1    1
    1          1    2    2         0    1
    1          1    3    3
    4          1    4    3

    1                    10
    0          9          18
   0.0       0.0        0.0    0     .002       15      .004    84637.1
   0.005   128876.8    .008    41863.7    .016   217803.0
   .012    285589.7    .01305   173449.1    .0111   318405.3
   0.0       0.0        .001    286497.5    .000    36762.3
   .003     54458.4    .004    18441.3    .003    80718.4
   .0055    96873.6    .01038   71822.4    .00728   124714.6
   0.0       0.0        .002    110794.1    .004     5078.9
   .006      7182.9     .008     2026.9    .016     9386.0
   .012      9576.5     .01412   8088.3    .01624  10100.5
   0.0       0.0        .004     9933.5    .000     8327.5
   .008     10781.7     .010     5603.5    .012    14472.3
   .014     15819.5     .016    12049.4    .018    17062.2
   .020     18853.4     .022    16947.7    .024    20306.5
   .026     21112.7     .028    19062.1    .036    22071.1
   .032     22471.9     .036    21645.6    .040    23033.7
   0.0       0.0        .02     22762.0    .04      8049.0
   0.0       9445.7     .10     5841.5    .15     12633.6
                                 11155.4
   0.0        .305      .001103   3582     .002307  .3494
   .003557   .3438      .004760   3390    .005826  .3350
   .000947   3321       .008070   3364    .009197  .3290
   .010324   3308       .011440   3329    .012558  .3358
   .01304    3308
   0.0        .48017    .000118    4636    .000274  .4418
   .001004    3755      .001627   3020    .002101  .3590
   .002740    3507      .003818   3600    .003804  .3578
   .004479    3552      .005078   3643    .005505  .3558
   .006325    3599      .006957   3656    .007582  .3670
   20920850. 18441390. 1313450. 1460878.  292075.
```

1COMPOSITE (0/-45/-45/90) ELEMENT ... NON-LINEAR DATA FILE ...

```
NUMBER OF NODAL POINTS-------------        4
NUMBER OF ELEMENTS-----------------        4
NUMBER OF DIFF. MATERIALS----------        1
NUMBER OF PRESSURE CARDSS----------        0
X-ACCELERATION---------------------   0.0000E+00
Y-ACCELERATION---------------------   0.0000E+00
REFERENCE TEMPERATURE--------------   0.0000E+00
MATERIAL COMBINATION
** ISO.=1 ANISO.=2 BOTH=3 **               2
NUMBER OF ISOTROPIC MATERIALS              0
TYPE OF OUTPUT---------------------        0
TYPE OF PUNCH OUTPUT---------------        0
NUMBER OF ITERATION----------------        0
NONLINEAR ANALYSIS NONLIN=1--------
LINEAR ANALYSIS NONLIN=0-----------        1
NONLIN-----------------------------        1
NDPSNR-----------------------------       15
MAX. NO. OF INRETS-MAXINR----------        4
MAXIMUM ELEM. OUTPUT MAXEL---------        4
MINIMUM ELEM. OUTPUT MINEL---------
DEPTH-WISE ELEMENTS MAXOPT---------
NDIS=0 FORCE LOADING
NDIS=1 DISPLACEMENT LOADING
TYPE OF LOADING  NDIS-------------         0
```

1NODAL POINT	TYPE	X ORDINATE	Y ORDINATE	X LOAD OR DISPLACEMENT	Y LOAD OR DISPLACEMENT	TEMPERATURE
1	1	0.00000	0.00000	0.00000E+00	0.00000E+00	0.000
2	11	0.00000	1.00000	0.00000E+00	0.00000E+00	0.000
3	10	0.00000	1.00000	0.00000E+00	0.00000E+00	0.000
4	0	1.00000	1.00000	0.00000E+03	0.00000E+00	0.000

				MATERIAL	ANGLE	THICKNESS
				1	0.00	0.021000
				1	45.00	0.021000
				1	-45.00	0.021000
				1	90.00	0.021000

1ELEMENT NO.	I	J	K	L
1	1	4	3	2
2	1	4	3	2
3	1	4	3	2
4	1	4	3	2

BAND WIDTH--------------   8

FOR THIS PROGRAM THE LOCATION OF AA USED IS = 320 AND IN IA IS = 35

MATERIAL 1

STRAIN 0 DEG. (TEN)	STRESS 0 DEG. (TEN)	STRAIN 0 DEG. (COM)	STRESS 0 DEG. (COM)	SHEAR STRAIN	SHEAR STRESS
0.00000E+00	0.00000E+00	0.00000E+00	0.00000E+00	0.00000E+00	0.00000E+00
0.20000E-02	0.41953700E+05	0.16000E-02	0.18441100E+05	0.00000E+00	0.68416500E+04

ITERATION CONTROLS
ITERATION   2   CHECK1
ITERATION CONTROLS
ITERATION   3   CHECK1
ITERATION CONTROLS
ITERATION   4   CHECK1
        LOAD INCREMENT   2
        DISPLACEMENTS

N.P.	UX	UY
1	0.00000000E+00	0.00000000E+00
4	0.5577883IE-02	0.5577883IE-02

STRESSES / STRAINS / ENERGY CONTRIBUTIONS

ELEM.	X	Y	-XX	-YY	-XY	-LL	-TT	-LT	ENER. LEVEL
1	0.500	0.500	0.1194E+06 / 0.8323E-02	-0.1001E+03 / -0.2008E-02	0.3104E-00 / 0.1004E-13	0.1194E+06 / 0.5677E-02	-0.1001E+03 / -0.2008E-02	0.3104E-00 / 0.1004E-13	0.1096E-00
2	0.500	0.500	0.2302E+05 / 0.5577E-02	0.1704E+05 / -0.2008E-02	-0.1734E+05 / 0.1004E-13	0.3781E+05 / 0.1755E-02	0.5143E+04 / 0.7845E-02	0.1228E-01	0.5073E-01
3	0.500	0.500	0.2302E+05 / 0.5677E-02	0.1704E+05 / -0.2008E-02	0.1734E+05 / 0.1004E-13	0.3781E+05 / 0.1755E-02	0.3143E+04 / -0.2637E-04	-0.7645E-02	0.5073E-01
4	0.500	0.500	0.6619E+04 / 0.5677E-02	-0.3676E+05 / -0.2008E-02	-0.1000E-00 / 0.1004E-13	-0.1744E-01 / 0.1744E-01	0.2100E+06 / 0.6010E+04	-0.2590E-07	0.5073E-01

ITERATION CONTROLS
ITERATION   2   CHECK1
ITERATION CONTROLS
ITERATION   3   CHECK1
ITERATION CONTROLS
ITERATION   4   CHECK1
        LOAD INCREMENT   3
        DISPLACEMENTS

N.P.	UX	UY
1	0.00000000E+00	0.00000000E+00
4	0.83225420E-02	-0.31026101E-02

STRESSES / STRAINS / ENERGY CONTRIBUTIONS

ELEM.	X	Y	-XX	-YY	-XY	-LL	-TT	-LT	ENER. LEVEL
1	0.500	0.500	0.1005E+06 / 0.8323E-02	-0.3541E+03 / -0.3103E-02	0.4070E-00 / 0.1001E-13	0.1005E+06 / 0.8323E-02	-0.3541E+03 / -0.3103E-02	0.4070E-00 / 0.1001E-13	0.4137E-00
2	0.500	0.500	0.3410E+05 / 0.8323E-02	0.2070E+05 / -0.3103E-02	-0.2591E+05 / 0.1001E-13	0.5646E+05 / 0.2610E-02	0.4574E+04 / 0.3606E-04	0.1143E-01	0.1126E-00
3	0.500	0.500	0.3410E+05 / 0.8323E-02	0.2070E+05 / -0.3103E-02	0.2591E+05 / 0.1001E-13	0.5646E+05 / 0.2610E-02	0.4574E+04 / -0.3606E-04	-0.1143E-01	0.1126E-00
4	0.500	0.500	0.9285E+04 / 0.8323E-02	-0.5822E+05 / -0.3103E-02	-0.2740E-00 / 0.1001E-13	0.8322E+05 / 0.6323E-02	0.8074E-07	-0.1326E-12	0.6717E+00

STRESSES / STRAINS / ENERGY CONTRIBUTIONS

ELEM.	X	Y	-XX	-YY	-XY	-LL	-TT	-LT	ENER. LEVEL

ITERATION CONTROLS
ITERATION   2   CHECK1
ITERATION CONTROLS
ITERATION   3   CHECK1
ITERATION CONTROLS
ITERATION   4   CHECK1
LOAD INCREMENT
DISPLACEMENTS

STRESSES / STRAINS / ENERGY CONTRIBUTIONS

ELEM.	X	Y	-XX	-YY	-XY	-LL	-TT	-LT	ENER. LEVEL

ITERATION CONTROLS
ITERATION   2   CHECK1
ITERATION CONTROLS
ITERATION   3   CHECK1
ITERATION CONTROLS
ITERATION   4   CHECK1
LOAD INCREMENT
DISPLACEMENTS

STRESSES / STRAINS / ENERGY CONTRIBUTIONS

ELEM.	X	Y	-XX	-YY	-XY	-LL	-TT	-LT	ENER. LEVEL

ELEM.   X   Y   S   T   -XX   -YY   -XY   -LL   -TT   -LT   ENER. LEVEL

STRESSES / STRAINS / ENERGY CONTRIBUTIONS

ITERATION CONTROLS
ITERATION   2   CHECK1   CHECK2
ITERATION CONTROLS
ITERATION   3   CHECK1   CHECK1
ITERATION CONTROLS
ITERATION   4   CHECK1   CHECK2
LOAD INCREMENT
DISPLACEMENTS
                UX   UY   N.P.   UX   UY

```
ITERATION CONTROLS
ITERATION  2  CHECK1        0.00000000E+00  CHECK2    0.42312125E+01  DECHK    0.10000000E+01 SCALE    0.10000000E+01
ITERATION  3  CHECK1        0.42312125E+01            0.42456190E+01  DECHK    0.33922776E-02 SCALE    0.10000000E+01
ITERATION  4  CHECK1        0.42456190E+01  CHECK2    0.42456619E+01  DECHK    0.10000007E-04 SCALE    0.10000000E+01
              LOAD INCREMENT   9

              DISPLACEMENTS
N.P.        UX                  UY                  UX              N.P.
 1   0.00000000E+00  0.00000000E+00     0.00000000E+00  -0.81062791E-02   2
 4   0.21703507E-01  0.00000000E+00     0.21703507E-01                    3   0.21703507E-01  -0.81062791E-02

                          STRESSES / STRAINS / ENERGY CONTRIBUTIONS

ELEM.  X      Y      -XX              -YY              -XY              -LL              -TT              -LT            ENER. LEVEL
 1   0.500  0.500  0.4857E-05   -0.5104E+03   0.1017E-06   0.4857E+00  -0.5104E-03   0.1017E-06
                   0.2179E-01   -0.8166E-02   0.4356E-13   0.2179E-01  -0.8166E-02   0.4356E-13
      L    T    S          ELEM. FAILING    2
 2   0.500  0.500  0.8706E-05   0.7261E+05  -0.7660E-05   0.1584E+05   0.2905E-01   0.9906E+00       0.1027E+01
                   0.2179E-01  -0.8166E-02   0.4356E-13   0.6814E-05   0.9205E-04   0.7271E-04
                                                           0.6814E-02   0.2900E-01
 3   0.500  0.500  0.8706E-05   0.7261E+05   0.7660E-05   0.1604E+05   0.2902E+00   0.1619E+00       0.7279E+00
                   0.2179E-01  -0.8166E-02   0.4356E-13   0.6814E-05   0.9206E-04   0.7271E-04
                                                           0.6814E-02  -0.2900E-01
 4   0.500  0.500  -0.2655E+04  -0.1445E+00  -0.7220E-06  -0.1445E+00   0.2902E+00   0.1619E+00       0.7279E+00
                   0.2179E-01  -0.8166E-02   0.4356E-13  -0.8166E-02   0.2655E-04  -0.1334E+00
      L    T    S          ELEM. FAILING    1                          0.8166E-02   0.2179E-01  -0.3493E-12
                                                                                                     0.1132E-01
ITERATION CONTROLS
ITERATION  2  CHECK1        0.00000000E+00  CHECK2    0.42577722E+00  DECHK    0.10000000E+01 SCALE    0.10000000E+01
ITERATION  3  CHECK1        0.42577722E+01  CHECK2    0.42876276E+01  DECHK    0.22609940E-02 SCALE    0.10000000E+01
ITERATION  4  CHECK1        0.42876276E+01  CHECK2    0.42876480E+01  DECHK    0.43423744E-05 SCALE    0.10000000E+01
              LOAD INCREMENT   10

              DISPLACEMENTS
N.P.        UX                  UY                  UX              N.P.
 1   0.00000000E+00  0.00000000E+00     0.00000000E+00  -0.92741322E-02   2
 4   0.24740426E-01  0.00000000E+00     0.24740426E-01                    3   0.24740426E-01  -0.92741322E-02

                          STRESSES / STRAINS / ENERGY CONTRIBUTIONS

ELEM.  X      Y      -XX              -YY              -XY              -LL              -TT              -LT            ENER. LEVEL
 1   0.500  0.500  0.5531E-05   -0.4722E-03  -0.3322E-09   0.5531E+00  -0.4722E-03  -0.3322E-09
                   0.2476E-01   -0.9274E-02   0.5018E-13   0.2476E-01  -0.9274E-02   0.5018E-13
      L    T    S          ELEM. FAILING    2
 2   0.500  0.500  0.9787E-05   0.8263E-05  -0.8078E-05   0.1716E+05   0.9478E-04   0.7622E-04       0.1027E+01
                   0.2476E-01  -0.9274E-02   0.5018E-13   0.7737E-02   0.7737E-02   0.3402E-01
 3   0.500  0.500  0.9787E-05   0.8263E-05   0.8078E-05   0.1716E+05   0.9478E-04   0.1999E+00       0.9232E+00
                   0.2476E-01  -0.9274E-02   0.5018E-13   0.7737E-02   0.7737E-02  -0.7622E-04
                                                                                  -0.3402E-01
 4   0.500  0.500  -0.5972E-04  -0.1648E+00  -0.8232E-06  -0.1648E+00   0.3466E+00   0.1999E+00       0.9232E+00
                   0.2476E-01  -0.9274E-02   0.5018E-13  -0.9274E-05  -0.5972E-04  -0.5972E-07
      L    T    S          ELEM. FAILING    1                          0.9274E-02   0.2476E-01  -0.3974E-12
                                                                                                     0.1132E-01
ITERATION CONTROLS
ITERATION  2  CHECK1        0.00000000E+00  CHECK2    0.42749042E-01  DECHK    0.10000000E+01 SCALE    0.10000000E+01
ITERATION  3  CHECK1        0.42749042E-01  CHECK2    0.42700392E-01  DECHK    0.11800937E-02 SCALE    0.10000000E+01
ITERATION  4  CHECK1        0.42700392E-01  CHECK2    0.42700342E-01  DECHK    0.92760115E-06 SCALE    0.10000000E+01
              LOAD INCREMENT   11

              DISPLACEMENTS
N.P.        UX                  UY                  UX
```

```
 1  0.00000000E+00  0.00000000E+00    2  0.00000000E+00  -0.10381966E-01    3  0.27713883E-01  -0.10381966E-01
 4  0.27713883E-01  0.00000000E+00
1

                                        STRESSES / STRAINS / ENERGY CONTRIBUTIONS

ELEM.   X        Y         -XX          -YY          -XY          -LL          -TT          -LT      ENER. LEVEL

 1    0.500    0.500    0.8287E+05   -0.4390E+03   -0.2283E-08    0.8287E+05   -0.4390E+03   -0.2283E-08
                        0.2771E-01   -0.1036E-01    0.5686E-13    0.2771E-01   -0.1036E-01    0.5686E-13
 L            S       ELEM. FAILING   2
 2    0.500    0.500    0.1000E+06    0.9276E+05   -0.9102E+05    0.9978E+00    0.2306E-01    0.0000E+00    0.1027E+01
                        0.2771E-01   -0.1036E-01    0.5686E-13    0.1917E+00    0.9935E+04    0.7917E+04
 L            S       ELEM. FAILING   3
 3    0.500    0.500    0.1000E+06    0.9276E+05    0.9102E+05    0.1917E+00    0.9931E+04    0.2306E+00    0.1137E+01
                        0.2771E-01   -0.1036E-01    0.5686E-13    0.4362E+00    0.4415E+00   -0.7917E+04
 L            S       ELEM. FAILING   4
 4    0.500    0.500   -0.9302E+04   -0.1051E+06   -0.9237E+00    0.8666E+02    0.8666E+02   -0.3816E-01    0.1137E+01
                        0.2771E-01   -0.1036E-01    0.5686E-13   -0.1051E+06    0.4416E+00    0.2306E+00
 L            S       ELEM. FAILING   1                        -0.4337E+00    0.6981E+00    0.0000E+00    0.1027E+01
```

Samples of Graphs and Contour Plots From
Finite Element Model Selection

All graphs and plots in this appendix represent stresses
derived assuming an isotropic material in the same geometry as
the test specimens with holes.
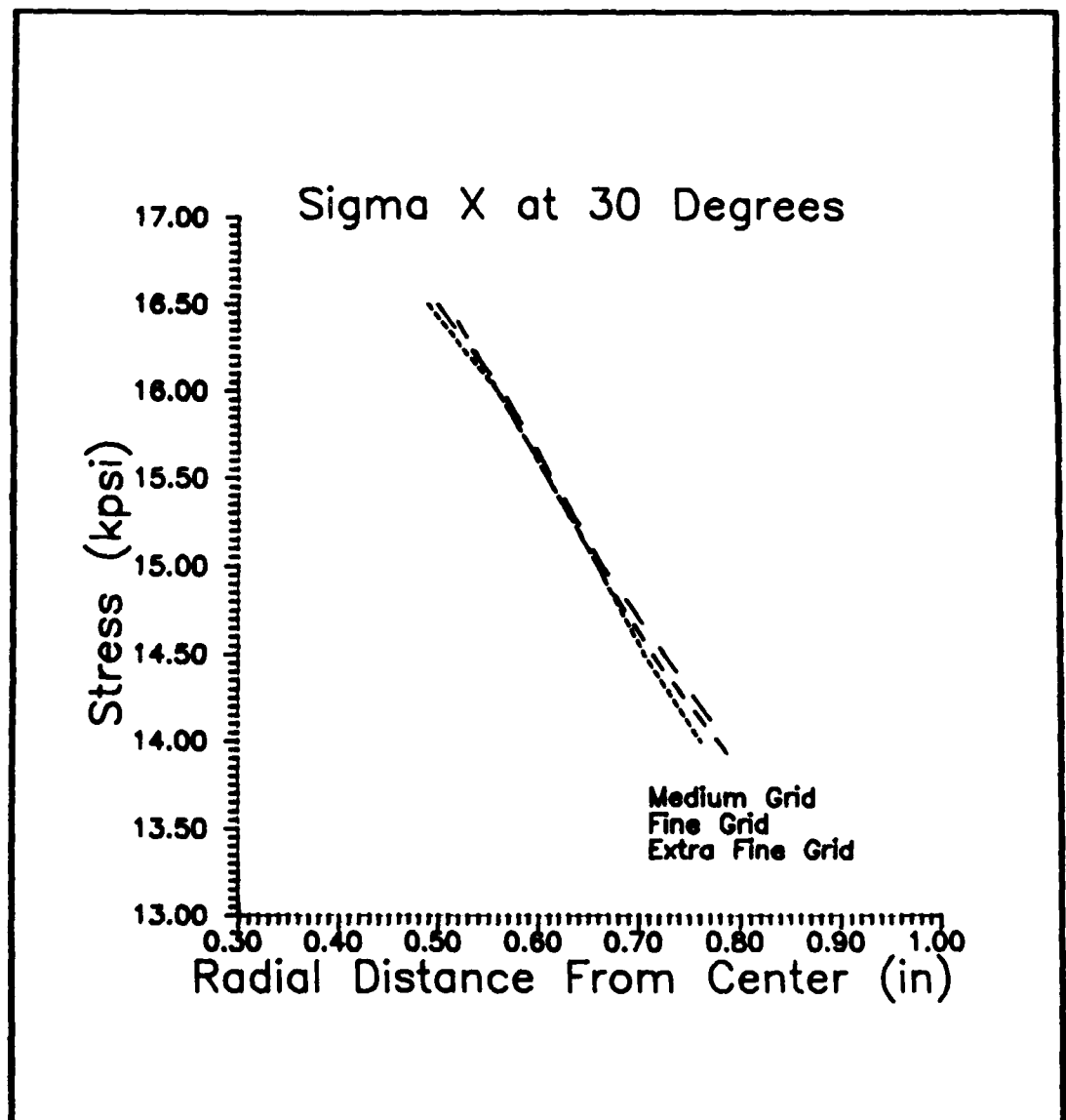
Figure B-1. Longitudinal Stress at the 30 Degree Ray
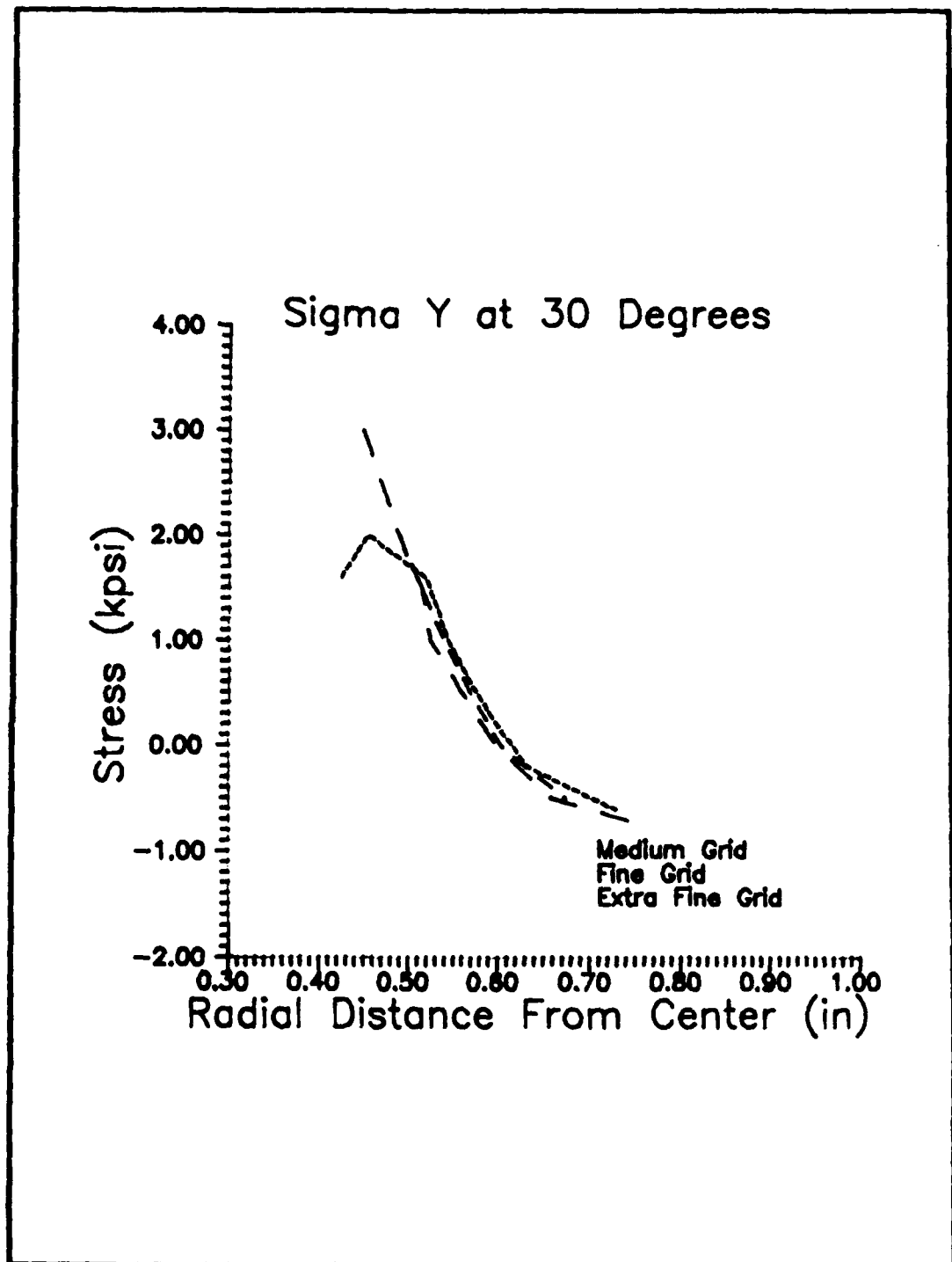
Figure B-2. Transverse Stress at the 30 Degree Ray
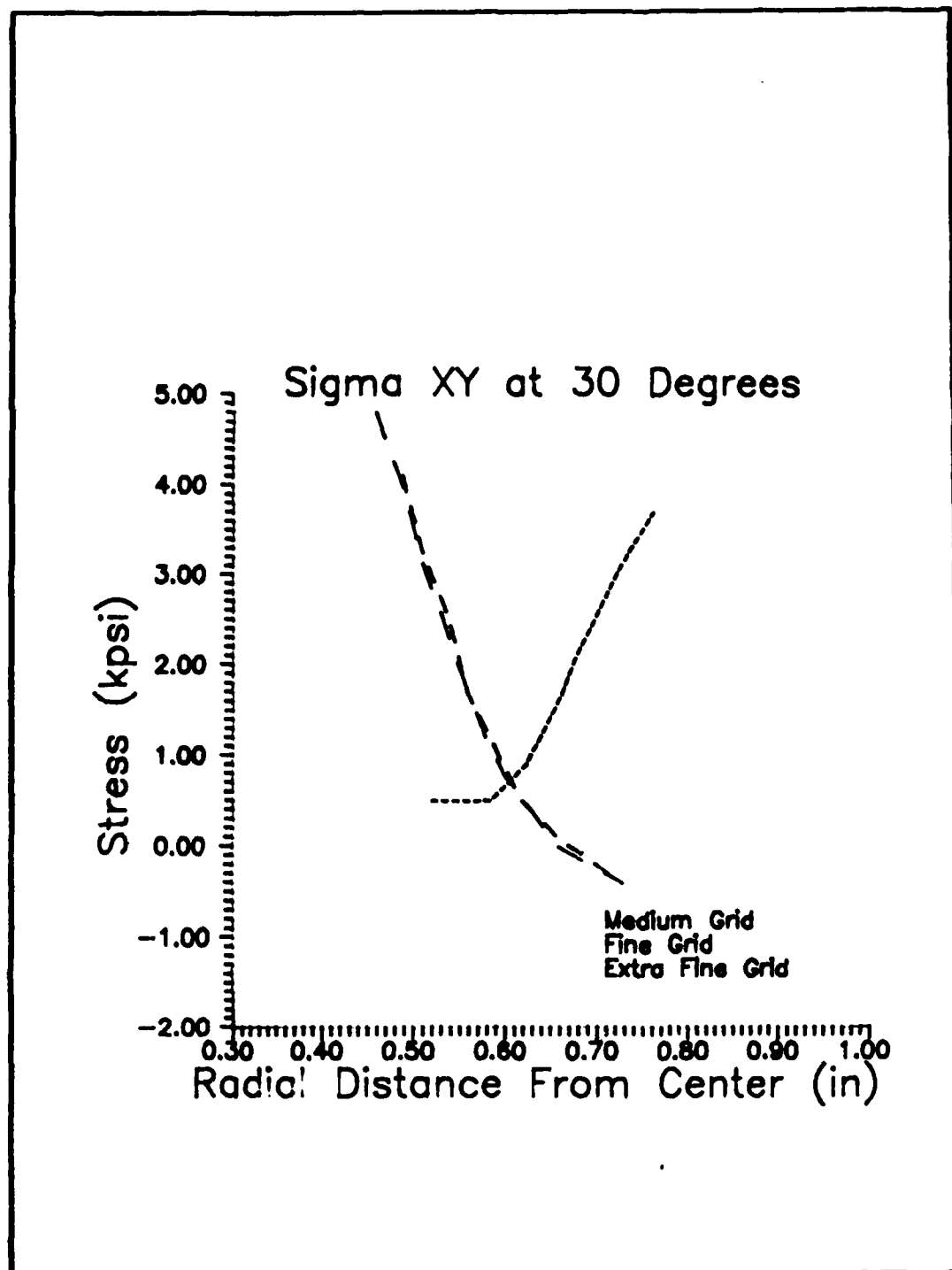
Figure B-3. Shear Stress at the 30 Degree Ray
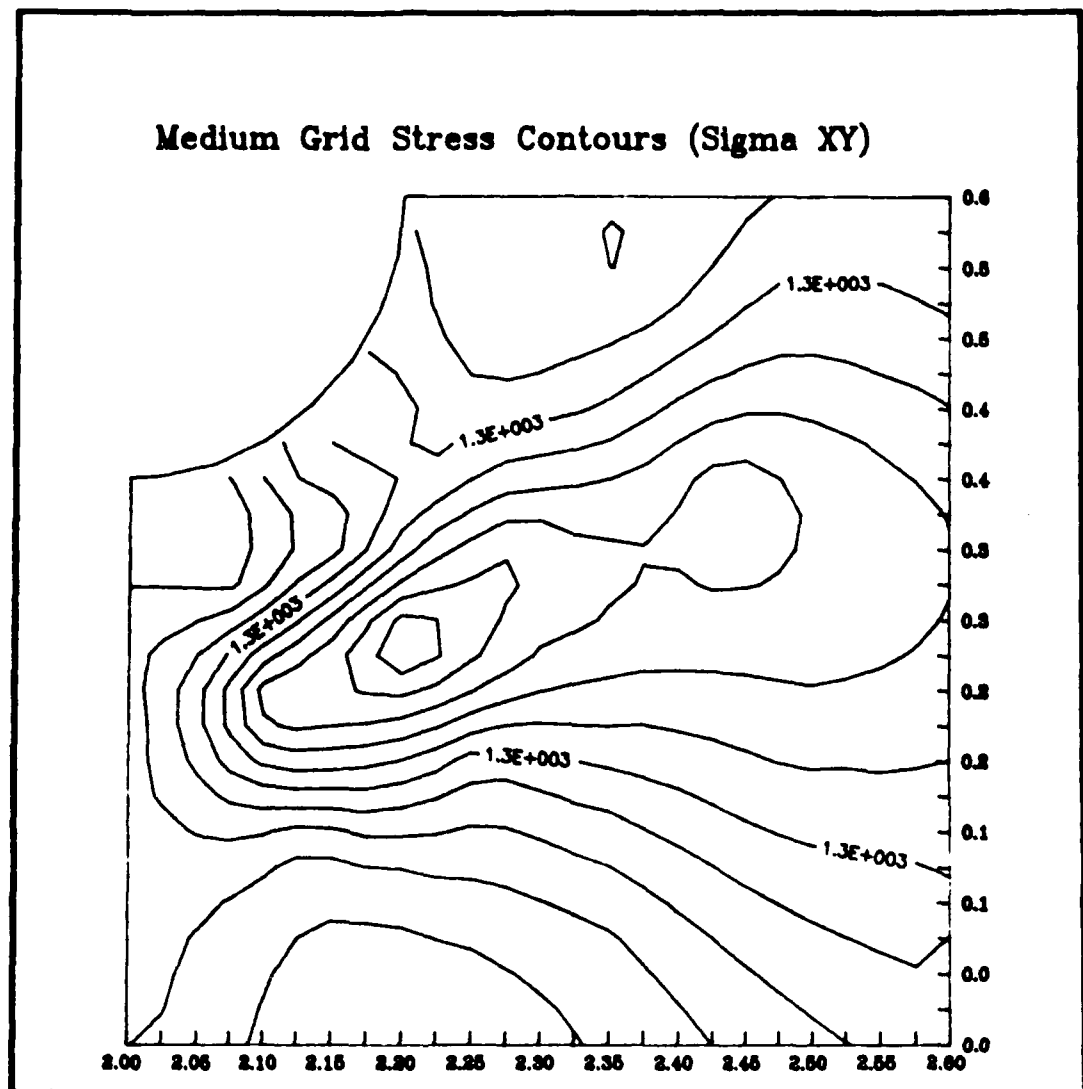
Figure B-4. Medium Grid Shear Stress Contour
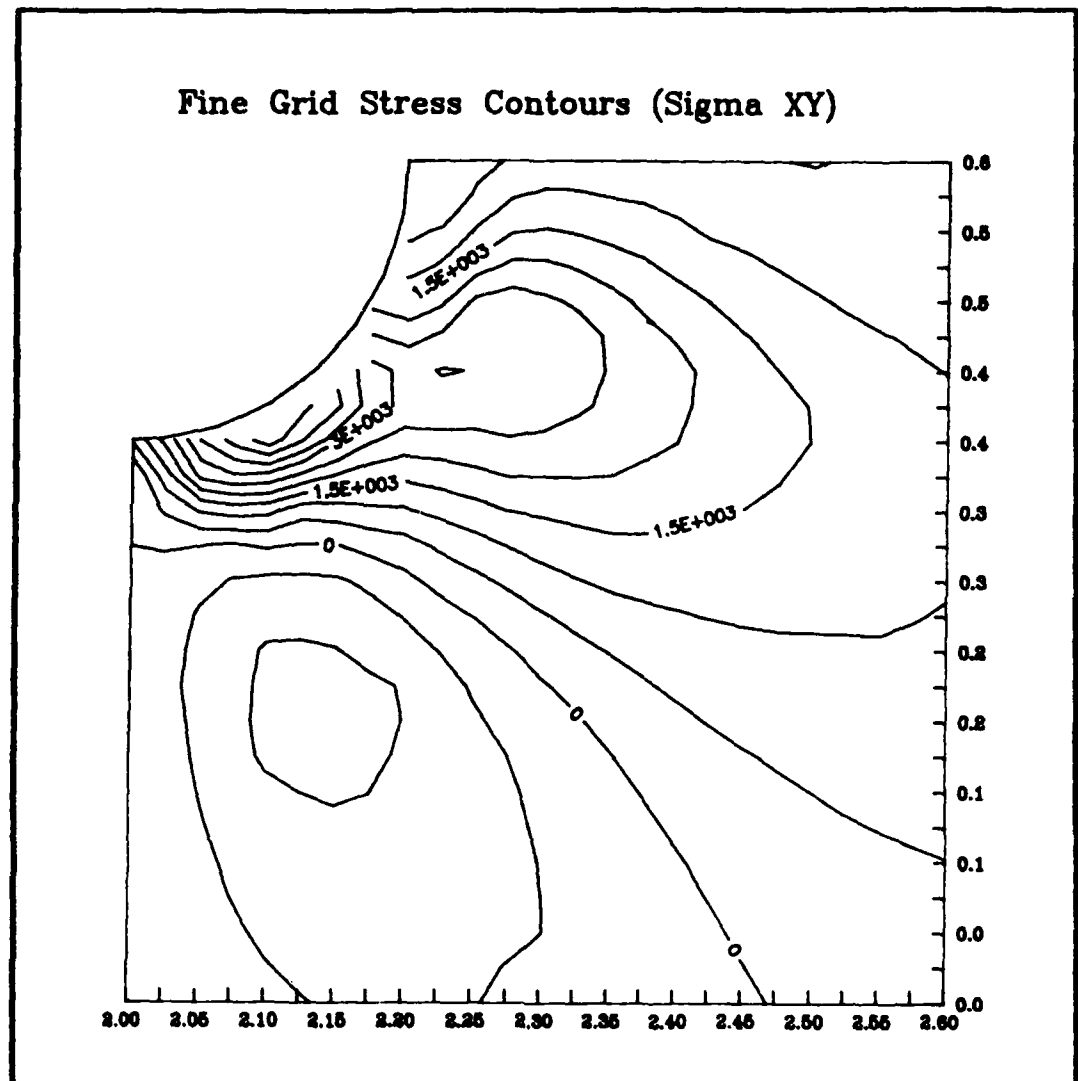
Figure B-5. Fine Grid Shear Stress Contour
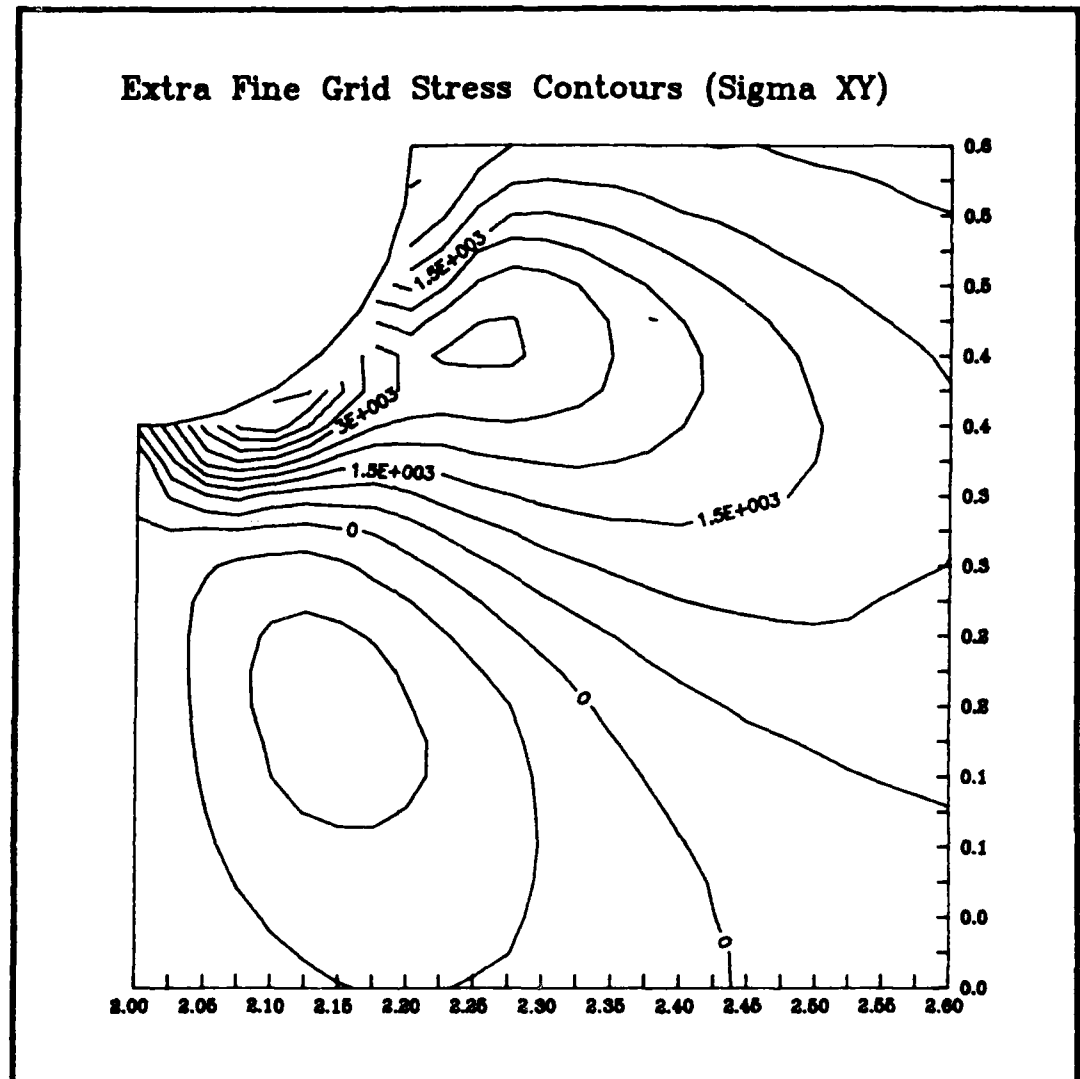
Figure B-6. Extra Fine Grid Shear Stress Contour

Appendix C. Tabular Experimental Data

Table C-1. Longitudinal Tension (E_1^t) Properties

Room Temperature		250 F	
Strain	Stress (ksi)	Strain	Stress (ksi)
0.00000	0.000	0.00000	0.0000
0.00100	19.500	0.00200	41.8537
0.00200	39.000	0.00400	84.6371
0.00300	58.500	0.00600	128.8788
0.00400	78.100	0.00800	173.4491
0.00500	97.800	0.01000	217.8030
0.00600	118.000	0.01200	262.5897
0.00700	138.500	0.01305	286.4975
0.00800	159.000	0.01410	310.4053
0.00900	180.000		
0.01000	202.000		
0.01100	224.500		
0.01200	247.500		
0.01300	271.000		
0.01400	295.000		
0.01410	297.393		

Table C-2. Transverse Tensile (E_2^t) Properties

Room Temperature		250 F	
Strain	Stress (ksi)	Strain	Stress (ksi)
0.00000	0.000	0.00000	0.0000
0.00100	1.550	0.00200	2.6269
0.00200	3.100	0.00400	5.0789
0.00300	4.600	0.00600	7.1829
0.00400	6.050	0.00800	8.6883
0.00500	7.450	0.01000	9.3866
0.00600	8.850	0.01200	9.6765
0.00700	10.200	0.01412	9.9335
0.00800	11.500	0.01624	10.1905
0.00900	12.550		
0.01000	13.300		
0.01100	13.900		
0.01200	14.300		
0.01290	14.586		

Table C-3.   Longitudinal Compression (E_1^C) Properties

Room Temperature		250 F	
Strain	Stress (ksi)	Strain	Stress (ksi)
0.00000	0.000	0.00000	0.0000
0.00080	15.000	0.00100	18.4413
0.00160	30.000	0.00200	36.7623
0.00240	44.500	0.00300	54.4584
0.00320	58.500	0.00400	71.8224
0.00400	72.500	0.00500	88.7184
0.00480	86.000	0.00550	96.8736
0.00560	99.000	0.00638	110.7941
0.00640	111.500	0.00726	124.7146
0.00720	124.000		
0.00800	136.000		
0.00880	148.000		
0.00960	159.000		
0.01040	170.000		
0.01101	178.000		

Table C-4. Transverse Compression (E_2^c) Properties

Room Temperature		250 F	
Strain	Stress (ksi)	Strain	Stress (ksi)
0.00000	0.000	0.00000	0.0000
0.00200	3.200	0.00400	5.6035
0.00400	6.400	0.00600	8.3275
0.00600	9.600	0.00800	10.7817
0.00800	12.750	0.01000	12.8404
0.01000	15.500	0.01200	14.4723
0.01200	18.000	0.01400	15.8195
0.01400	20.250	0.01600	16.9477
0.01600	22.200	0.01800	17.9622
0.01800	24.050	0.02000	18.8534
0.02000	25.730	0.02200	19.6521
0.02200	27.300	0.02400	20.3865
0.02400	28.700	0.02600	21.1127
0.02600	29.900	0.02800	21.6456
0.02800	30.900	0.03000	22.0711
0.03000	31.800	0.03200	22.4719
0.03200	32.500	0.03600	22.7528
0.03400	33.100	0.00400	23.0337
0.03520	33.400		

Table C-5. Shear (G_{12}) Properties

Room Temperature		250 F	
Strain	Stress (ksi)	Strain	Stress (ksi)
0.00000	0.000	0.00000	0.0000
0.00400	3.090	0.02000	5.8415
0.00800	5.200	0.04000	8.0496
0.01200	6.535	0.06000	9.4457
0.01600	7.440	0.10000	11.1554
0.02000	8.080	0.15000	12.6336
0.02400	8.610	0.20000	13.7560
0.02800	9.020	0.25000	14.9054
0.03200	9.330	0.30000	15.7844
0.03600	9.578	0.40000	17.9831
0.04000	9.810	0.48520	20.4634
0.04400	10.030	0.57040	22.9437
0.04800	10.230		
0.05600	10.540		

Table C-6. Poisson's Ratio at 250 F

Room Temperature		250 F	
Strain	ν_{12}^{t}	Strain	ν_{12}^{c}
0.00000	.3549	0.00000	.4802
0.000094	.3617	0.000110	.4636
0.000236	.3644	0.000274	.4416
0.000474	.3608	0.001084	.3755
0.001193	.3562	0.001627	.3620
0.002387	.3494	0.002181	.3590
0.003557	.3438	0.002746	.3587
0.004700	.3389	0.003318	.3583
0.005826	.3350	0.003894	.3570
0.006947	.3321	0.004479	.3552
0.008070	.3304	0.005078	.3543
0.009197	.3299	0.005695	.3558
0.010324	.3308	0.006326	.3599
0.011440	.3329	0.006957	.3655
0.012550	.3358	0.007582	.3676
0.013640	.3386		

Table C-7. Ultimate Tensile Strength of Ply Lay-ups

Ply Lay-up	Ultimate Tensile Strength (ksi)
$[0]_{16}$	55.556
$[90]_{16}$	4.851
$[\pm 45]_{4S}$	21.329
$[0,\pm 45,90]_{2S}$	38.690

Appendix D: Equipment List

Strain Gages

Micro Measurements Stacked Rosette - two for each UT specimen

P/N: WK - 08 - 060WR - 350

Micro Measurements Rosettes - two for each of the 0° and 90° tension and as farfield gages for all specimens with holes

P/N: CEA - 03 - 125UR - 350

Micro Measurements Rosettes - two each for the compression specimens

P/N: CEA - 03 - 062UR - 350

Electrix Industries High Elongation/High Temperature Rosettes - increasingly smaller sizes were used on the shear specimens

P/N: PAHE - 03 - 250RB - 350 LEN

P/N: PAHE - 03 - 125RB - 350 LEN

P/N: PAHE - 03 - 062RB - 350 LEN

Strain Gage Adhesive

Micro Measurements M-Bond AE - 10/15 adhesive for all but the stacked rosettes

Micro Measurements M-Bond 200 adhesive for the stacked rosettes

Tab Adhesive

Scotch 3M Structural Adhesive AF - 163 - 2 for all tabs but the compression specimens

BLH Electronics SR - 4 Adhesive for tabs of the compression specimens

Miscellaneous Equipment

Spin Physics SP2000 High Speed Video System

Sony video recorder and camera

Instron 20 kip universal test machine

Dataplate Control Unit

Rolfes Compression Test Fixture

Heat Chamber

Hot Air Gun w/ Rheostat (2 each)

Voltmeter

Summagraphics Digitizer

Vita

Capt Fisher was born in Mt. Clemens, Michigan and raised
in the shadow of the space program in Merritt Island,
Florida. After high school, he entered the USAF as a Nuclear
Weapons Specialist and was stationed in some of the garden
spots of the world: Minot, North Dakota and Erhac, Turkey.
Partially to avoid these cultural meccas, he left the
USAF in 1980 to attend the University of New Mexico. He
rejoined the USAF in 1982 through the College Senior
Engineering Program (CSEP) and graduated in 1983 with a B.S.
in Mechanical Engineering. After passing through Lackland
AFB for the second time, he was commissioned as a 2nd
Lieutenant and stationed at Tyndall AFB, Florida. At Tyndall
AFB, he was a project manager responsible for modifications
to full scale and subscale target drones and for testing many
of the drone command and control systems. After Capt Fisher
rejoins the world of eight hour days and three day weekends,
he will be assigned to Robbins AFB, Georgia.

REPORT DOCUMENTATION PAGE	Form Approved OMB No. 0704-0188

1a. REPORT SECURITY CLASSIFICATION UNCLASSIFIED	1b. RESTRICTIVE MARKINGS

2a. SECURITY CLASSIFICATION AUTHORITY	3. DISTRIBUTION / AVAILABILITY OF REPORT
2b. DECLASSIFICATION / DOWNGRADING SCHEDULE	Approved for public release; distribution unlimited.

4. PERFORMING ORGANIZATION REPORT NUMBER(S) AFIT/GAE/AA/88D-15	5. MONITORING ORGANIZATION REPORT NUMBER(S)

6a. NAME OF PERFORMING ORGANIZATION School of Engineering	6b. OFFICE SYMBOL (If applicable) AFIT/ENY	7a. NAME OF MONITORING ORGANIZATION

6c. ADDRESS (City, State, and ZIP Code) Air Force Institute of Technology Wright-Patterson AFB OH 45433-6583	7b. ADDRESS (City, State, and ZIP Code)

8a. NAME OF FUNDING / SPONSORING ORGANIZATION AFSC/FDL	8b. OFFICE SYMBOL (If applicable) AFWAL/FIBC	9. PROCUREMENT INSTRUMENT IDENTIFICATION NUMBER

8c. ADDRESS (City, State, and ZIP Code) Wright-Patterson AFB OH 45433	10. SOURCE OF FUNDING NUMBERS			
	PROGRAM ELEMENT NO. 62201F	PROJECT NO. 2401	TASK NO. 03	WORK UNIT ACCESSION NO. 66

11. TITLE (Include Security Classification)
A STUDY OF THE FAILURE CHARACTERISTICS OF A THERMOPLASTIC COMPOSITE MATERIAL AT HIGH TEMPERATURE

12. PERSONAL AUTHOR(S)
James M. Fisher, Capt, USAF

13a. TYPE OF REPORT MS Thesis	13b. TIME COVERED FROM _____ TO _____	14. DATE OF REPORT (Year, Month, Day) 1988 December	15. PAGE COUNT 201

16. SUPPLEMENTARY NOTATION

17. COSATI CODES			18. SUBJECT TERMS (Continue on reverse if necessary and identify by block number)
FIELD	GROUP	SUB-GROUP	Composite Materials, Gr/PEEK, Finite Element Analysis, Nonlinear Analysis, Failure Criteria.
11	04		
13	13		

19. ABSTRACT (Continue on reverse if necessary and identify by block number)

Thesis Advisor: Dr. Anthony N. Palazotto

20. DISTRIBUTION / AVAILABILITY OF ABSTRACT ☒ UNCLASSIFIED/UNLIMITED ☐ SAME AS RPT. ☐ DTIC USERS	21. ABSTRACT SECURITY CLASSIFICATION UNCLASSIFIED
22a. NAME OF RESPONSIBLE INDIVIDUAL Anthony N. Palazotto, Professor	22b. TELEPHONE (Include Area Code) 513-255-3517	22c. OFFICE SYMBOL AFIT/ENY

DD Form 1473, JUN 86   Previous editions are obsolete.   SECURITY CLASSIFICATION OF THIS PAGE

The purpose of this thesis was to study the failure characteristics of the thermoplastic composite Graphite/Polyetheretherketone (Gr/PEEK) at 250 F. Specimens of Gr/PEEK containing a hole (1/3 diameter to width ratio) were tested at 250 F to determine stress-strain response near the hole, the progression of failure, and ultimate tensile strength. The ply lay-ups of these specimens were: $[0]_{16}$, $[90]_{16}$, $[\pm 45]_{4S}$, and $[0,\pm 45,90]_{2S}$. Using ASTM standards, specimens of Gr/PEEK were also tested at 250 F to determine the nonlinear material properties of Gr/PEEK. These material properties were used to predict the stress-strain behavior, propagation of failure, and ultimate failure of a model of the specimens with a hole.

Testing of the specimens containing ± 45 degree fibers was complicated when the high temperature coupled with the high strains caused the strain gages to become unglued prematurely. Optical techniques of measuring strains were used on both the basic property $[\pm 45]_{4S}$ specimens and the $[\pm 45]_{4S}$ specimens with a hole to determine the feasibility of these techniques and to provide an experimental basis for comparison for the analysis.

A high speed video camera was used to record failure of the specimens with holes. Data on approximately how rapidly the different ply lay-ups fail is valuable in modeling the progression of failure analytically. Although the video camera was capable of frame rates high enough to capture the failure process, the high frame rate is at the expense of photographic resolution. Although the images do provide some insight into how rapidly the specimens fail, the images recorded are of relatively poor quality.